



UNIVERSITY OF TWENTE.

Faculty of Electrical Engineering,
Mathematics & Computer Science

On the effect of antenna coupling on spectrum sensing using a cross-correlation spectrum analyser with two antennas

P.J. Prins, Bsc.

MSc. Thesis
January 2012

Supervisors

prof.dr.ir.ing. F.B.J. Leferink
dr.ir. M.J. Bentum
dr.ir. A.B.J. Kokkeler
M.S. Oude Alink, Msc.

Chair of Telecommunication Engineering &
Chair of Integrated Circuit Design,
Faculty of Electrical Engineering,
Mathematics and Computer Science
University of Twente
P.O. Box 217
7500 AE Enschede
The Netherlands

Summary

Spectrum sensing for cognitive radio is a technique to find unused pieces of spectrum which can then be used to transmit and receive data. This requires sensitive, low noise, measuring. For that purpose it has been proposed to use a cross-correlation spectrum analyser. Such a system can use one antenna and a splitter to two receiver paths. Alternatively, a second antenna can be used instead of a splitter.

In this report the signal reception and system noise reduction of both designs are compared analytically, in case the antennas are dipole antennas, positioned in parallel, collinear or in echelon. The antenna coupling is described using an impedance matrix of which the entries are expressed according to the induced electromagnetic force method. For this purpose it is assumed that the environment is reflection-free and time-invariant.

The contribution of signals and (thermal) noise from the passive front-end, consisting of an H-type resistive attenuator, to the best achievable signal to noise ratio at the output of the receivers is derived. Some approaches for optimization of the two-antenna design are discussed, supported by plots.

Contents

Contents	v
List of abbreviations and symbols	vii
List of abbreviations	vii
List of symbols	vii
1 Introduction	1
1.1 Cognitive radio	1
1.2 Previous work	3
1.3 Goal of this work	4
1.4 Outline	5
2 System overview of a correlation spectrum analyser	7
2.1 Principle of a correlation spectrum analyser	7
2.2 Definitions of signals and noise in energy detection for cognitive radio	9
2.3 Assumptions to accommodate analysis	11
2.4 Receiver circuit	12
3 Antenna coupling	15
3.1 Impedance of a dipole antenna	15
3.2 Mutual impedance of two dipole antennas in echelon	18
3.3 Matrix description of multiple dipole antennas in echelon	26
3.4 Optimal load impedance of coupled antennas	31
3.5 Summary	41
4 Signal and noise propagation in a cross correlation spectrum analyser	43
4.1 Determining the propagation of signal and noise	43
4.2 Calculation of transfer functions	51
4.3 Plots	55
4.4 Summary	73
5 Conclusion and recommendations	75
5.1 Conclusion	75
5.2 Recommendations	77
A Correlation	79
A.1 Stochastic process	79

A.2	Cumulative probability distribution function	79
A.3	Probability density function	80
A.4	Averages	80
A.5	Autocorrelation	81
A.6	Cross-correlation	81
A.7	Correlation estimator	83
B	Derivation of the self-impedance of a dipole antenna	87
	Bibliography	93

List of abbreviations and symbols

List of abbreviations

ADC	Analog-to-digital converter	7, 11, 45, 46, 75
CR	Cognitive radio	1–3, 9, 10, 50, 76
DFT	Discrete fourier transform	7–9
EM	Electromagnetic	1, 9, 10, 51
EMF	Electromagnetic force	15, 20, 87
EMI	Electromagnetic interference	2, 10
EMS	Electromagnetic susceptibility	2
LAN	Local area network	2
LO	Local oscillator	7–9
PDF	Probability density function	8, 80
PSD	Power spectral density	7–9, 11, 12, 45, 46, 48–51, 53, 55, 56, 59, 60, 63, 68, 69, 72, 73, 75, 76, 81, 85
SA	Spectrum analyser	3, 7
SNR	Signal-to-noise-ratio	8, 11, 44, 45, 47–51, 69, 73, 75
SSID	Service set identifier	2
TV	Television	1
VFD	Variable frequency drive	2
XCSA	Cross-correlation spectrum analyser	3–5, 7, 8, 43, 44, 49, 51, 75, 76

List of symbols

a	(m)	Antenna radius	16–19, 30, 31, 37–39, 56, 60, 63, 66, 69, 87–90
\mathbf{a}^*		Column vector of exponential integrals	21
A		Average	81–83
\mathbf{b}		Row vector of sums and differences of complex exponentials	21
c	(ms^{-1})	Speed of light in free space ($299792458 \text{ ms}^{-1}$)	15, 19, 23–25, 30, 31, 37–40, 57, 58, 60–62, 64–68, 70, 71
Ci		Cosine integral	18, 91
\mathbf{d}	(m)	Column vector of sum and difference distances	21
e		Euler’s number (2.72...)	16, 17, 20, 87, 88
\mathbf{e}	(V)	Excitation vector	27, 32, 34
E		Expectation	80–83

E_z	(Vm ⁻¹)	Phasor of the z-component of a potential field 16, 20
E_1		Exponential integral 17, 21, 88–91
f	(s ⁻¹)	Frequency 15, 19, 23–25, 30, 31, 37–40, 57, 58, 60–62, 64–68, 70, 71
f_*		Probability density function 80, 81
F_*		Cumulative probability distribution function 80
G		Gain 8, 9
h_{**}		Transfer function in the time domain 82, 83
H_{**}		Transfer function in the frequency domain . 29, 44–55, 57, 58, 60–62, 64, 66, 67, 70, 71, 83
H		Transfer matrix 26, 27, 29–31, 40
i	(A)	Current phasor vector 26, 27, 32, 34
I_m	(A)	Maximum amplitude of a standing current wave 15–17, 20
I_z	(A)	Phasor of the current in the z-direction . . . 15–18, 20, 26
j		Imaginary unit 16, 17, 20, 21, 81, 82, 84, 85, 87–91
J_z	(Am ⁻²)	Phasor of the z-component of the current distribution 16, 20
k	(m ⁻¹)	Wave number 15–21, 23–31, 33, 36–40, 52, 55, 57, 58, 60–62, 64–68, 70, 71, 87–90
k_B	(JK ⁻¹)	Boltzmann's constant (1.38 10 ⁻²³ JK ⁻¹) 49, 50
ℓ	(m)	Length of one of the two dipole elements . . 13, 15–31, 33, 36–40, 52, 55–71, 75, 87–90
\mathbf{M}_*	($\Omega^{\text{rank}(\mathbf{Z})-1}$)	Minor matrix of ($\mathbf{Z}_0 + \mathbf{Z}_{l*}$) 33, 34
N_*	(Vs)	Noise in frequency domain representation . 44, 46–48, 52, 54
P		Probability 80
\mathcal{P}	(W)	Power 16, 50
r	(m)	Radial coordinate in a spherical coordinate system 15–17, 19, 20, 87
r_s	(m)	Orthogonal distance between two dipole antennas. 19–25, 30, 31, 37–40, 57, 58
r_z	(m)	Longitudinal distance between two dipole antennas 18–26, 30, 31, 37–40
r_φ	(RAD)	Azimuth between two dipole antennas 20
R_{a*}	(Ω)	Input series resistance of an attenuator 12, 13, 52, 54, 56, 60, 63, 66, 69–71
R_{b*}	(Ω)	Shunt resistance of an attenuator . . 12, 13, 52, 54, 56, 60, 63, 66, 69
R_{c*}	(Ω)	Output series resistance of an attenuator . . 12, 13, 52, 54, 56, 60, 63, 66, 69
R_s	(Ω)	Splitter input resistance 12, 13, 52, 56, 60, 63, 66, 69
R_{l*}	(Ω)	Load resistance 13, 50, 52, 54, 56, 60, 63, 66, 69
R_1	(m)	Distance from the upper end of a dipole antenna to a field point 15–17, 19, 20, 87

R_2	(m)	Distance from the lower end of a dipole antenna to a field point.....15–17, 19, 20, 87
R_{**}		Correlation 81–83
s		Radial coordinate in a cylindrical coordinate system15–17, 19, 20, 87
s		Sample.....79–83
S_{**}		Power spectral density.....43–48, 50, 81–85
S		Power spectral density for which at the output of the system, the magnitude of the signal contribution is equal to the magnitude of the thermal noise of the front end.. 51, 58, 59, 61, 65, 68, 71
S		Diagonal matrix of sine functions.....26–29
Si		Sine integral 18, 91
t	(s)	Time.....79–85
T	(s)	Time period..... 81, 83–85
\mathcal{T}	(K)	Temperature.....49, 50
\mathbf{u}	(V)	Voltage phasor vector.....26, 27, 32, 34
U	(V)	Phasor of the antenna voltage 16, 18, 20, 26
U_I	(V)	Phasor of the second mixer input voltage in a two-antenna system.....13, 54
U_I	(V)	Phasor of the first mixer input voltage in a two-antenna system.....13, 54
U_O	(V)	Phasor of the second mixer input voltage in a one-antenna system.....13, 52
U_{Ξ}	(V)	Phasor of the source voltage of a sending antenna 13, 52, 54
U_{Ψ}	(V)	Phasor of the first mixer input voltage in a one-antenna system.....13, 52
z		Third coordinate in a Cartesian or cylindrical coordinate system.....15–20, 87–89
Z_l	(Ω)	Load impedance 26–40
\mathbf{Z}_l	(Ω)	Matrix of load impedances.....27–29, 40
Z_m	(Ω)	Antenna impedance related to the maximum current amplitude.....16–21, 23–27, 29, 33, 36, 52, 55, 87–90
\mathbf{Z}_m	(Ω)	Matrix of antenna impedances related to the maximum current amplitude.....13, 26–29, 41, 54
Z_{Ξ}	(Ω)	Source impedance of a transmitting antenna.. 12, 13, 52, 54–56, 60, 63, 66, 69
Z_0	(Ω)	Antenna impedance at the terminals... 12, 16–20, 23–27, 31–39
\mathbf{Z}_0	(Ω)	Matrix of antenna impedances at the terminals26–29, 32, 41, 52, 54, 56, 60, 63, 66, 69
γ		Euler-Mascheroni constant (0.577...).....17, 18, 89, 90

Γ	(Vs)	Signal in the second circuit in a two-antenna system in frequency domain representation 13, 45–48, 50, 54, 56, 60, 63, 66, 69
δ		Dirac delta function 16, 20, 84, 85
ϵ		Small positive real number 80, 84, 89, 90
η	(Ω)	Impedance of free space ($\approx 120\pi\Omega$). 16–18, 20, 21, 87–90
Θ	(V^2s)	Power spectral density of Ξ : $S_{\Xi\Xi}$ 48, 49
I	(Vs)	Signal in the first circuit in a two-antenna system in frequency domain representation . . 13, 45–48, 50, 54, 56, 60, 63, 66, 69
λ	(m)	Wavelength . . . 19, 21, 23–25, 30, 31, 37–40, 57–62, 64–68, 70, 71
Λ_*	(V^2s)	Power spectral density of N_* : $S_{N_*N_*}$ 48–51, 57, 62, 66, 70
Ξ	(Vs)	Source signal in frequency domain representation . . 44–47
O	(Vs)	Signal in the second circuit in a one-antenna system in frequency domain representation . . . 12, 13, 47, 48, 50, 52, 56, 60, 63, 66, 69
π		Archimedes' constant (3.14. . .) 15–21, 23–25, 29–31, 37–40, 57, 58, 60–62, 64–68, 70–72, 84, 85, 87–91
Π	(V^2s)	Cross power spectral density of I and Γ : $S_{I\Gamma}$ 48
τ	(s)	Time shift 81–84
Υ_*	(Vs)	Signal that enters the correlator in frequency domain representation 44, 46, 47
φ	(RAD)	Azimuth in a spherical coordinate system 20
Φ	(V^2s)	Cross power spectral density of Ψ and O : $S_{\Psi O}$ 48
Ψ	(Vs)	Signal in the first circuit in a one-antenna system in frequency domain representation . . 12, 13, 47, 48, 50, 52, 56, 60, 63, 66, 69
ω	(RAD s^{-1})	Angular frequency 18, 81–85

Chapter 1

Introduction

1.1 Cognitive radio

The paradigm

A cognitive radio (CR) is a wireless communication device which automatically adjusts its transmission and reception parameters to avoid interference with other wireless communication, while optimizing communication along the line or network it is part of. These parameters include channel and transmission power. Ideally two or more of these devices can be put anywhere to set up a network along which they can communicate without interfering with other licensed or unlicensed users of the electromagnetic (EM) spectrum. This requires scanning and monitoring of the radio environment and adjusting transmission accordingly.

A spectrum sensing CR is a type of CR that regularly scans the EM spectrum for (currently) unused frequency bands and sets up transmission within this band. Compared to other kinds of CR, in a spectrum sensing CR only frequency divided channels are considered and not for example time, space or code-divided channels. Furthermore only free channels are used, while the wider definition of CR would allow communication along channels in use as long as harmful interference with the other user is averted somehow.

Scanning and monitoring of the EM spectrum without prior or external knowledge can only be done by some form of energy detection. If there is more EM energy in a frequency band than some threshold above the background noise level, the band is assumed to be occupied. Other methods can be more sensitive, but rely on information of the signal that can be present. For example when looking for an empty television (TV) band, information on the local protocol for television broadcast can help distinguishing a TV channel in use from background noise. In practice that means that weaker TV signals can still be detected than with energy detection. However, having this information is a concession on the CR paradigm in which *any* other usage of the EM spectrum needs to be detected.

Spectrum sensing

Energy detection for the purpose of CR is meant to prevent re-using a frequency band that is already in use. That would be unwanted for two reasons. First, it

might interfere with the reception at a receiver for which some signal was sent. Therefore it is undesirable to re-use a channel to which a receiver is listening. Second, to use a channel in which already a lot of power is present, would require extra power compared to using an empty channel. Because of this it is undesirable to re-use a channel on which an other transmitter is sending, as long as there are other channels with less power present. Any or both of these two reasons may apply. General examples of each case are given in Table 1.1.

	Other transmitter active	No other transmitter active
Other receiver listening	<ul style="list-style-type: none"> •Communication in progress 	<ul style="list-style-type: none"> •Idle time during communication •Electromagnetic susceptibility (EMS)
No other receiver listening	<ul style="list-style-type: none"> •Unattended broadcast •Electromagnetic interference (EMI) 	<ul style="list-style-type: none"> •Unassigned unused band •Assigned but unused band

Table 1.1: Examples of bands with or without an active transmitter and/or a receiver listening

On the left hand side of the table we find examples of cases in which a transmitter (other than our own) is sending. This could mean there is a receiver listening to what is being sent. In that case we can speak of communication in progress. In this case reuse of the channel by a CR will likely cause harmful interference, which would therefore be forbidden in most cases, because that reuse is undesirable to other users of the spectrum.

Conversely: a transmitter can also be sending, while there is no receiver to listen. Examples include a radio station that is broadcasting music all night, while perhaps no radio is tuned to that particular station at that time, or a wireless local area network (LAN) router that is broadcasting its service set identifier (SSID) while there is no mobile device within reach to use that information. Another kind of transmitter to which no receiver is listening is an unintentional transmitter: an electromagnetic interferer. If we have for instance a variable frequency drive (VFD)¹ that is causing EMI, there is probably no receiver intentionally listening to it.² In all cases where there is no receiver listening, no harm is done by a CR reusing that particular channel, as the sender will not even take notice.

On the right hand side of Table 1.1 are examples in which no transmitter is sending. This can be the case when there is no sender as well: the band is unused. The use of such a band will cause no harm, but whether it is *allowed* to use a channel that is possibly assigned to an other user or for another purpose, will depend on local regulations. There are also cases in which there is an active receiver, but no transmitter. One can think of a receiver waiting for an interrupted or unstarted transmission, like a receiver for radio astronomy or a pager waiting for a message to come. Also equipment suffering from EMS like medical equipment can be seen as a receiver in the absence of a transmitter. A CR can cause harmful interference to such a device without being able to detect that.

¹A VFD is a system to control the speed of an electric motor by controlling the frequency of the power to that motor. Due to the combination of high powers and high frequencies, such systems are infamous for causing EMI.

²There may be a victim system that is “unintentionally listening” to EMI, but that is usually called *hearing* rather than listening.

All examples on the left hand side of table 1.1 are possibly detectable, but certainly not distinguishable by means of energy detection only. Therefore when using energy detection as the only means of spectrum sensing, both harmful and unarmful reuse needs to be avoided. Furthermore some additional knowledge is required to avoid certain channels in which no transmitter is active, required by local regulations, or by the presence of a legitimate receiver to which no harmful interference may be caused. Although this tells us that implementing a CR with spectrum sensing as its only channel selection mechanism will not suffice, the remainder of this report will be confined to spectrum sensing, or, more specifically, spectrum sensing by means of energy detection.

A reliable implementation of a CR based on energy detection requires a high sensitivity. This puts severe demands on the noise floor of the receiver and the spectrum analyser (SA), because a weak signal can only be recognised when the uncertainty of the level of the noise floor is lower. Furthermore the system needs to be sufficiently linear, because strong higher harmonics or intermodulation products will be recognised as separate occupied bands, preventing the system from using these possibly empty bands. To meet these requirements it was proposed to implement the SA as a cross-correlation spectrum analyser (XCSA), which will be discussed in Chapter 2.

1.2 Previous work

Correlation spectrum analysers are widely known for a long time and through the years several approaches were studied to optimize its design. Sampietro et al. [1] showed that using a XCSA with two independent amplifier paths in a measurement instrument instead of a traditional system, improved the sensitivity by at least 50 dB. A slightly different implementation was chosen by Ciofi et al. [2]. Instead of calculating the cross-correlation between the two receiver paths, he chose to approximate the autocorrelation of the sum and the difference between the two paths. This had the advantage that the correlation could be estimated in the time-domain, if desired. Kokkeler and Gunst [3] derived a general expression for the correlation function in the case of cross-correlating multi-bit quantized signals. With this expression the response of the active part of a correlation amplifier to noise and periodic signals can be analysed. The use of more than two amplifiers to be able to reduce the system noise even further than with two amplifiers, was discussed by Crupi et al. [4]. They found that in principle their method would allow complete elimination of the noise introduced by the amplifiers. Oude Alink [5] elaborated on improving the linearity and reducing the variance of an XCSA with two paths. One of his design decisions to improve the linearity, was attenuating the input signal. His design is the basis for the spectrum analysers discussed in this report. Heskamp and Slump [6] compared three designs for a correlation receiver for the purpose of energy detection for the purpose of CR and concluded that only the two front-end design was promising. An implementation of an XCSA was published by Oude Alink et al. [7, 8]. This design includes the front-end attenuation. Measurements showed that this design was more linear than a receiver with a single path, while reducing the noise figure within an acceptable amount of time. In [9] the uncertainty of the noise level in a cross-correlation receiver was

analysed, compared to an autocorrelation receiver.

For an XCSA the signal needs to be directed to both paths of the receiver. The splitter that is required to do so, is a weak point in the design, because system noise can travel through the splitter to the other path. Therefore, it was suggested to replace the splitter by a second antenna. Domizioli et al. [10] presented a mathematical description of the correlation of noise in a two-antenna XCSA, in which the antenna coupling is assumed to be known as an impedance matrix. Results are shown in case of parallel dipole antennas at the frequency for which the total length of the antennas equals a half wavelength. Smeenge [11], Oude Alink et al. [12] addressed the problem of having two antennas that receive an unequal signal. Non-ideal effects like multipath, fading and the Doppler effect were explored using a far-field antenna model.

1.3 Goal of this work

An XCSA with two antennas is supposed to lower the system noise compared to an XCSA with only one antenna. Whether that is actually the case, is determined by the amount of system noise that is transmitted via the antennas to the other receiver path, compared to the amount of noise that is passed by a splitter. Furthermore, two antennas are not at the same spot, so they receive signals slightly different. This has a negative influence on the correlation of signals. If the deterioration of the signal reception is bigger than the reduction of the noise, using two antennas will not be beneficial.

The transmission of system noise via the antennas is determined by the (near-field) coupling of the antennas. This depends on the type, size and position of the antennas, which also effects the reception of signals. Reducing noise coupling and maintaining signal reception are conflicting requirements in designing the antennas. To make a good design, one needs to model the effect of the design parameters on these requirements. This leads to the following research question:

“What is the effect of antenna coupling on spectrum sensing for cognitive radio using a cross-correlation spectrum analyser with two antennas?”

To answer this question, we use the following sub-questions:

- How can we model antenna coupling?
- How is the propagation of system noise to the output effected by antenna coupling in a two-antenna XCSA?
- How is the measurement of signals effected by using two antennas instead of one?
- Which antenna designs are promising for a two-antenna XCSA for cognitive radio?

1.4 Outline

In the next chapter, we will give an overview of the spectrum analyser designs that will be compared. We will start with a description of the evolution of an autocorrelation spectrum analyser via a one-antenna XCSA to a two-antenna XCSA and briefly discuss the advantages and disadvantages of these systems. We continue with the definition of signal and noise we will use throughout this report and end with the assumptions we will use while modelling the systems.

Chapter 3 will be about modelling the coupling between two or more dipole antennas in a parallel, echelon or collinear position. Starting with a derivation of the impedance of a dipole antenna and the mutual impedance between two dipole antennas, we will describe the antenna coupling as an impedance matrix. It will be shown how to calculate the transfer function in case we connect the antennas to (Thévenin equivalent) sources. We will end this chapter with a derivation of the optimal load impedances we should ideally connect to (strongly coupled) dipole antennas.

In Chapter 4 we will derive equations that describe the propagation of several system noise components to the output of a one-antenna and a two-antenna XCSA. Parallel dipole antennas are assumed, but most of the equations can be used for any linear time-invariant antenna configuration of which the impedance matrix is known by calculation or by measurement. This chapter ends with a series of plots that aim to show the effect of design parameters and the unknown direction of a transmitter on measurement by both a two-antenna XCSA and a similar one-antenna XCSA.

The mathematical background of cross-correlation can be found in Appendix A.

Chapter 2

System overview of a correlation spectrum analyser

2.1 Principle of a correlation spectrum analyser

This section is meant to give a qualitative description of different kinds of correlation SAs: an autocorrelation SA, an XCSA with one antenna and an XCSA with two antennas. This will allow us to compare these systems conceptually without losing track because of the mathematics. The terminology and general mathematics of stochastic signals are found in Appendix A. The mathematical description of both kinds of XCSAs is found in the remainder of this report, starting from the next chapter.

Autocorrelation spectrum analyser

The autocorrelation of a random signal is well known to reveal how the energy of that signal is spread among different frequencies. [13]

To show the advantages of an XCSA, let us first have a look at a receiver with an autocorrelation SA. A block diagram of such a receiver is shown in figure 2.1. The signal from the antenna is often amplified first before passing to the mixer to improve the signal strength. After mixing down with a local oscillator (LO), the resulting signal is further amplified. Next the signal is passed through an analog-to-digital converter (ADC) after which the discrete Fourier transform (DFT) is taken. Taking the product of this complex-valued spectrum and its complex conjugate, results in an estimation of the power spectral density (PSD) of the signal. This can be seen as the discrete time equivalent for the cross-spectrum estimation shown in Equation A.36 on Page 85 in Appendix A. By choosing a larger number of samples in the DFT-window the frequency resolution of this estimation is enlarged. The variance of this estimation can be reduced by repeating this process several times for the required number of samples and by taking the average of all obtained spectra.[5, 7, 11]

The accuracy of this kind of system is severely limited by the internal noise of the receiver. Noise that is generated between the antenna and the DFT adds up to the antenna signal and cannot be distinguished from the resulting power spectrum. In most cases the PSD of the system noise is not exactly known. When detecting energy in a certain band at the system output, there is uncertainty whether a high amount of system noise, or a signal with a small

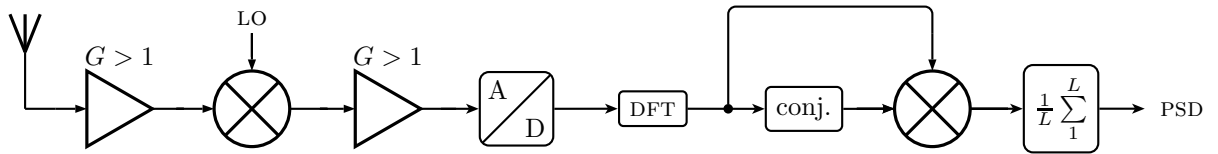


Figure 2.1: Block diagram of an autocorrelation receiver

amount of system noise is observed. In this way signals that appear weaker than the uncertainty of the system noise cannot be reliably detected. The straightforward way of improving this system is trying to reduce the amount of noise generated by the system, but that is limited by other performance parameters, as noise reduction is generally a trade-off with parameters like linearity, measurement time or power consumption. An approach to improve the receiver even further is discussed in the next subsection.

Cross correlation spectrum analyser with one antenna

A cross correlation receiver uses an XCSA. This system makes use of the fact that noise from different sources is usually not correlated. Figure 2.2 shows this system doubles some components and adds a splitter. The pre-amplifiers are in this design replaced by attenuators, which will be explained in a moment.

In both the upper and the lower branch of the system, noise is generated. If all these components are equal and the system is thus symmetric, the noise process in the upper and lower branch will even have the same probability density function (PDF). However, because the noise comes from different sources, their cross correlation can be expected to be zero. When there is no transfer of noise between the branches before the correlator circuit, the noise contribution is expected to be zero in the cross-PSD. Nevertheless, noise that is generated between the antenna and the splitter has a non-zero contribution to the PSD. Furthermore both the splitters and the attenuators need to be passive electrical components to maintain the systems linearity. As a drawback, noise can travel from the upper attenuator via the passive splitter to the lower branch and vice versa. This will result in some noise contribution of the attenuators to the cross-PSD. However, when using sufficient time to estimate the cross-PSD, the resulting system noise contribution to the output can be made smaller than the system noise of an autocorrelation receiver.

Part of the improved signal-to-noise-ratio (SNR) can be traded off against an increase in the systems linearity. This was done by Oude Alink et al. [7] by replacing the amplifiers between the antenna and the mixers by passive attenuators. In this way a smaller range of the mixers is used, making the mixers more linear and reducing higher harmonics. Higher harmonics and intermodulation products from strong signals can cause false positives of occupied bands that may or may not actually be occupied.

Cross correlation spectrum analyser with two antennas

As the splitter was the main cause for noise coupling between the branches of the cross correlation receiver with one antenna, its noise performance can be

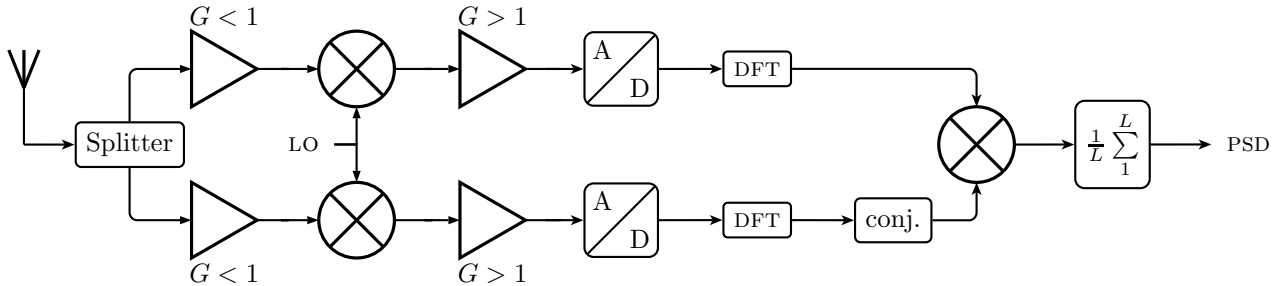


Figure 2.2: Block diagram of a cross correlation receiver with one antenna

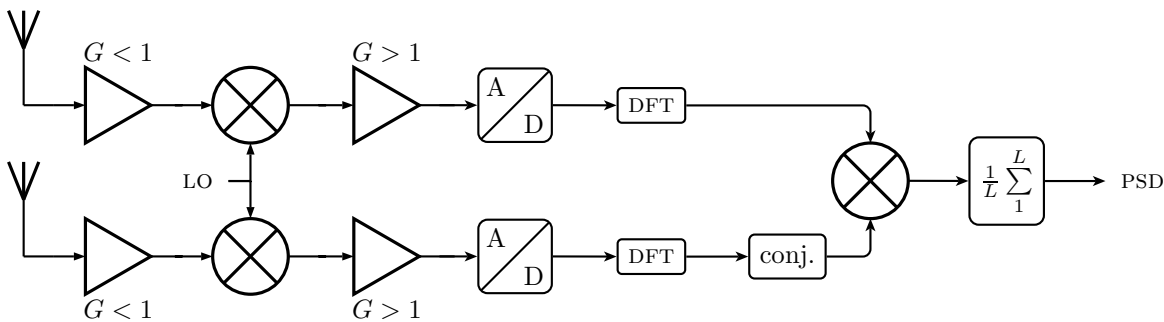


Figure 2.3: Block diagram of a cross correlation receiver with two antennas

further improved by removing this splitter.[7] To still get the signal to both branches, a second antenna needs to be added. A block diagram of this is shown in figure 2.3. This can be advantageous as far as the system noise is concerned, because the amount of noise that is passed between the branches can be made smaller compared to the amount passed by the splitter. This requires reducing the coupling between the antennas, suggesting to put them apart as far as possible. Doing that will unfortunately have a drawback in the detection of a signal. Because the signal that is passed to both branches is no longer exactly the same, depending on the direction from which the signal to be detected is coming, the estimated signal PSD will alter. This will be shown in Chapter 4.

2.2 Definitions of signals and noise in energy detection for cognitive radio

Definition of a signal

According to [14], a signal is “an impulse or a fluctuating electric quantity, such as voltage, current, or electric field strength, whose variations represent coded information” The information to be revealed for a CR by means of energy detection, is how much power is present at different frequency bands of the EM spectrum.

signal a fluctuating electric quantity whose variations represent the amount of power that is present at different frequency bands of the EM spectrum.

Referring to Table 1.1 on Page 2 there are three types of transmission we would like to detect using energy detection. These are the cases on the left hand side of the table, in which some other transmitter is active.

- Transmission of information to which a receiver is listening: communication in progress,
- Transmission of information to which no receiver is listening, like unattended broadcast,
- Unintentional transmission: EMI.

All of these cases can cause a certain amount of power to be present in certain bands of the EM spectrum. Consequently the amount of power being transmitted in any of these cases is a quantity whose variations represent information that is to be revealed by means of energy detection: a signal.

One could argue that the third case should be referred to as noise, because the energy that is being transmitted was not intended to deliver information to a receiver. That would indeed be the case if we were discussing a receiver for communication purposes, that is meant to receive information that was deliberately coded and sent to be received. In such a system, a signal would be characterised by the fact that it is a fluctuating electric field strength to which the receiver is listening. In that case in Table 1.1 the top row shows examples of signals, while the bottom row shows examples of noise.

In this report EMI will be considered a signal, because just like the other cases, in the case of energy detection, the presence of EMI can be a contraindication for a reusable channel. Whether there is a receiver listening to it or whether the power was even radiated with the intention for it to be received is an insignificant detail with respect to the subject at hand, as the difference cannot be detected with energy detection.

As discussed in Section 1.1, a CR will need other sources of information if it has to meet certain local regulations, like ensuring to avoid using certain bands, even if little or no power is present. As these other sources are meant to reveal other information, a discussion of these other sources would require an other definition of a signal.

Definition of noise

According to [14], noise is “a disturbance, especially a random and persistent disturbance, that obscures or reduces the clarity of a signal”. As all power in some band of the EM spectrum is a signal by definition, any disturbance of the signal must not be in the EM spectrum. Consequently no noise is received. The only remaining disturbances come from within the energy detector.

noise a disturbance originating from the energy detector itself that obscures or reduces the clarity of the signal

Examples of noise sources are thermal noise, higher harmonics and quantization noise.

2.3 Assumptions to accommodate analysis

Correlator

As only the passive front ends differ between the one-antenna receiver and the two-antenna receiver, we are only interested in the influence of this part of the systems with respect to the output of the systems. The purpose of the rest of the systems is estimation of the cross-PSD, so it makes sense to model these parts with their idealized relevant behaviour: as a black box that outputs the cross-PSD of the two signals that enter it, with any noise they already contain. If any noise is added within this black-boxed part of the system, it will assumably add that noise both in the one-antenna and two-antenna system, so it has no effect on the comparison of both systems.

This way of thinking can be described as a “preservation of correlated system noise”, in which the amount of correlated noise that enters the correlator cannot diminish with respect to the signal towards the output of the system. This is not generally true, as will be mathematically shown in Chapter 4. For the time being the reasoning is as described in the following two paragraphs.

Both signals that enter the mixers are a linear combination of the signal and noise from one or more sources. This means that for each of these sources there are two “inverse” linear operations that add the noise from that source up to zero in one of the two branches of the system. In that case the resulting cross correlation of that noise component will be zero as well. That same inverse linear operation will not cause that cancellation for the signal component as well, because it will enter the mixer in a different linear combination than the noise. From this we can see that it is possible to have a linear operation that cancels noise while leaving some part of the signal. This means there is no “preservation of correlated system noise”, even if the parts of the system behind the mixers are idealized as some linear operation.

In practice there might be some coupling between the branches of the system, but of course it is highly improbable that this causes complete cancellation of a noise component. However, the fact that it is possible that the SNR, the ratio between the amount of signal and the amount of noise in the cross correlation between the two branches, is increased by cross talk between the branches, shows some additional assumption is required to allow a part of the system to be modelled as an ideal cross correlator black box. To be able to say anything about the influence of the coupling at the passive front end with respect to the correlated noise at the output, we must either know what coupling takes place between both paths behind the mixer inputs, or we must assume there is no coupling at all in this part of the system. The latter assumption will be used. We have to keep in mind that in case some receiver design actually does have a significant amount of coupling between both signal paths in the mixers, the amplifiers or the ADCs, the noise performance of one receiver type might actually get better while the performance of the other receiver type gets worse.

Antennas

To facilitate a theoretical analysis of the receivers, all antennas are assumed to be parallel dipole antennas, because the electric properties of these antennas can be derived mathematically reasonably well. In Chapter 3 the dipole

antenna behaviour will be described as an impedance matrix Z_0 . When the system needs to be modelled with other antennas, this impedance matrix can be replaced by another one that describes these antennas. This matrix can either be derived mathematically or be measured. The only limitations are that the antenna setup can be regarded as a linear time-invariant system and that the antennas by itself are passive.

Signal source

Although many signal sources can be present at the same time, only one will be used in the analysis. When source antennas are sufficiently far apart, they will not influence the signal an other source is sending. In that case the presence of multiple source antennas can be seen as a superposition of multiple cases with one source antenna and the reception of these cases can be added to model the multiple source case. This simplification greatly reduces the mathematical complexity, because the matrices that are used in the equations are not bigger than 3×3 , describing the coupling between one source antenna and one or two antennas in the receiver.

2.4 Receiver circuit

Under the assumption that there is no coupling between the signal paths behind the mixer inputs, the required performance measures of both receiver types can be calculated by only taking into account the signals that enter the mixers. Figures 2.4 and 2.5 show only the parts of the circuit prior to the mixers. The systems are assumed to be balanced, but not necessarily equal in both branches.

The source is modelled as a voltage source U_{Ξ} with an internal impedance Z_{Ξ} which is connected to a dipole antenna.

The n -port (where n equals the number of receiving antennas plus one sending antenna) models the coupling between the antennas. Its parameters depend on the length of the dipole antennas and their mutual position. This will be elaborated in Chapter 3.

The splitter of the one-antenna receiver is modelled as a star-type resistive splitter, consisting of the balanced noisy resistors R_s and a part of $R_{a\psi}$ and $R_{a\phi}$, that are also part of the attenuator.

The attenuator is modelled as an H-type (also known as balanced T-type) resistive attenuator, consisting of all noisy resistors with indices a , b and c .

The load is formed by a resistor that models the input impedance of the mixers. As this load models the mixer input rather than an actual resistor, the load impedances are not modelled with thermal noise, but with a noise process of which the PSD is unknown.

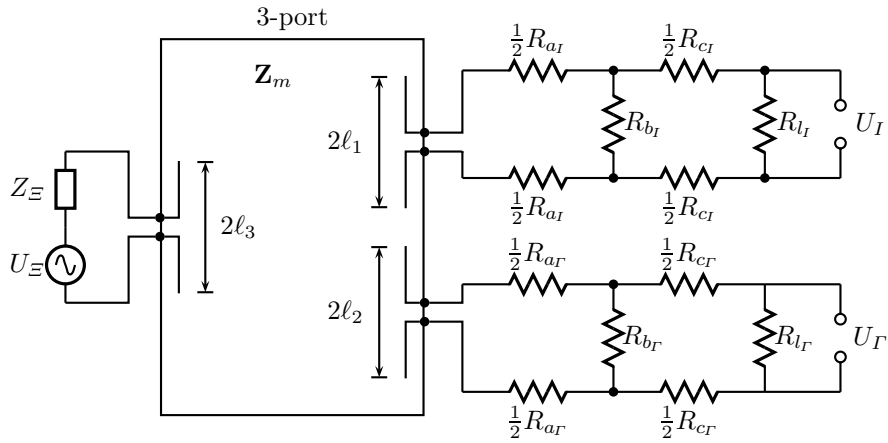


Figure 2.4: Circuit drawing of the two-antenna receiver

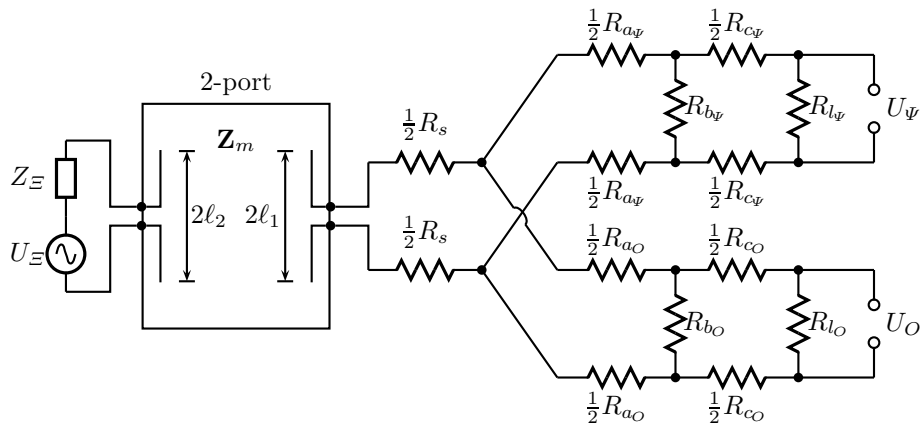


Figure 2.5: Circuit drawing of the one-antenna receiver

Chapter 3

Antenna coupling

3.1 Impedance of a dipole antenna

The description of the behaviour of an antenna starts with a calculation of its impedance. The method used in this section to calculate the impedance of a dipole antenna is known as the induced electromagnetic force (EMF) method. For this method the ohmic losses in the antenna are neglected and the current in the antenna is simplified to a perfect cylindrical surface current. Because of this, currents are considered to be flowing only in the z -direction. As a consequence only the z -component of the electric field is of interest. This reduces the computational complexity at the cost of less accuracy in the result.¹

When the current is only flowing in the longitudinal direction, either side of the dipole antenna can be modelled like a standing wave tube or a string that is attached on one end. At the outer ends of the antenna the current can go no further, so it must be zero. This forces a so called node at these ends in the standing wave tube model, as shown in Figure 3.1. When being driven by a signal consisting of one frequency, the standing wave takes the shape of a sine along both sides of the antenna, the wavelength of which is determined by the wave number $k = 2\pi f c^{-1}$ [15]:

$$I_z(z) = I_m \cdot \sin(k(\ell - |z|)) \quad (3.1)$$

¹These inaccuracies include the effect of non-homogeneous currents at the connections in relatively thick antennas.

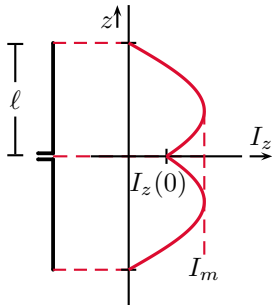


Figure 3.1: Sinusoidal current distribution in a dipole antenna

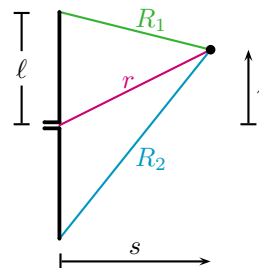


Figure 3.2: Vectors to fieldpoints around a dipole antenna

In this equation I_z is the phasor of the current in the z -direction and I_m is the maximum amplitude of a standing current wave. If we idealize this current as a uniform sheet current along the perimeter of the antenna, the current distribution is approximated by:

$$J_z = \begin{cases} \frac{I_m}{2\pi a} \sin(k(\ell - |z|)) \cdot \delta(s - a) & |z| \leq \ell \\ 0 & |z| > \ell \end{cases} \quad (3.2)$$

In this formula δ is the Dirac delta function, a is the antenna radius, s is the radial coordinate in a cylindrical coordinate system and J_z is the phasor of the z -component of the current distribution. The z -component of the electric field of a finite-length electric dipole, assuming a sinusoidal current distribution as shown in Figure 3.1, is given in [15, p. 408]:

$$E_z = -j \frac{\eta I_m}{4\pi} \left(\frac{\exp(-jkR_1)}{R_1} + \frac{\exp(-jkR_2)}{R_2} - 2 \cos(k\ell) \frac{\exp(-jkr)}{r} \right) \quad (3.3)$$

The parameter η is the impedance of free space ($\approx 120\pi \Omega$). The parameters R_1 , R_2 and r are the lengths of the vectors from the dipole endpoints and midpoint respectively to some field-point. Referring to Figure 3.2:

$$r = \sqrt{s^2 + z^2} \quad (3.4)$$

$$R_1 \triangleq \sqrt{s^2 + (z - \ell)^2} \quad (3.5)$$

$$R_2 \triangleq \sqrt{s^2 + (z + \ell)^2} \quad (3.6)$$

In these formulas s and z refer to the cylindrical coordinates with respect to the dipole. The antenna impedance at its terminals ($z = 0$) is then given by [15–17]:

$$\begin{aligned} Z_0 \triangleq \frac{U(0)}{I_z(0)} &= -\frac{1}{I_z^2(0)} \iiint_{\text{all space}} E_z \cdot J_z \, dV = -\frac{1}{I_z^2(0)} \int_{-\ell}^{\ell} E_z \Big|_{s=a} \cdot I_z \, dz \\ &= \frac{I_m^2}{I_z^2(0)} \int_{-\ell}^{\ell} \frac{j\eta}{4\pi} \left(\frac{e^{-jkR_1}}{R_1} + \frac{e^{-jkR_2}}{R_2} - 2 \cos(k\ell) \frac{e^{-jkr}}{r} \right) \Big|_{s=a} \cdot \sin(k(\ell - |z|)) \, dz \end{aligned} \quad (3.7)$$

The antenna impedance can not only be modelled as an impedance at the terminals, but also as an impedance at some distance from the antenna terminals. As long as the same amount of power is radiated for every possible input current, both ways of modelling will be equivalent. If we choose that distance such that the location at which the impedance is modelled coincides with a maximum of the standing current wave (known as an anti-node), we obtain:

$$\mathcal{P}_{\text{radiated}} = I_z^2(0) \cdot Z_0 = I_m^2 \cdot Z_m = \frac{I_z^2(0)}{\sin^2(k\ell)} \cdot Z_0 \quad (3.8)$$

$$\Rightarrow Z_m \triangleq \sin^2(k\ell) \cdot Z_0 \quad (3.9)$$

The location of the antenna impedance related to the maximum current amplitude Z_m depends on k and thus on the frequency. When the antenna is smaller than a half wavelength, there is not even an anti-node in the antenna, so the physical interpretation of Z_m vanishes, but it can still be calculated, using Equation 3.9 as a definition. The importance of using Z_m instead of Z_0 is of mathematical nature, which will become clear in Section 3.3. Using Equation 3.8 in Equation 3.7 yields:

$$\begin{aligned} \frac{4\pi}{\eta} Z_m &= \frac{4\pi I_z^2(0)}{\eta I_m^2} Z_0 \\ &= \int_{-\ell}^{\ell} j \sin(k(\ell - |z|)) \left(\frac{e^{-jkR_1}}{R_1} + \frac{e^{-jkR_2}}{R_2} - 2 \cos(k\ell) \frac{e^{-jkr}}{r} \right) \Big|_{s=a} dz \end{aligned} \quad (3.10)$$

The derivation of the solution of this integral is shown in Appendix B on Page 87. This solution cannot be expressed in closed form. Instead, the solution can be given in terms of the E_1 -function:

$$E_1(z) \triangleq \int_z^{\infty} \frac{\exp(-w)}{w} dw \quad \Re(z) \geq 0 \quad (3.11)$$

$$E'_1(a, x) \triangleq E_1(jk(\sqrt{a^2 + x^2} + x)) \quad (3.12)$$

$$\begin{aligned} \frac{4\pi}{\eta} Z_m &= -\exp(2jk\ell) \cdot E'_1(a, 2\ell) + (2 \cdot \exp(2jk\ell) + 2) \cdot E'_1(a, \ell) \\ &\quad + (-\exp(2jk\ell) - \exp(-2jk\ell) - 4) \cdot E'_1(a, 0) \\ &\quad + (2 \cdot \exp(-2jk\ell) + 2) \cdot E'_1(a, -\ell) - \exp(-2jk\ell) \cdot E'_1(a, -2\ell) \\ &= 2E'_1(a, \ell) - 4E'_1(a, 0) + 2E'_1(a, -\ell) + \cos(2k\ell) \\ &\quad \cdot \left[-E'_1(a, 2\ell) + 2E'_1(a, \ell) - 2E'_1(a, 0) + 2E'_1(a, -\ell) - E'_1(a, -2\ell) \right] \\ &\quad + j \sin(2k\ell) \cdot \left[-E'_1(a, 2\ell) + 2E'_1(a, \ell) - 2E'_1(a, -\ell) + E'_1(a, -2\ell) \right] \end{aligned} \quad (3.13)$$

As explained in Appendix B, Equation 3.13 can cause large inaccuracies when used in a numerical evaluation. The following approximation can be used when $a \ll \ell$, which is often the case:

$$\begin{aligned} \frac{4\pi}{\eta} Z_m &\approx 2 E_1(2jk\ell) + 2\gamma + j\pi + 2 \ln(2k\ell) \\ &\quad + \cos(2k\ell) \left[-E_1(4jk\ell) + 2 E_1(2jk\ell) + \gamma + \frac{j\pi}{2} + \ln(k\ell) \right] \\ &\quad + j \sin(2k\ell) \left[-E_1(4jk\ell) + 2 E_1(2jk\ell) + \gamma + \frac{j\pi}{2} + \ln\left(\frac{ka^2}{\ell}\right) \right] \end{aligned} \quad (3.14)$$

In these equations γ is the Euler-Mascheroni constant (0.577...). The real and

imaginary part of the impedance related to the current maxima yield:

$$\begin{aligned} \frac{4\pi}{\eta} \Re\{Z_m\} = & 2 \operatorname{Ci}(2k\ell) + 2\gamma + 2 \ln(2k\ell) \\ & + \cos(2k\ell) [-\operatorname{Ci}(4k\ell) + 2 \operatorname{Ci}(2k\ell) + \gamma + \ln(k\ell)] \\ & + \sin(2k\ell) [\operatorname{Si}(4k\ell) - 2 \operatorname{Si}(2k\ell)] \end{aligned} \quad (3.15)$$

$$\begin{aligned} \frac{4\pi}{\eta} \Im\{Z_m\} = & 2 \operatorname{Si}(2k\ell) + \cos(2k\ell) [-\operatorname{Si}(4k\ell) + 2 \operatorname{Si}(2k\ell)] \\ & + \sin(2k\ell) \left[-\operatorname{Ci}(4k\ell) + 2 \operatorname{Ci}(2k\ell) - \operatorname{Ci}\left(\frac{ka^2}{\ell}\right) \right] \end{aligned} \quad (3.16)$$

with:

$$\operatorname{Si}(x) \triangleq \int_0^x \frac{\sin(w)}{w} dw \quad (3.17)$$

$$\operatorname{Ci}(x) \triangleq \int_x^\infty \frac{\cos(w)}{w} dw \quad (3.18)$$

Equations 3.15 and 3.16 are also found in [15], but in that book an alternative definition of the Ci-function is used and the antenna length parameter equals 2ℓ . Using Equation 3.9 the antenna impedance at the terminals Z_0 can be found from the antenna impedance related to the maximum current amplitude Z_m . As these impedances appear to depend mostly on the value $2k\ell$, they can be plotted as a function of this value. This value becomes more easy to interpret after dividing by 2π , after which it can be interpreted as a normalized frequency. The only remaining independent parameter is the antenna radius a . The real and imaginary part and the magnitude of the impedances are shown in Figure 3.3 for $a = \ell/100$. The corresponding phase plot is shown in Figure 3.4. The real part of the antenna impedance is positive at every frequency, because it is a passive device.

3.2 Mutual impedance of two dipole antennas in echelon

When two dipole antennas are placed next to each other, a current in one antenna will cause an electric field around the other antenna, which causes an open terminal voltage across the terminals of the other antenna. The (complex) ratio of the two is defined as the mutual impedance as shown in Equation 3.19. From the Rayleigh-Carson reciprocity theorem, the relation in Equation 3.20 can be derived, provided that the medium between the two antennas is linear, passive and isotropic [15, 16].

$$Z_{0,12} \triangleq -\frac{U_1(0)}{I_{z2}(r_{z2})} \Big|_{I_{z1}(0)=0} \quad (3.19)$$

$$Z_{0,12}(\omega) \equiv Z_{0,21}(\omega) \triangleq -\frac{U_2(r_{z2})}{I_{z1}(0)} \Big|_{I_{z2}(r_{z2})=0} \quad (3.20)$$

The value $I_{z2}(r_{z2})$ is the current at the terminal pair of the second dipole antenna, which is not (necessarily) located at $z=0$. The mutual impedance describes the electric coupling between two ports. In this case these ports

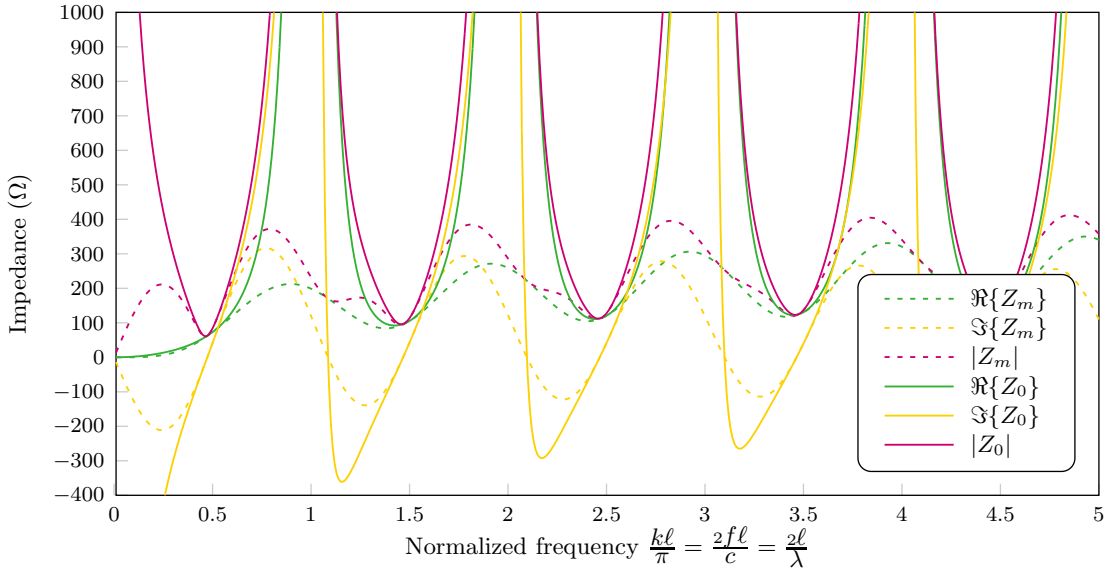


Figure 3.3: Impedance of a dipole antenna with $a = \ell/100$

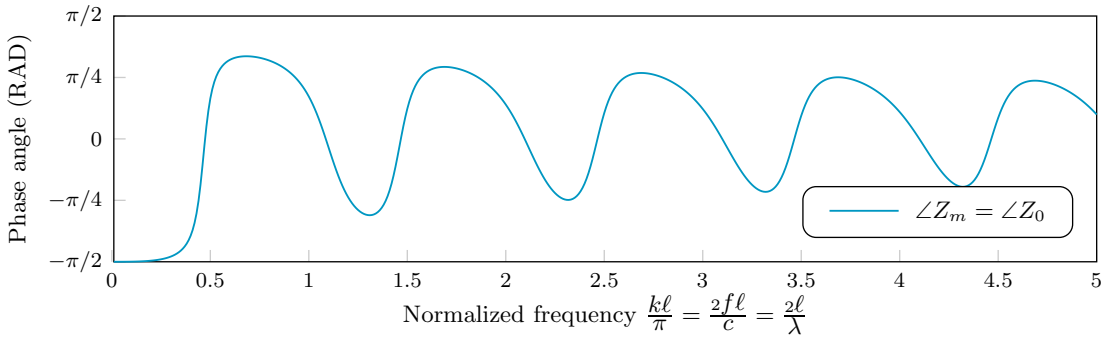


Figure 3.4: Phase angle of the impedance of a dipole antenna with $a = \ell/100$

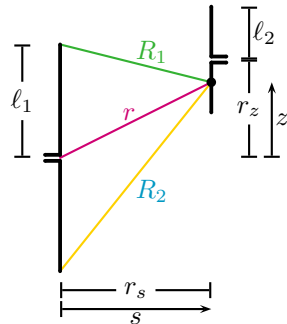


Figure 3.5: Two parallel dipole antennas of arbitrary length in echelon

are the terminal pairs of two dipole antennas. Together with the impedance of both antennas, the electric properties of a linear time-invariant two-port is fully described. This will be shown in Section 3.3. In the current section, the mutual impedance of two dipole antennas that are positioned in echelon (in parallel at any distance, as shown in Figure 3.5) will be modelled. The induced EMF method can be used to calculate their mutual impedance. The electric field of the first dipole antenna is just as in Equation 3.3 and the current in the second dipole antenna can be modelled as a line current parallel to the first dipole antenna. This is a current with an infinitesimal cross section area:

$$E_{z1} = -j \frac{\eta I_{m1}}{4\pi} \left(\frac{\exp(-jkR_1)}{R_1} + \frac{\exp(-jkR_2)}{R_2} - 2 \cos(k\ell) \frac{\exp(-jkr)}{r} \right) \quad (3.21)$$

$$I_{z2}(z) = I_{m2} \cdot \sin(k(\ell_2 - |z - r_z|)) \quad (3.22)$$

$$J_{z2} = \begin{cases} I_{m2} \sin(k(\ell_2 - |z - r_z|)) \cdot \delta(s - r_s) \cdot \delta(\varphi - r_\varphi) & |z - r_z| \leq \ell_2 \\ 0 & |z - r_z| > \ell_2 \end{cases} \quad (3.23)$$

The variables s , z and φ refer to the cylindrical coordinates with respect to the first dipole antenna. The variables r_s , r_z and r_φ refer to the coordinates of the center of the second dipole antenna, as shown in Figure 3.5. The mutual impedance between the antennas is then given by [15, 17, 18]:

$$\begin{aligned} Z_{0,12} &\triangleq \frac{U_1(0)}{I_{z2}(r_z)} = -\frac{1}{I_{z1}(0)I_{z2}(r_z)} \iiint_{\text{all space}} E_{z1} \cdot J_{z2} dV \\ &= -\frac{1}{I_{z1}(0)I_{z2}(r_z)} \int_{r_z - \ell_2}^{r_z + \ell_2} E_{z1} \Big|_{s=r_s} \cdot I_{z2} dz = \frac{I_{m1}I_{m2}}{I_{z1}(0)I_{z2}(r_z)} \cdots \\ &\cdot \int_{r_z - \ell_2}^{r_z + \ell_2} \frac{j\eta}{4\pi} \left(\frac{e^{-jkR_1}}{R_1} + \frac{e^{-jkR_2}}{R_2} - 2 \cos(k\ell_1) \frac{e^{-jkr}}{r} \right) \Big|_{s=r_s} \cdot \sin(k(\ell_2 - |z - r_z|)) dz \end{aligned} \quad (3.24)$$

Noting that according to Equation 3.1 and Equation 3.22

$$\frac{I_{m1}I_{m2}}{I_{z1}(0)I_{z2}(r_z)} = \frac{1}{\sin(k\ell_1) \sin(k\ell_2)} \quad (3.25)$$

it makes sense to define:

$$\begin{aligned} Z_{m12} &\triangleq \sin(k\ell_1) \cdot \sin(k\ell_2) \cdot Z_{0,12} = \\ &\int_{r_z - \ell_2}^{r_z + \ell_2} \frac{j\eta}{4\pi} \left(\frac{e^{-jkR_1}}{R_1} + \frac{e^{-jkR_2}}{R_2} - 2 \cos(k\ell_1) \frac{e^{-jkr}}{r} \right) \Big|_{s=r_s} \cdot \sin(k(\ell_2 - |z - r_z|)) dz \end{aligned} \quad (3.26)$$

This integral can be solved by following the same procedure as is shown for the impedance in Appendix B, but because of the two extra parameters

the equations in both the derivation and the solution will become even longer. In [15] a solution is given that is only valid for dipole antennas for which both ℓ_1 and ℓ_2 are odd multiples of $\lambda/2$. Because we are interested in the wide-band behaviour of the antenna system, these equations do not suffice. A more general equation is given in [18]. A more compact and computationally efficient form of the result of [18] is given below. The real and imaginary part are merged into one complex equation by using the “mapping” between the real and imaginary part provided by King [18] and noting its relation to the exponential integral. Then the geometric factors can be merged into exponential factors, after writing products of geometric factors as a sum. The length of the equation is further reduced by sorting the addition by equal exponential integrals. As a result, the 32 trigonometric factors of King [18] per required Z_{m12} -value are replaced by four, while the 96 trigonometric integrals of King [18] are replaced by eighteen complex exponential integrals.

$$\mathbf{d} \triangleq \begin{bmatrix} 1 & 1 & 1 & 1 & 1 & 1 & 1 & 1 & 1 \\ -1 & -1 & -1 & 0 & 0 & 0 & 1 & 1 & 1 \\ -1 & 0 & 1 & -1 & 0 & 1 & -1 & 0 & 1 \end{bmatrix}^T \cdot \begin{bmatrix} r_z \\ \ell_1 \\ \ell_2 \end{bmatrix} \quad (3.27)$$

$$\mathbf{a}_n^+ \triangleq E_1 \left(jk \left(\sqrt{r_s^2 + \mathbf{d}_n^2} + \mathbf{d}_n \right) \right) \quad \forall n \in \{1, 2, 3, \dots, 9\} \quad (3.28)$$

$$\mathbf{a}_n^- \triangleq E_1 \left(jk \left(\sqrt{r_s^2 + \mathbf{d}_n^2} - \mathbf{d}_n \right) \right) \quad \forall n \in \{1, 2, 3, \dots, 9\} \quad (3.29)$$

$$\mathbf{b} \triangleq \begin{bmatrix} \exp(jk \mathbf{d}_1) \\ \exp(jk \mathbf{d}_3) \\ \exp(jk \mathbf{d}_7) \\ \exp(jk \mathbf{d}_9) \end{bmatrix}^T \cdot \begin{bmatrix} -1 & 1 & 0 & 1 & -1 & 0 & 0 & 0 & 0 \\ 0 & 1 & -1 & 0 & -1 & 1 & 0 & 0 & 0 \\ 0 & 0 & 0 & 1 & -1 & 0 & -1 & 1 & 0 \\ 0 & 0 & 0 & 0 & -1 & 1 & 0 & 1 & -1 \end{bmatrix} \quad (3.30)$$

$$Z_{m12} = \frac{\eta}{8\pi} (\mathbf{a}^+ \cdot \mathbf{b} + \mathbf{a}^- \cdot \bar{\mathbf{b}}) \quad (3.31)$$

In the latter equation a line above a symbol indicates the (element by element) complex conjugate. From this, the mutual impedance related to the antenna terminals can be found using Equation 3.26. The mutual impedance according to this model appears to depend on the lengths of both antennas and their position with respect to each other. In Figure 3.6 some parallel antennas of equal length are shown. The magnitude of the mutual impedance between the black antenna and either of the coloured antennas is shown in Figure 3.8 and its phase angle in Figure 3.9. In Figure 3.7 some antennas of equal length are shown at a constant distance in different directions from each other. The corresponding mutual impedances are shown in Figure 3.10 and in Figure 3.11. In Figure 3.12 and Figure 3.13 the mutual impedances of two parallel antennas of different lengths are shown.

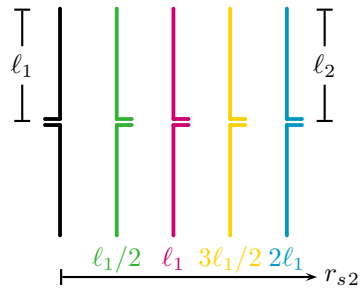


Figure 3.6: Two dipole antennas of equal length in parallel with $r_z = 0$ at different distances

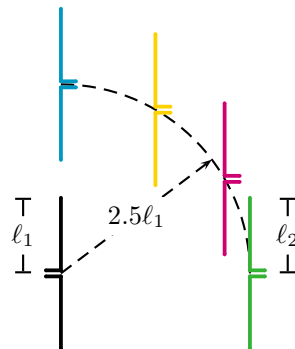


Figure 3.7: Two dipole antennas of equal length in echelon with a distance between its centers of $2.5l$ at different angles

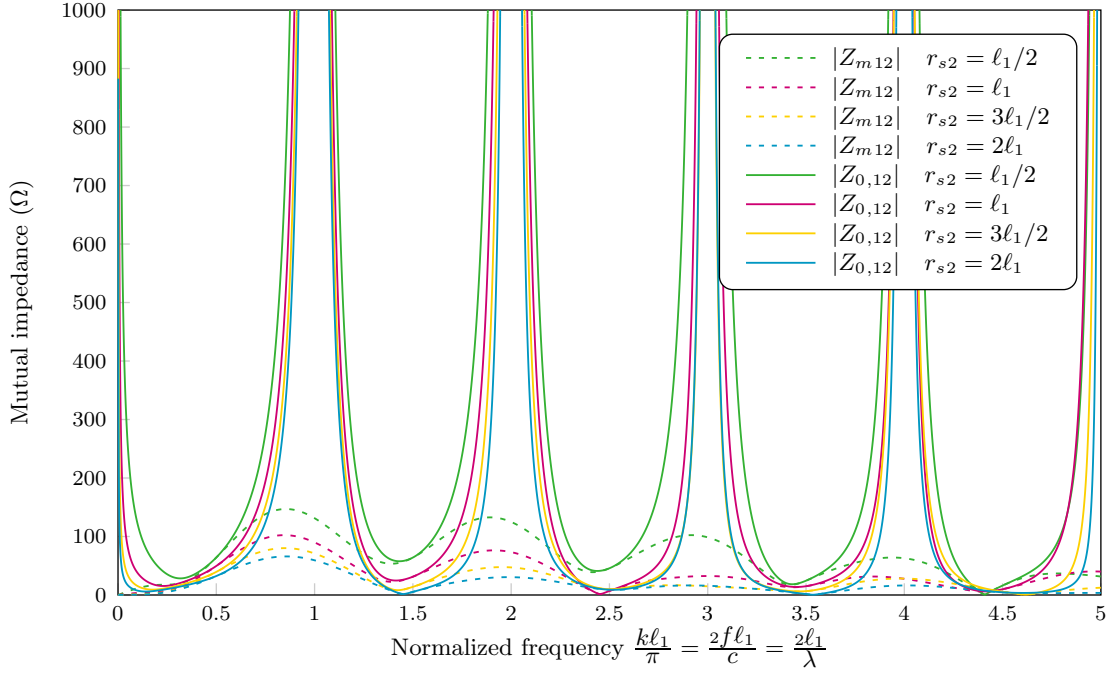


Figure 3.8: Mutual impedance of two dipole antennas of equal length in parallel with $r_{z2} = 0$ at different distances

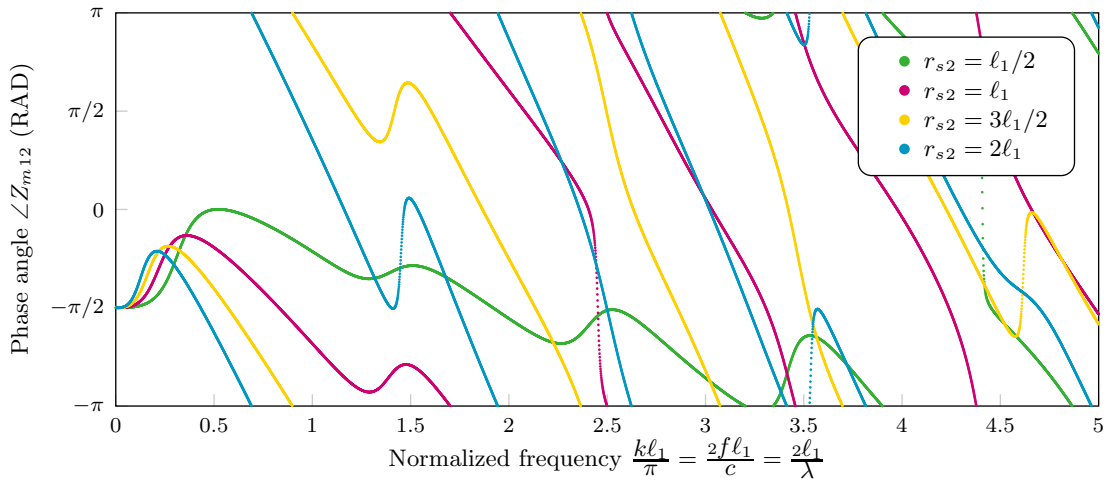


Figure 3.9: Phase angle of the mutual impedance of two dipole antennas of equal length in parallel with $r_{z2} = 0$ at different distances

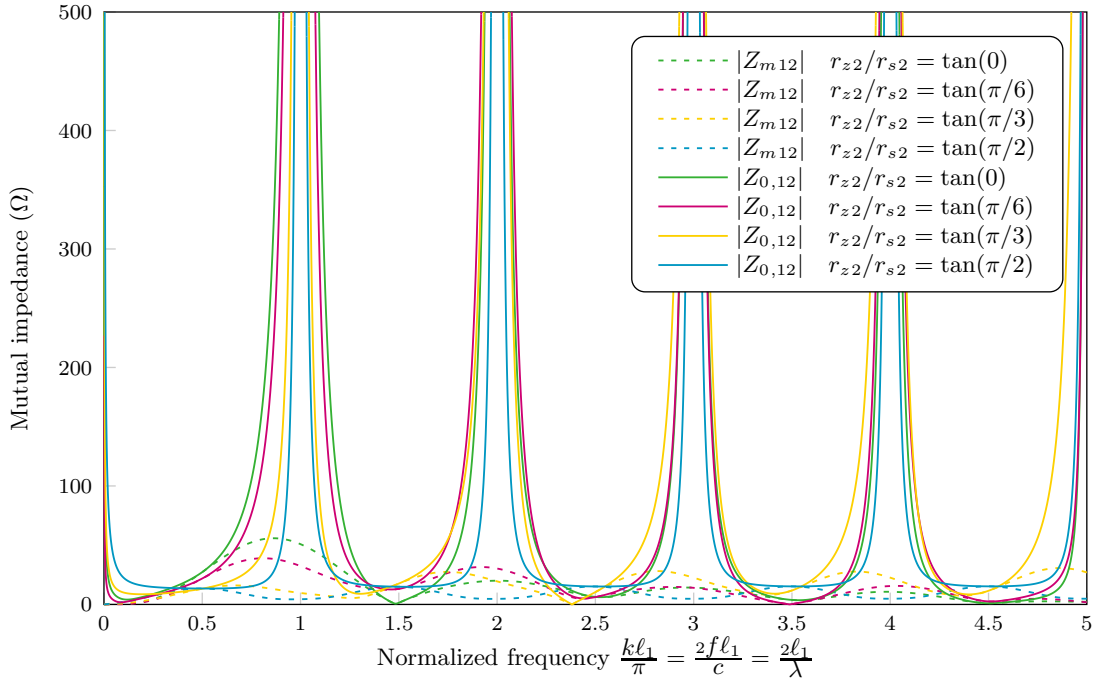


Figure 3.10: Mutual impedance of two dipole antennas of equal length in echelon with a distance between its centers of 2.5ℓ at different angles

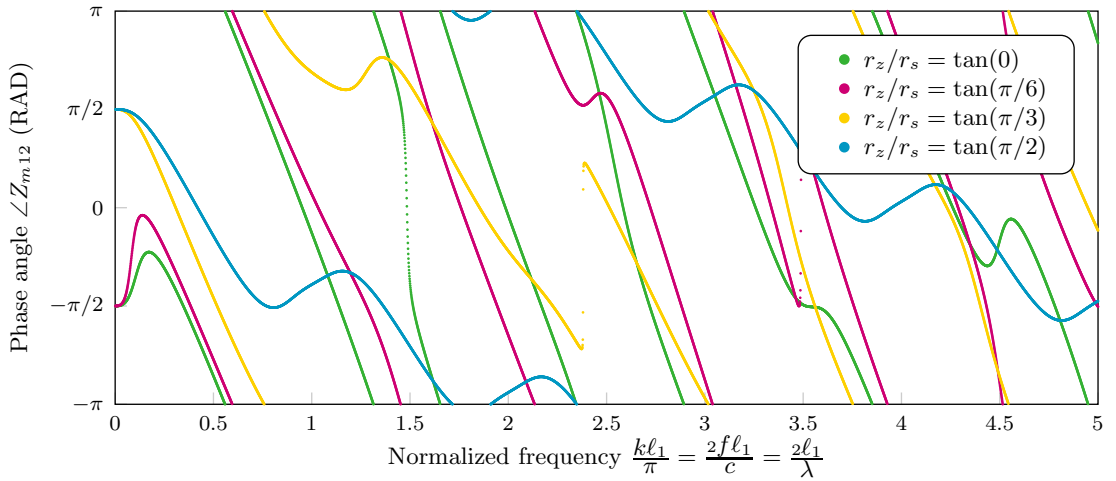


Figure 3.11: Phase angle of the mutual impedance of two dipole antennas of equal length in echelon with a distance between its centers of 2.5ℓ at different angles

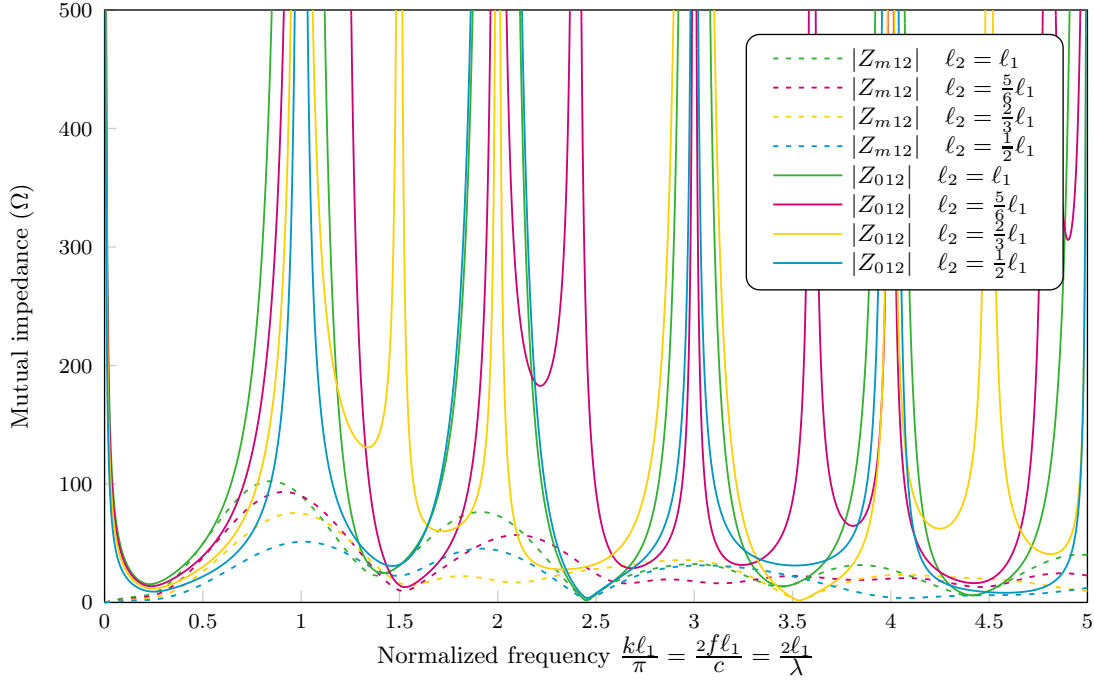


Figure 3.12: Mutual impedance of two dipole antennas of different length in parallel with $r_{s2} = \ell_1$ and $r_{z2} = 0$

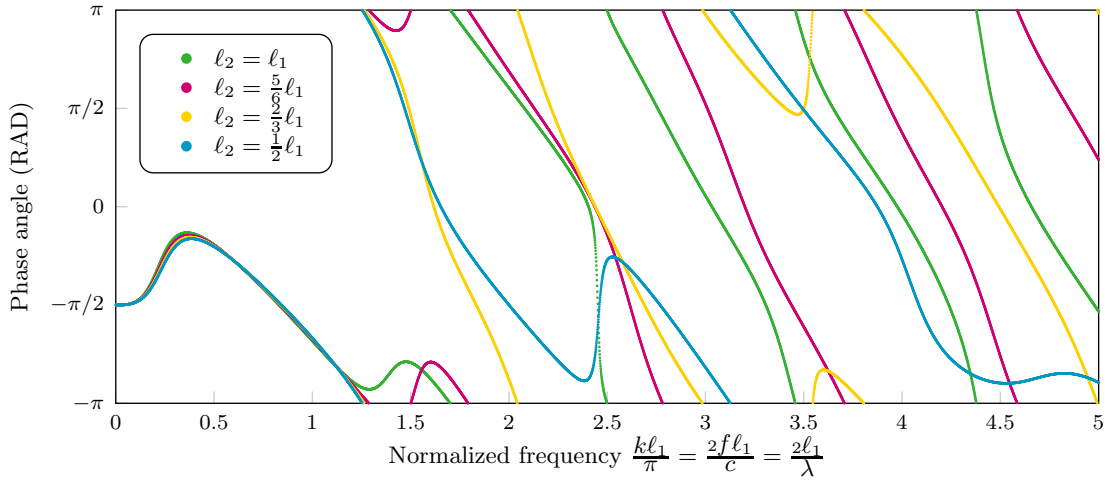


Figure 3.13: Phase angle of the mutual impedance of two dipole antennas of different length in parallel with $r_{s2} = \ell_1$ and $r_{z2} = 0$

3.3 Matrix description of multiple dipole antennas in echelon

The electric behaviour at the ports of a linear time invariant n -port that consists of n dipole antennas in echelon, can be completely described by the n antenna impedances and the $n(n-1)/2$ distinct mutual impedances. This can be compactly written in matrix notation. We define:

$$\mathbf{u} \triangleq \begin{bmatrix} U_1(0) \\ U_2(r_{z2}) \\ \vdots \\ U_n(r_{zn}) \end{bmatrix} \quad \mathbf{i} \triangleq \begin{bmatrix} I_{z1}(0) \\ I_{z2}(r_{z2}) \\ \vdots \\ I_{zn}(r_{zn}) \end{bmatrix} \quad \mathbf{Z}_0 \triangleq \begin{bmatrix} Z_{0,11} & Z_{0,12} & \cdots & Z_{0,1n} \\ Z_{0,21} & Z_{0,22} & \cdots & Z_{0,2n} \\ \vdots & \vdots & \ddots & \vdots \\ Z_{0,n1} & Z_{0,n2} & \cdots & Z_{0,nn} \end{bmatrix}$$

The parameters r_z refer to the location of the antenna terminals. This parameter was necessary to derive the mutual impedances. Normally in an electric circuit model we are not interested in the location of the components, so this parameter can be omitted. In the impedance matrix the diagonal elements $Z_{0,mm}$ are the self impedances of the antennas, while the non-diagonal elements are mutual impedances between pairs of antennas. This matrix is symmetric, which can be concluded from Equation 3.20. According to the definitions of the (mutual) antenna impedance in Equation 3.7 and Equation 3.24:

$$\mathbf{u} = \mathbf{Z}_0 \cdot \mathbf{i} \quad (3.32)$$

We further define:

$$\mathbf{S} \triangleq \begin{bmatrix} \sin(k\ell_1) & 0 & \cdots & 0 \\ 0 & \sin(k\ell_2) & & 0 \\ \vdots & & \ddots & \vdots \\ 0 & 0 & \cdots & \sin(k\ell_n) \end{bmatrix} \quad (3.33)$$

$$\mathbf{Z}_m \triangleq \begin{bmatrix} Z_{m,11} & Z_{m,12} & \cdots & Z_{m,1n} \\ Z_{m,21} & Z_{m,22} & \cdots & Z_{m,2n} \\ \vdots & \vdots & \ddots & \vdots \\ Z_{m,n1} & Z_{m,n2} & \cdots & Z_{m,nn} \end{bmatrix} \quad (3.34)$$

Then the following relation holds, as can be checked using Equation 3.9 and Equation 3.26.

$$\mathbf{Z}_0 = \mathbf{S}^{-1} \cdot \mathbf{Z}_m \cdot \mathbf{S}^{-1} \quad (3.35)$$

When multiple dipole antennas are placed next to each other, a signal can be sent from any antenna to the others. This voltage to voltage transmission can be described as a transfer matrix \mathbf{H} . In this case the ports of the n -port are assumed to be loaded with some load impedance Z_l , as shown in Figure 3.14.

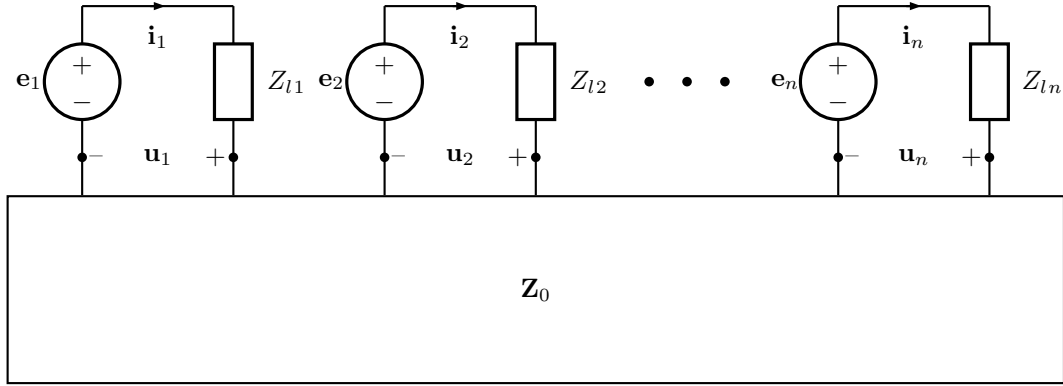


Figure 3.14: An n -port with load impedances

In matrix notation:

$$\mathbf{u} - \mathbf{e} = \mathbf{H} \cdot \mathbf{e} \quad (3.36)$$

$$\mathbf{Z}_l \triangleq \begin{bmatrix} Z_{l1} & 0 & \cdots & 0 \\ 0 & Z_{l2} & & 0 \\ \vdots & & \ddots & \vdots \\ 0 & 0 & \cdots & Z_{ln} \end{bmatrix} \quad (3.37)$$

$$\begin{aligned} \mathbf{u} - \mathbf{e} &= -\mathbf{Z}_l \cdot \mathbf{i} \\ &= -\mathbf{Z}_l \cdot (\mathbf{Z}_0 + \mathbf{Z}_l)^{-1} \cdot \mathbf{e} \\ &= -\mathbf{Z}_l \cdot (\mathbf{S}^{-1} \mathbf{Z}_m \mathbf{S}^{-1} + \mathbf{Z}_l)^{-1} \cdot \mathbf{e} \\ &= -\mathbf{Z}_l \cdot (\mathbf{S}^{-1} (\mathbf{Z}_m + \mathbf{S} \mathbf{Z}_l \mathbf{S}) \mathbf{S}^{-1})^{-1} \cdot \mathbf{e} \\ &= -\mathbf{Z}_l \cdot \mathbf{S} (\mathbf{Z}_m + \mathbf{S} \mathbf{Z}_l \mathbf{S})^{-1} \mathbf{S} \cdot \mathbf{e} \end{aligned} \quad (3.38)$$

$$\Rightarrow \mathbf{H} = -\mathbf{Z}_l \mathbf{S} (\mathbf{Z}_m + \mathbf{S} \mathbf{Z}_l \mathbf{S})^{-1} \mathbf{S} \quad (3.39)$$

In case of a receiver with only one antenna, receiving from only one other antenna, the transmission matrix can be calculated from Equation 3.39 using 2×2 matrices. This results in:

$$\mathbf{H} = \frac{\begin{bmatrix} -Z_{l1} \sin^2(kl_1) (Z_{m22} + Z_{l2} \sin^2(kl_2)) & Z_{m12} Z_{l1} \sin(kl_1) \sin(kl_2) \\ Z_{m21} Z_{l2} \sin(kl_1) \sin(kl_2) & -Z_{l2} \sin^2(kl_2) \cdot (Z_{m11} + Z_{l1} \sin^2(kl_1)) \end{bmatrix}}{(Z_{m11} + Z_{l1} \sin^2(kl_1))(Z_{m22} + Z_{l2} \sin^2(kl_2)) - Z_{m12} Z_{m21}} \quad (3.40)$$

In case $Z_{m12} = Z_{m21}$ is very small compared to the antenna and load impedances, which is the case if the antennas are far apart, it is seen that:

$$\mathbf{H}_{11} \approx \frac{-Z_{l1} \sin^2(kl_1)}{Z_{m11} + Z_{l1} \sin^2(kl_1)} = \frac{-Z_{l1}}{Z_{0,11} + Z_{l1}} \quad (3.41)$$

This is just a voltage divider of the load impedance and the antenna impedance, as could be expected.

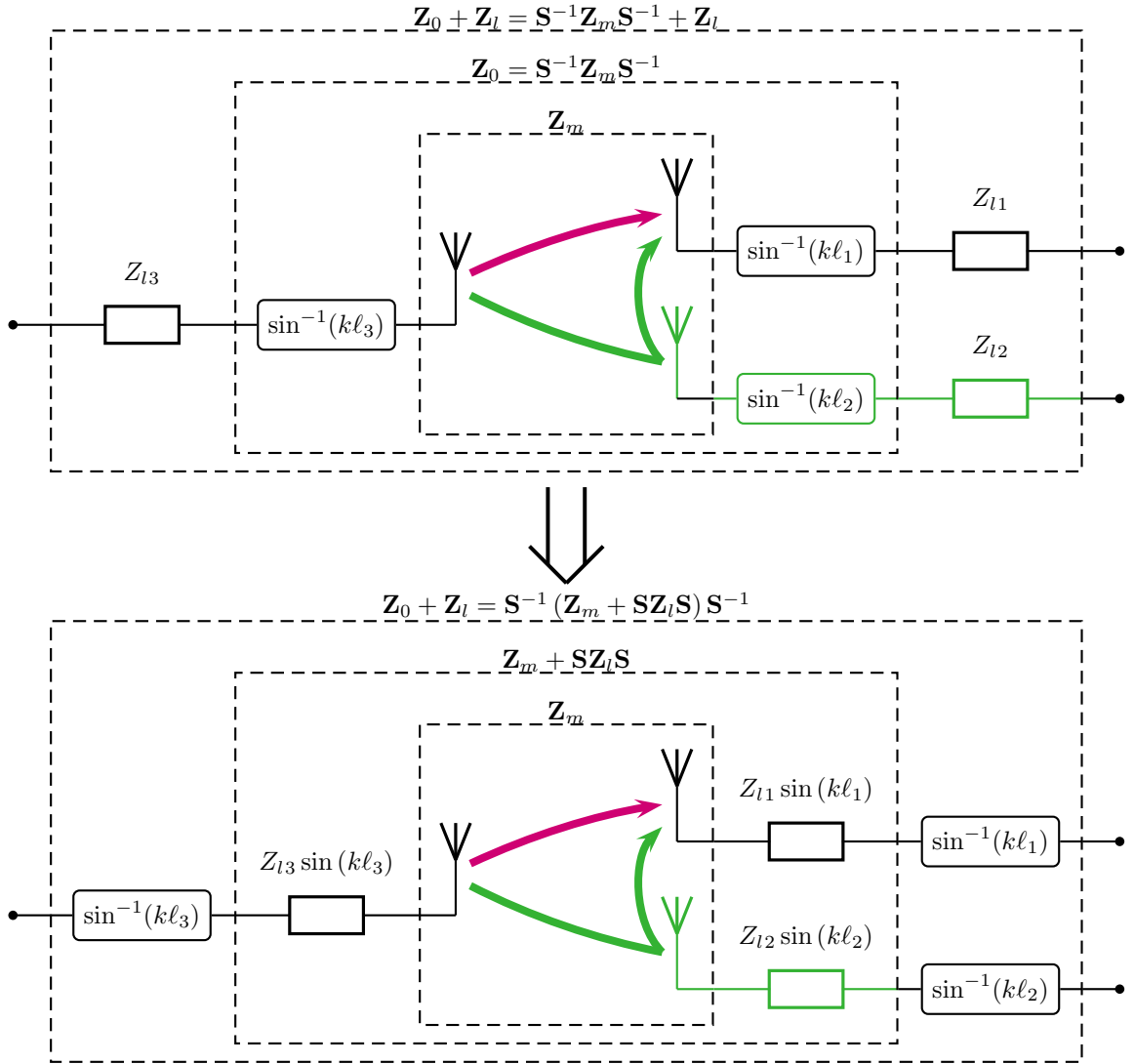


Figure 3.15: Graphical interpretation of Equation 3.38

In Equation 3.41 we see that all occurrences of the load impedances Z_{ln} appear as a multiplication with $\sin(k\ell_n)$, whereas the elements of the matrix \mathbf{Z}_m , where these sine-functions came from, appear solo. To show why this is the case, Figure 3.15 shows two diagrams of the three-antenna case. In the upper diagram the straightforward calculation of \mathbf{H} is shown. Suppose we want to calculate \mathbf{H}_{31} , there are multiple contributing signal paths. The two shortest paths are shown: directly and via a reflection at antenna 2. This reflection depends on the load impedance of antenna 2, Z_{l2} . Suppose furthermore that antenna 2 has a different length than the other two antennas. If we try to calculate \mathbf{H}_{13} at a frequency for which $(k\ell_2)$ is a multiple of π , such that $\sin(k\ell_2) = 0$, we will find that $\mathbf{Z}_{022} \rightarrow \infty$, according to Equation 3.9 on Page 16. As a consequence, if we try to calculate $(\mathbf{S}^{-1}\mathbf{Z}_m\mathbf{S}^{-1} + \mathbf{Z}_l)^{-1}$, we will get a singularity. That is unnecessary, because all the condition “ $\sin(k\ell_2) = 0$ ” says, is that according to Equation 3.1 on Page 15, there is no current flowing at the terminals of antenna 2, which should not prohibit the calculation of the transfer \mathbf{H}_{13} between antenna 1 and antenna 3. In the lower diagram of Figure 3.15 Equation 3.39 is illustrated. The load impedances are transferred to the “reference plain” of \mathbf{Z}_m , whereas in the upper diagram the antenna impedance \mathbf{Z}_m was transferred to the “reference plain” of \mathbf{Z}_0 . If we now try to calculate \mathbf{H}_{13} in case $\sin(k\ell_2) = 0$, we find that the virtual load impedance of antenna 2, $Z_{l2} \sin(k\ell_2)$ is zero. This causes no singularity in the calculation of \mathbf{H}_{13} . Because of the use of these virtual load impedances, the load impedances Z_{ln} appear as a multiplication with $\sin(k\ell_n)$ in Equation 3.41. Hereby it is also shown why using \mathbf{Z}_m in calculations is more favourable than \mathbf{Z}_0 : it prevents unnecessary singularities in the results of these calculations.

The transfer functions between different antennas show that although the mutual impedances between two antennas are generally equal ($Z_{m12} = Z_{m21}$) for any antenna positioning and size, the corresponding transfer functions are only equal if and only if the load impedances are equal:

$$Z_{l1} \equiv Z_{l2} \iff H_{12} \equiv H_{21} \tag{3.42}$$

Some examples of transfer functions are shown in graphs. In Figure 3.16 the transfer function of two dipole antennas of equal length with aligned axes is shown where the load impedances are altered. The phase plot of this transfer function is shown in Figure 3.17. It can be seen that a higher load impedance yields wider lobes in the magnitude of the transfer function and a less steep phase curve. In Figure 3.16 the magnitude transfer function between two parallel antennas of equal length with a quite large range of distances is shown, where both have a 50Ω load impedance. It is seen that a ten times bigger distance yields about 20 dB of attenuation. As the energy at a ten times larger distance spreads over a 100 times larger surface, the attenuation in decibels yields $10 \log(1/100) = -20\text{dB}$. However, at short distances this appears not to be valid: The shape of the curve is less regular. This shows it is difficult to show representative graphs about the near field antenna coupling, as the curve shapes vary greatly within a short distance. The phase plot corresponding to this magnitude plot is not shown, because this plot becomes too steep to read at the larger distances.

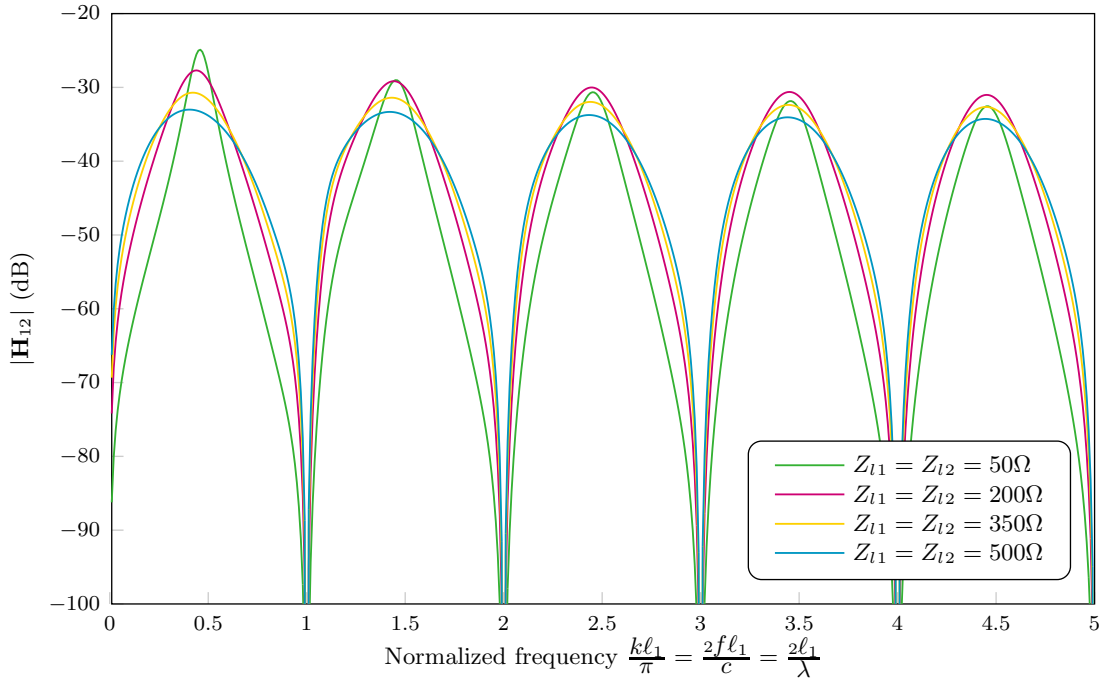


Figure 3.16: Magnitude of the transfer function of two dipole antennas of equal length with different ohmic loads, with $a_1 = a_2 = \ell_1/100$, $r_{s2} = 0$ and $r_{z2} = 2.5\ell_1$

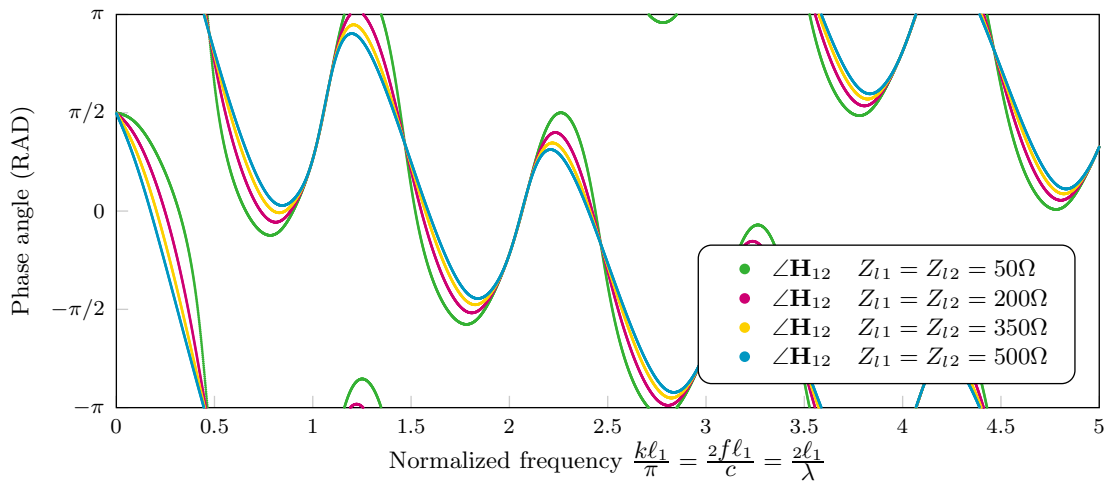


Figure 3.17: Phase angle of the transfer function of two dipole antennas of equal length with different ohmic loads, with $a_1 = a_2 = \ell_1/100$, $r_{s2} = 0$ and $r_{z2} = 2.5\ell_1$

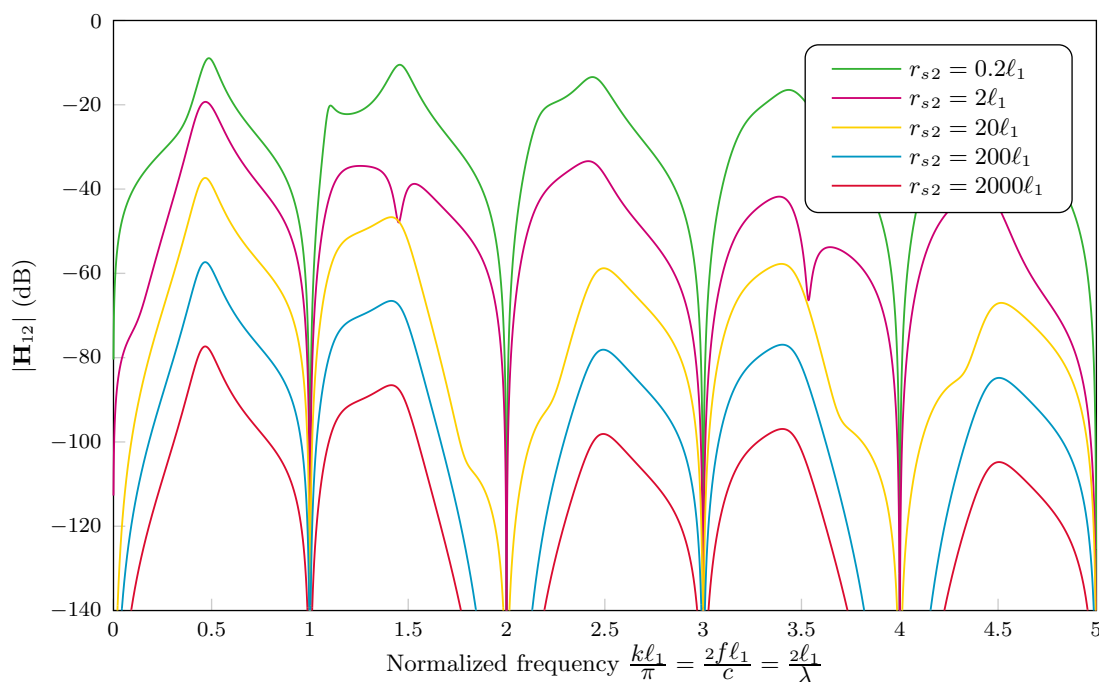


Figure 3.18: Magnitude of the transfer function of two parallel dipole antennas of equal length at different distances, with $a_1 = a_2 = \ell_1/100$, $Z_{l1} = Z_{l2} = 50\Omega$ and $r_{z2} = 0$

3.4 Optimal load impedance of coupled antennas

By matching the input impedances of the receiver circuit to the antenna, the transfer of signals between the antenna and the circuit can be optimized. There are two kinds of impedance matching: Choosing the input impedance equal to the antenna impedance ($Z_l = Z_0$) yields no reflections at the connection between the antenna and the circuit. Choosing the input impedance equal to the complex conjugate of the antenna impedance ($Z_l = \overline{Z_0}$) yields a maximum power transfer from the antenna to the circuit.

When two dipole antennas are put close to each other, their radiation impedance is altered. Consequently both types of optimal matching impedances, are altered as well. In this section these impedances are calculated. These values will not be practically achievable, nor will they be accurate in practice due to other objects surrounding the antennas, but it is meant to give a rough idea of the influence of a close antenna spacing to the radiation impedance.

Reflection-free matching

In case of one dipole antenna, the optimal matching impedance to prevent reflection equals the dipole impedance related to its terminals. In case of two coupled dipole antennas, the optimal matching impedance for each antenna equals the equivalent impedance at the antenna terminals. This depends on all

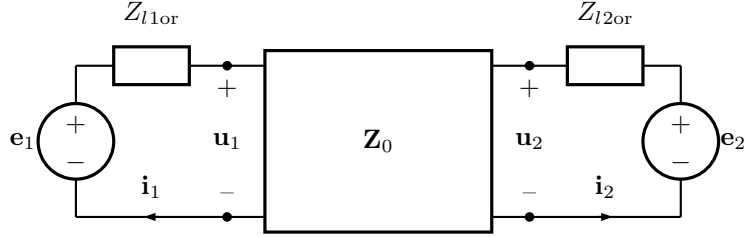


Figure 3.19: Two-port with optimal load impedances

parameters of the respective impedance matrix as well as the load impedance of the other dipole antenna. The optimal matching impedances for a reflection-free connection are found as:

$$\begin{cases} Z_{l1or} = \frac{\mathbf{u}_1}{\mathbf{i}_1} \Big|_{e_2=0} \\ Z_{l2or} = \frac{\mathbf{u}_2}{\mathbf{i}_2} \Big|_{e_1=0} \end{cases} \quad (3.43)$$

The corresponding circuit is shown in Figure 3.19. The calculation below is valid in case both dipole antennas have their optimal load impedance. Applying these optimal load impedances ensures that there are no reflections, but does not say anything about the mutual coupling.

$$\begin{cases} \begin{bmatrix} \mathbf{u}_1 \\ \mathbf{u}_2 \end{bmatrix}_{e_2=0} = \begin{bmatrix} \mathbf{u}_1 \\ -\mathbf{i}_2 Z_{l2or} \end{bmatrix} = \begin{bmatrix} Z_{0,11} & Z_{0,12} \\ Z_{0,21} & Z_{0,22} \end{bmatrix} \cdot \begin{bmatrix} \mathbf{i}_1 \\ \mathbf{i}_2 \end{bmatrix} \\ \begin{bmatrix} \mathbf{u}_1 \\ \mathbf{u}_2 \end{bmatrix}_{e_1=0} = \begin{bmatrix} -\mathbf{i}_1 Z_{l1or} \\ \mathbf{u}_2 \end{bmatrix} = \begin{bmatrix} Z_{0,11} & Z_{0,12} \\ Z_{0,21} & Z_{0,22} \end{bmatrix} \cdot \begin{bmatrix} \mathbf{i}_1 \\ \mathbf{i}_2 \end{bmatrix} \end{cases} \quad (3.44)$$

$$\Rightarrow \begin{cases} \begin{bmatrix} \mathbf{u}_1 \\ 0 \end{bmatrix} = \begin{bmatrix} Z_{0,11} & Z_{0,12} \\ Z_{0,21} & Z_{0,22} + Z_{l2or} \end{bmatrix} \cdot \begin{bmatrix} \mathbf{i}_1 \\ \mathbf{i}_2 \end{bmatrix} \\ \begin{bmatrix} 0 \\ \mathbf{u}_2 \end{bmatrix} = \begin{bmatrix} Z_{0,11} + Z_{l1or} & Z_{0,12} \\ Z_{0,21} & Z_{0,22} \end{bmatrix} \cdot \begin{bmatrix} \mathbf{i}_1 \\ \mathbf{i}_2 \end{bmatrix} \end{cases} \quad (3.45)$$

$$\Rightarrow \begin{cases} \begin{bmatrix} \mathbf{i}_1 \\ \mathbf{i}_2 \end{bmatrix} = \begin{bmatrix} Z_{0,11} & Z_{0,12} \\ Z_{0,21} & Z_{0,22} + Z_{l2or} \end{bmatrix}^{-1} \cdot \begin{bmatrix} \mathbf{u}_1 \\ 0 \end{bmatrix} \\ \begin{bmatrix} \mathbf{i}_1 \\ \mathbf{i}_2 \end{bmatrix} = \begin{bmatrix} Z_{0,11} + Z_{l1or} & Z_{0,12} \\ Z_{0,21} & Z_{0,22} \end{bmatrix}^{-1} \cdot \begin{bmatrix} 0 \\ \mathbf{u}_2 \end{bmatrix} \end{cases} \quad (3.46)$$

Using Equation 3.43:

$$\Rightarrow \begin{cases} Z_{l1or}^{-1} = \left(\begin{bmatrix} Z_{0,11} & Z_{0,12} \\ Z_{0,21} & Z_{0,22} + Z_{l2or} \end{bmatrix}^{-1} \right)_{11} = \frac{\mathbf{M}_{or,11}}{\begin{vmatrix} Z_{0,11} & Z_{0,12} \\ Z_{0,21} & Z_{0,22} + Z_{l2or} \end{vmatrix}} \\ Z_{l2or}^{-1} = \left(\begin{bmatrix} Z_{0,11} + Z_{l1or} & Z_{0,12} \\ Z_{0,21} & Z_{0,22} \end{bmatrix}^{-1} \right)_{22} = \frac{\mathbf{M}_{or,22}}{\begin{vmatrix} Z_{0,11} + Z_{l1or} & Z_{0,12} \\ Z_{0,21} & Z_{0,22} \end{vmatrix}} \end{cases} \quad (3.47)$$

Here, \mathbf{M}_{or} is the minor matrix of $(\mathbf{Z}_0 + \mathbf{Z}_{lor})$.

$$\Rightarrow \begin{cases} Z_{l1or} = \frac{\begin{vmatrix} Z_{0,11} + Z_{l1or} & Z_{0,12} \\ Z_{0,21} & Z_{0,22} + Z_{l2or} \end{vmatrix} - Z_{l1or} \cdot \mathbf{M}_{or,11}}{\mathbf{M}_{or,11}} \\ Z_{l2or} = \frac{\begin{vmatrix} Z_{0,11} + Z_{l1or} & Z_{0,12} \\ Z_{0,21} & Z_{0,22} + Z_{l2or} \end{vmatrix} - Z_{l2or} \cdot \mathbf{M}_{or,22}}{\mathbf{M}_{or,22}} \end{cases} \quad (3.48)$$

$$\Rightarrow \begin{cases} Z_{l1or} = \frac{\begin{vmatrix} Z_{0,11} + Z_{l1or} & Z_{0,12} \\ Z_{0,21} & Z_{0,22} + Z_{l2or} \end{vmatrix}}{2\mathbf{M}_{or,11}} \\ Z_{l2or} = \frac{\begin{vmatrix} Z_{0,11} + Z_{l1or} & Z_{0,12} \\ Z_{0,21} & Z_{0,22} + Z_{l2or} \end{vmatrix}}{2\mathbf{M}_{or,22}} \end{cases} \quad (3.49)$$

The equations up until Equation 3.49 can be generalized for receivers with three or more antennas, but the further derivation will be quite lengthy. In the present case of two antennas we obtain:

$$\Rightarrow \begin{cases} 2Z_{l1or}(Z_{0,22} + Z_{l2or}) = (Z_{0,11} + Z_{l1or})(Z_{0,22} + Z_{l2or}) - Z_{0,12}Z_{0,21} \\ 2Z_{l2or}(Z_{0,11} + Z_{l1or}) = (Z_{0,11} + Z_{l1or})(Z_{0,22} + Z_{l2or}) - Z_{0,12}Z_{0,21} \end{cases} \quad (3.50)$$

$$\Rightarrow \begin{cases} Z_{0,12}Z_{0,21} = Z_{0,11}Z_{0,22} - Z_{l1or}Z_{l2or} \\ Z_{0,11}Z_{l1or} = Z_{0,22}Z_{l2or} \end{cases} \quad (3.51)$$

$$\Rightarrow \begin{cases} Z_{l1or}^2 = Z_{0,11}^2 - Z_{0,11} \frac{Z_{0,12}Z_{0,21}}{Z_{0,22}} = \sin^{-4}(k\ell_1) \left(Z_{m11}^2 - Z_{m11} \frac{Z_{m12}Z_{m21}}{Z_{m22}} \right) \\ Z_{l2or}^2 = Z_{0,22}^2 - Z_{0,22} \frac{Z_{0,12}Z_{0,21}}{Z_{0,11}} = \sin^{-4}(k\ell_2) \left(Z_{m22}^2 - Z_{m22} \frac{Z_{m12}Z_{m21}}{Z_{m11}} \right) \end{cases} \quad (3.52)$$

As could be expected, the optimal matching impedance is about equal to the antenna impedance, but with a correction that depends on the coupling with the other antenna and the impedance of the other antenna.

Conjugate matching

In case of one dipole antenna, the matching impedance for optimal power transfer equals the complex conjugate of the dipole impedance related to its termi-

nals. In case of two coupled dipole antennas, the optimal matching impedance for each antenna equals the complex conjugate of the equivalent impedance at the antenna terminals. The optimal matching impedances for maximum power transfer are found as:

$$\begin{cases} \overline{Z_{l1op}} = \frac{\mathbf{u}_1}{\mathbf{i}_1} \Big|_{\mathbf{e}_2=0} \\ \overline{Z_{l2op}} = \frac{\mathbf{u}_2}{\mathbf{i}_2} \Big|_{\mathbf{e}_1=0} \end{cases} \quad (3.53)$$

The first part of the calculation is similar to the case of reflection-free matching. Equation 3.54 can be derived just like Equation 3.47.

$$\begin{cases} \overline{Z_{l1op}^{-1}} = \left(\begin{bmatrix} Z_{0,11} & Z_{0,12} \\ Z_{0,21} & Z_{0,22} + Z_{l2op} \end{bmatrix}^{-1} \right)_{11} = \frac{\mathbf{M}_{op,11}}{\begin{vmatrix} Z_{0,11} & Z_{0,12} \\ Z_{0,21} & Z_{0,22} + Z_{l2op} \end{vmatrix}} \\ \overline{Z_{l2op}^{-1}} = \left(\begin{bmatrix} Z_{0,11} + Z_{l1op} & Z_{0,12} \\ Z_{0,21} & Z_{0,22} \end{bmatrix}^{-1} \right)_{22} = \frac{\mathbf{M}_{op,22}}{\begin{vmatrix} Z_{0,11} + Z_{l1op} & Z_{0,12} \\ Z_{0,21} & Z_{0,22} \end{vmatrix}} \end{cases} \quad (3.54)$$

Here, \mathbf{M}_{op} is the minor matrix of $(\mathbf{Z}_0 + \mathbf{Z}_{lop})$.

$$\Rightarrow \begin{cases} \overline{Z_{l1op}} = \frac{\begin{vmatrix} Z_{0,11} + Z_{l1op} & Z_{0,12} \\ Z_{0,21} & Z_{0,22} + Z_{l2op} \end{vmatrix} - Z_{l1op} \cdot \mathbf{M}_{op,11}}{\mathbf{M}_{op,11}} \\ \overline{Z_{l2op}} = \frac{\begin{vmatrix} Z_{0,11} + Z_{l1op} & Z_{0,12} \\ Z_{0,21} & Z_{0,22} + Z_{l2op} \end{vmatrix} - Z_{l2op} \cdot \mathbf{M}_{op,22}}{\mathbf{M}_{op,22}} \end{cases} \quad (3.55)$$

$$\Rightarrow \begin{cases} (Z_{l1op} + \overline{Z_{l1op}})(Z_{0,22} + Z_{l2op}) = (Z_{0,11} + Z_{l1op})(Z_{0,22} + Z_{l2op}) - Z_{0,12}Z_{0,21} \\ (Z_{l2op} + \overline{Z_{l2op}})(Z_{0,11} + Z_{l1op}) = (Z_{0,11} + Z_{l1op})(Z_{0,22} + Z_{l2op}) - Z_{0,12}Z_{0,21} \end{cases} \quad (3.56)$$

$$\Rightarrow \begin{cases} Z_{l1op} + \overline{Z_{l1op}} = Z_{0,11} + Z_{l1op} - \frac{Z_{0,12}Z_{0,21}}{Z_{0,22} + Z_{l2op}} \\ Z_{l2op} + \overline{Z_{l2op}} = Z_{0,22} + Z_{l2op} - \frac{Z_{0,12}Z_{0,21}}{Z_{0,11} + Z_{l1op}} \end{cases} \quad (3.57)$$

$$\Rightarrow \begin{cases} \overline{Z_{l1op}} - Z_{0,11} + \frac{Z_{0,12}Z_{0,21}}{2\Re\{Z_{0,22}\} - \frac{\overline{Z_{0,12}Z_{0,21}}}{Z_{0,11} + Z_{l1op}}} = 0 \\ \overline{Z_{l2op}} - Z_{0,22} + \frac{Z_{0,12}Z_{0,21}}{2\Re\{Z_{0,11}\} - \frac{\overline{Z_{0,12}Z_{0,21}}}{Z_{0,22} + Z_{l2op}}} = 0 \end{cases} \quad (3.58)$$

If we take the complex conjugate and multiply by $(2\Re\{Z_{0,22}\})(Z_{0,11} + Z_{l1op}) -$

$Z_{0,12}Z_{0,21}$) or $(2\Re\{Z_{0,11}\}(Z_{0,22} + Z_{l_{2op}}) - Z_{0,12}Z_{0,21})$ respectively, we obtain:

$$\Rightarrow \begin{cases} 2\Re\{Z_{0,22}\}Z_{l_{1op}}^2 + 2\Re\{Z_{0,22}\}Z_{0,11}Z_{l_{1op}} - 2\Re\{Z_{0,22}\}\overline{Z_{0,11}}Z_{l_{1op}} \\ - Z_{0,12}Z_{0,21}Z_{l_{1op}} + \overline{Z_{0,12}}Z_{0,21}Z_{l_{1op}} + \overline{Z_{0,11}}Z_{0,12}Z_{0,21} \\ + Z_{0,11}\overline{Z_{0,12}}Z_{0,21} - 2\Re\{Z_{0,22}\}Z_{0,11}\overline{Z_{0,11}} = 0 \\ 2\Re\{Z_{0,11}\}Z_{l_{2op}}^2 + 2\Re\{Z_{0,11}\}Z_{0,22}Z_{l_{2op}} - 2\Re\{Z_{0,11}\}\overline{Z_{0,22}}Z_{l_{2op}} \\ - Z_{0,12}Z_{0,21}Z_{l_{2op}} + \overline{Z_{0,12}}Z_{0,21}Z_{l_{2op}} + \overline{Z_{0,22}}Z_{0,12}Z_{0,21} \\ + Z_{0,22}\overline{Z_{0,12}}Z_{0,21} - 2\Re\{Z_{0,11}\}Z_{0,22}\overline{Z_{0,22}} = 0 \end{cases} \quad (3.59)$$

Dividing by $2\Re\{Z_{0,22}\}$ and $2\Re\{Z_{0,11}\}$ respectively and collecting conjugate pairs, yields:

$$\Rightarrow \begin{cases} Z_{l_{1op}}^2 + \left(2\Im\{Z_{0,11}\} - \frac{\Im\{Z_{0,12}Z_{0,21}\}}{\Re\{Z_{0,22}\}}\right)jZ_{l_{1op}} \\ + \left(\frac{\Re\{\overline{Z_{0,11}}Z_{0,12}Z_{0,21}\}}{\Re\{Z_{0,22}\}} - |Z_{0,11}|^2\right) = 0 \\ Z_{l_{2op}}^2 + \left(2\Im\{Z_{0,22}\} - \frac{\Im\{Z_{0,12}Z_{0,21}\}}{\Re\{Z_{0,11}\}}\right)jZ_{l_{2op}} \\ + \left(\frac{\Re\{\overline{Z_{0,22}}Z_{0,12}Z_{0,21}\}}{\Re\{Z_{0,11}\}} - |Z_{0,22}|^2\right) = 0 \end{cases} \quad (3.60)$$

From these quadratic equations $Z_{l_{1op}}$ and $Z_{l_{2op}}$ can be solved. Using Equation 3.61 to Equation 3.64, the result can be written as shown in Equation 3.65 or as shown in Equation 3.66.

$$\Re\{\overline{Z_{0,11}}Z_{0,12}Z_{0,21}\} \equiv \Re\{Z_{0,11}\}\Re\{Z_{0,12}Z_{0,21}\} + \Im\{Z_{0,11}\}\Im\{Z_{0,12}Z_{0,21}\} \quad (3.61)$$

$$\Re\{\overline{Z_{0,22}}Z_{0,12}Z_{0,21}\} \equiv \Re\{Z_{0,22}\}\Re\{Z_{0,12}Z_{0,21}\} + \Im\{Z_{0,22}\}\Im\{Z_{0,12}Z_{0,21}\} \quad (3.62)$$

$$|Z_{0,11}|^2 - (\Im\{Z_{0,11}\})^2 \equiv (\Re\{Z_{0,11}\})^2 \quad (3.63)$$

$$|Z_{0,22}|^2 - (\Im\{Z_{0,22}\})^2 \equiv (\Re\{Z_{0,22}\})^2 \quad (3.64)$$

$$\Rightarrow \left\{ \begin{array}{l} Z_{l1\text{op}} = \sqrt{(\Re\{Z_{0,11}\})^2 - \frac{\Re\{Z_{0,11}\}\Re\{Z_{0,12}Z_{0,21}\}}{\Re\{Z_{0,22}\}} - \left(\frac{\Im\{Z_{0,12}Z_{0,21}\}}{2\Re\{Z_{0,22}\}}\right)^2} \\ + \left(\frac{\Im\{Z_{0,12}Z_{0,21}\}}{2\Re\{Z_{0,22}\}} - \Im\{Z_{0,11}\}\right)j \\ \\ Z_{l2\text{op}} = \sqrt{(\Re\{Z_{0,22}\})^2 - \frac{\Re\{Z_{0,22}\}\Re\{Z_{0,12}Z_{0,21}\}}{\Re\{Z_{0,11}\}} - \left(\frac{\Im\{Z_{0,12}Z_{0,21}\}}{2\Re\{Z_{0,11}\}}\right)^2} \\ + \left(\frac{\Im\{Z_{0,12}Z_{0,21}\}}{2\Re\{Z_{0,11}\}} - \Im\{Z_{0,22}\}\right)j \end{array} \right. \quad (3.65)$$

$$\Rightarrow \left\{ \begin{array}{l} Z_{l1\text{op}} = \left(\sqrt{(\Re\{Z_{m11}\})^2 - \frac{\Re\{Z_{m11}\}\Re\{Z_{m12}Z_{m21}\}}{\Re\{Z_{m22}\}} - \left(\frac{\Im\{Z_{m12}Z_{m21}\}}{2\Re\{Z_{m22}\}}\right)^2} \right. \\ \left. + \left(\frac{\Im\{Z_{m12}Z_{m21}\}}{2\Re\{Z_{m22}\}} - \Im\{Z_{m11}\}\right)j \right) \cdot \sin^{-2}(k\ell_1) \\ \\ Z_{l2\text{op}} = \left(\sqrt{(\Re\{Z_{m22}\})^2 - \frac{\Re\{Z_{m22}\}\Re\{Z_{m12}Z_{m21}\}}{\Re\{Z_{m11}\}} - \left(\frac{\Im\{Z_{m12}Z_{m21}\}}{2\Re\{Z_{m11}\}}\right)^2} \right. \\ \left. + \left(\frac{\Im\{Z_{m12}Z_{m21}\}}{2\Re\{Z_{m11}\}} - \Im\{Z_{m22}\}\right)j \right) \cdot \sin^{-2}(k\ell_2) \end{array} \right. \quad (3.66)$$

We can verify that in case the mutual impedances are zero, which is nearly the case if the antennas are far apart, the conjugate matching impedances are equal to the complex conjugate of the antenna impedances:

$$\lim_{Z_{m,12} \rightarrow 0} Z_{l1\text{op}} = \Re\{Z_{0,11}\} - \Im\{Z_{0,11}\} = \overline{Z_{0,11}} \quad (3.67)$$

$$\lim_{Z_{m,12} \rightarrow 0} Z_{l2\text{op}} = \Re\{Z_{0,22}\} - \Im\{Z_{0,22}\} = \overline{Z_{0,22}} \quad (3.68)$$

Plots

In Figure 3.20 and Figure 3.21 the optimal impedance for reflection-free matching is compared to the antenna impedance. In Figure 3.22 and Figure 3.23 the optimal conjugate matched impedance is compared to the complex conjugate of the antenna impedance. In both cases it is seen that only if the second antenna is really close, the optimal matching impedances differ significantly from the antenna impedance or its complex conjugate respectively. In Figure 3.24 the transfer between parallel antennas is compared in case they are both connected to a 50Ω impedance, to their optimal matching impedance for reflection-free matching or to their complex conjugate matched impedances. In the both matching cases the zeros at integer values of the normalized frequency disappear, but the transfers are still far from flat. As expected the complex matched designs yield the highest transfer. Especially the lower frequencies in the complex conjugate matching case stand out, as the transfer is larger than 0 dB. Looking at figure Figure 3.21 and Figure 3.23, we see that in this frequency region the antenna impedance is nearly pure inductive, so its complex conjugate match is nearly pure capacitive. Consequently, the antenna and the complex conjugate matched load form a resonator. Resonance in the receiver

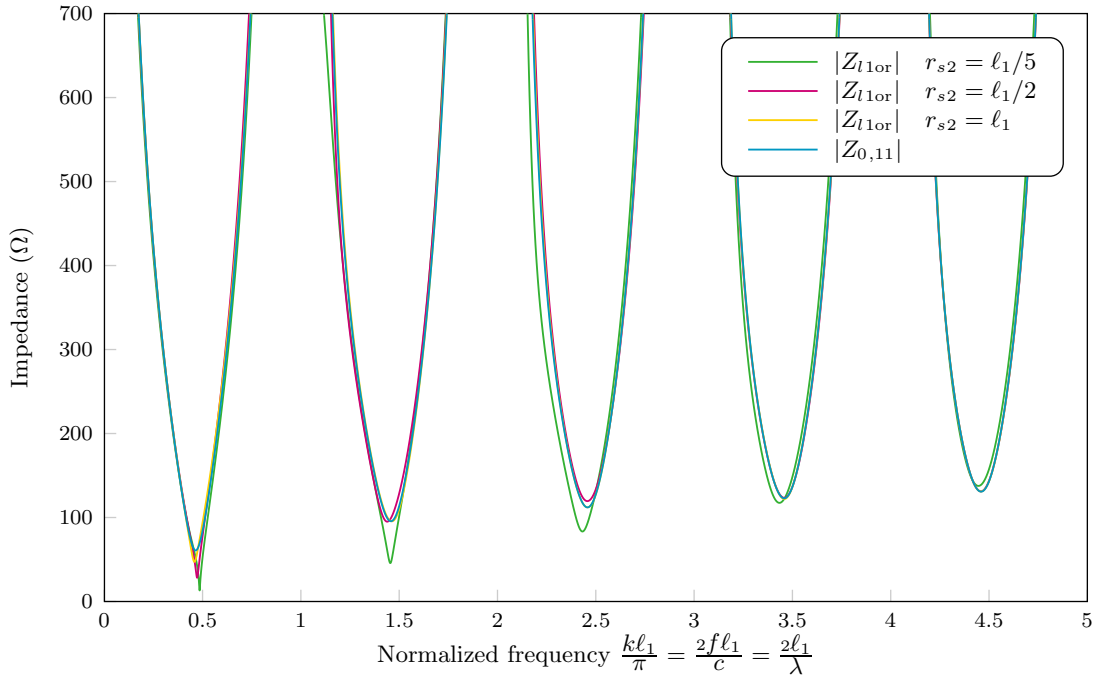


Figure 3.20: Optimal load impedance for reflection-free matching of a dipole antenna in parallel to a second dipole antenna of equal length, compared to the impedance of the first antenna with $a_1 = a_2 = \ell_1/100$ and $r_{z2} = 0$

is undesired, because it would increase the demands on the dynamic range of the system and slow the system down with respect to time-variant signals. In practice we will have to make sure that the amount of ohmic resistance in the antenna load is sufficient in case the load is chosen partly capacitive.

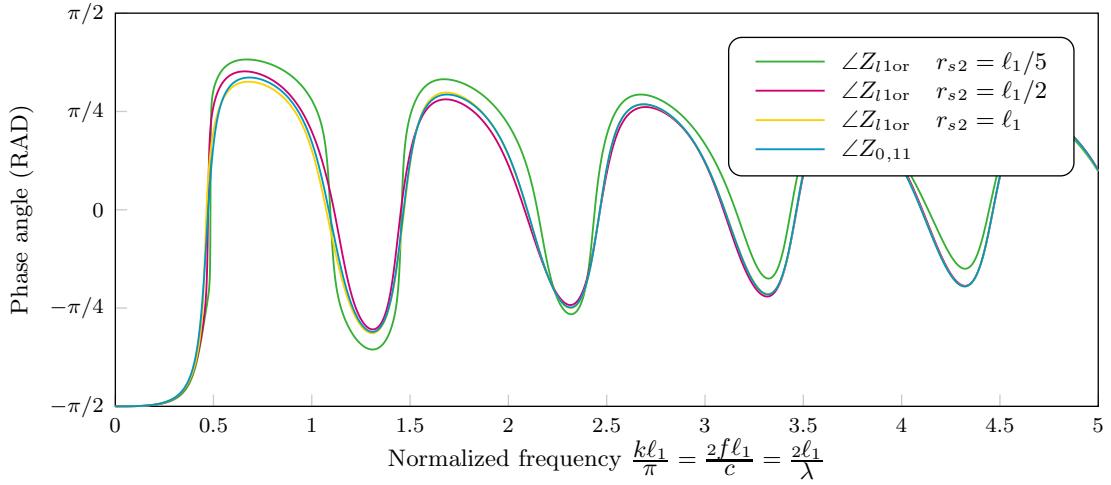


Figure 3.21: Phase angle of the optimal load impedance for reflection-free matching of a dipole antenna in parallel to a second dipole antenna of equal length, compared to the impedance of the first antenna with $a_1 = a_2 = \ell_1/100$ and $r_{z2} = 0$

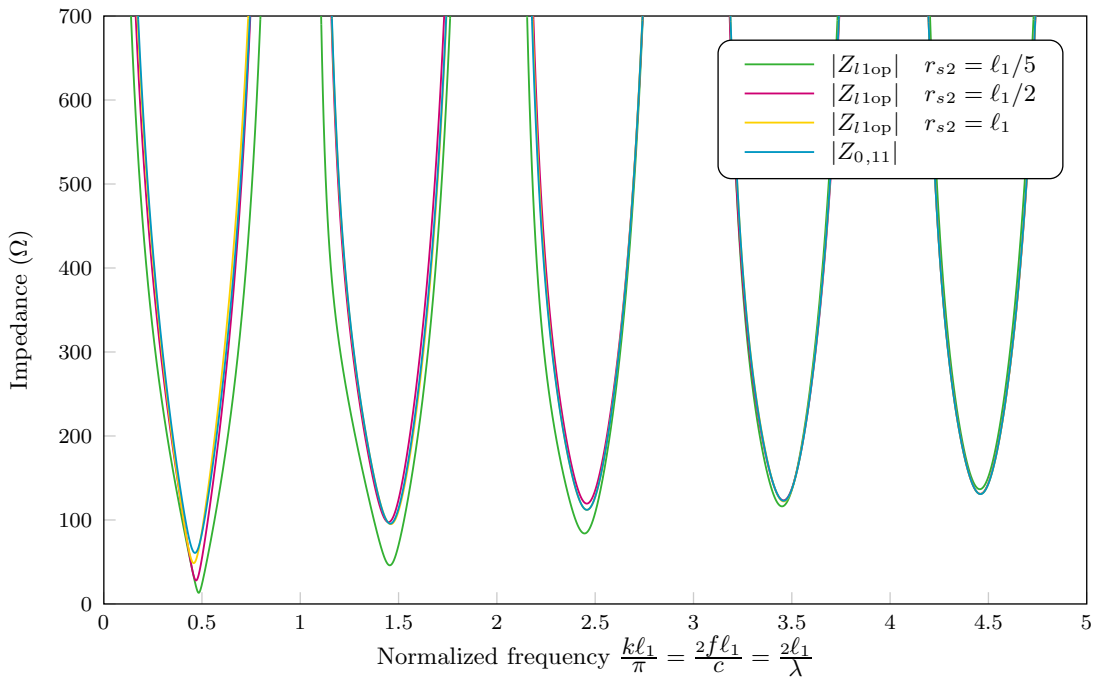


Figure 3.22: Optimal conjugate matched load impedance of a dipole antenna in parallel to a second dipole antenna of equal length, compared to the impedance of the first antenna with $a_1 = a_2 = \ell_1/100$ and $r_{z2} = 0$

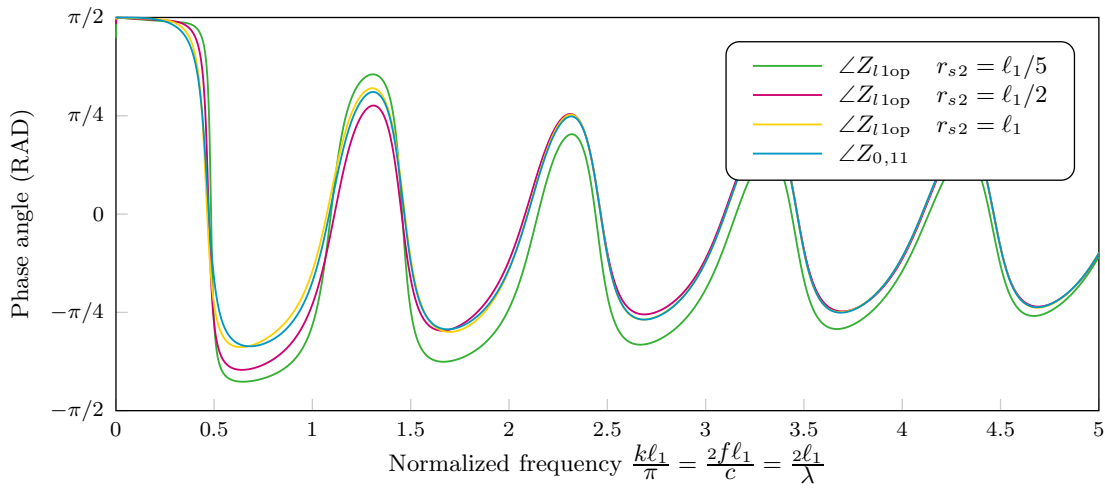


Figure 3.23: Phase angle of the optimal conjugate matched load impedance of a dipole antenna in parallel to a second dipole antenna of equal length, compared to the complex conjugate of the impedance of the first antenna with $a_1 = a_2 = \ell_1/100$ and $r_{z2} = 0$

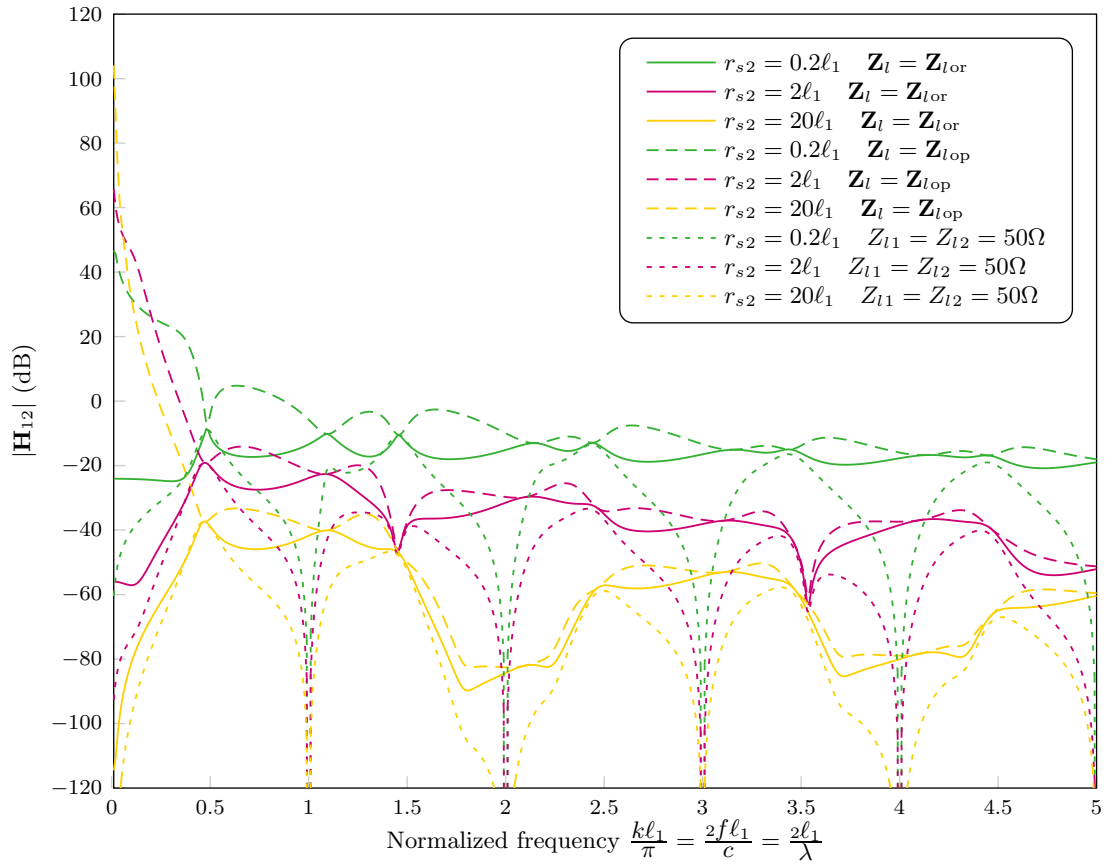


Figure 3.24: Transfer functions of parallel dipole antennas of equal length at different distances, both connected to 50Ω or one of the optimal matching impedances respectively, with $r_{s2} = 0$

3.5 Summary

In this chapter, expressions were presented to calculate the impedance of a dipole antenna in a reflection-free environment and for the mutual impedance between two dipole antennas of unequal length in echelon position. These parameters were used to describe the electric circuit behaviour of several dipole antennas in a parallel, echelon or collinear position with respect to each other in a reflection-free environment as an impedance matrix \mathbf{Z}_0 . These results will be used in the next chapter to model the propagation of signals and noise in a receiver front-end, using circuit-theory.

Furthermore, an expression for the transfer matrix was derived in case the antennas are all connected to some voltage source in series with a load impedance. These transfer functions include all direct and indirect paths between the dipole antennas. It was shown to be beneficial to express the dipole antenna coupling with respect to the amplitude of the standing wave in the antenna instead of the current amplitude at the antenna terminals to obtain the matrix \mathbf{Z}_m . This is mainly because it reduces the amount of indeterminate values when calculating transfer functions.

To show the effect of close antenna spacing on the apparent impedance of the antennas, expressions were derived for the required load impedances to prevent reflections at the antenna terminals or to maximize power transfer to the load impedance, respectively. Although these load impedances cannot be realised in practice for a broadband system, its values may serve as a reference for designing a receiver front-end.

Chapter 4

Signal and noise propagation in a cross correlation spectrum analyser

4.1 Determining the propagation of signal and noise

Signals with additive noise

We will analyse the propagation of signals and noise through the receiver systems, by starting from a simple model and gradually working to a more more precise description. The most idealised model of an XCSA is an ideal correlator. The stochastic signals that enter the correlator will in general both comprise of a signal component and a noise component. The most basic model of this is shown in Figure 4.1. For simplicity we will analyse a situation with only one external signal source and noise from internal noise sources first. As the noise components are uncorrelated to the signal components, the cross spectrum will consist of the cross spectrum of both signal components added to the cross spectrum of both noise components according to Equation A.22 on Page 82, as

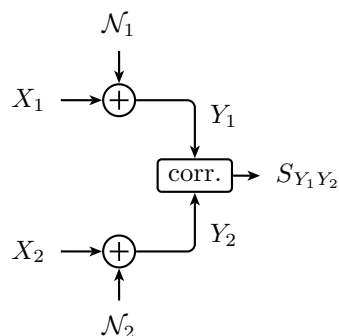


Figure 4.1: Block diagram of the cross correlation of signals with additive noise

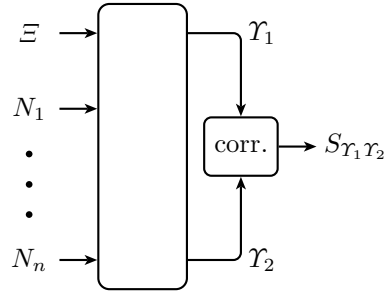


Figure 4.2: Block diagram of the cross correlation of a linear combination of signal and noise

indicated in Equation 4.3.

$$Y_1 = X_1 + \mathcal{N}_1 \quad (4.1)$$

$$Y_2 = X_2 + \mathcal{N}_2 \quad (4.2)$$

$$S_{Y_1 Y_2} = S_{X_1 X_2} + \underbrace{S_{X_1 \mathcal{N}_2}}_0 + \underbrace{S_{\mathcal{N}_1 X_2}}_0 + S_{\mathcal{N}_1 \mathcal{N}_2} \quad (4.3)$$

We can explain Equation 4.3 as: We want to measure $S_{X_1 X_2}$ using as XCSA, but due to additive noise from within this system we measure $S_{Y_1 Y_2}$ instead. The signal to noise ratio at the output of this simplified model is thus given by:

$$\text{SNR} = \frac{S_{X_1 X_2}}{S_{\mathcal{N}_1 \mathcal{N}_2}} \quad (4.4)$$

Signals and noise transferred from their sources

In all correlation receivers the signal components entering the correlator are transferred from a transmitter, through the air, via some path through the receiver to the correlator. The internal noise components are transferred from some point within the receiver to the correlator. We will call the signal as transmitted at the source Ξ and the noise components as created at their source N_n with n replaced by a symbol referring to the specific noise source. The signals that enter the ideal correlator will be referred to as \mathcal{Y}_1 and \mathcal{Y}_2 . The model is illustrated in Figure 4.2. If we assume these transfers to be linear, the signals entering the correlator can be expressed as in Equation 4.5 and Equation 4.6.

$$\mathcal{Y}_1 = H_{\mathcal{Y}_1 \Xi} \Xi + \sum_n H_{\mathcal{Y}_1 N_n} N_n \quad (4.5)$$

$$\mathcal{Y}_2 = H_{\mathcal{Y}_2 \Xi} \Xi + \sum_n H_{\mathcal{Y}_2 N_n} N_n \quad (4.6)$$

Using Equation A.25 on Page 83, this results in expression 4.7 for the cross spectrum, where a line above a variable indicates the complex conjugate of that variable.

$$S_{\mathcal{Y}_1 \mathcal{Y}_2} = \overline{H_{\mathcal{Y}_1 \Xi}} H_{\mathcal{Y}_2 \Xi} \cdot S_{\Xi \Xi} + \sum_n \overline{H_{\mathcal{Y}_1 N_n}} H_{\mathcal{Y}_2 N_n} \cdot S_{N_n N_n} \quad (4.7)$$

This cross spectrum is seen to be linearly dependent on the PSD of the signal Ξ that was to be measured. Furthermore, the output spectrum has a term that is linearly dependent on the noise. If the transfer from a noise source to either of the correlator inputs is zero, the noise source does not contribute to the output noise, independent of the transfer to the other correlator input. From Equation 4.7 we find at the output:

$$\text{SNR} = \frac{\overline{H_{\mathcal{R}_1 \Xi} H_{\mathcal{R}_2 \Xi}} \cdot S_{\Xi \Xi}}{\sum_n \overline{H_{\mathcal{R}_1 N_n} H_{\mathcal{R}_2 N_n}} \cdot S_{N_n N_n}} \quad (4.8)$$

The SNR is often expressed in decibels to be able to handle the large range of this parameter more conveniently. In this case a problem rises: The autocorrelation spectra $S_{\Xi \Xi}$ and $S_{N_n N_n}$ are always real positive, but this is not generally the case for the transfer functions that relate them to the output cross correlation spectra. Consequently, the SNR can be a complex value, which cannot be expressed in decibels using the normal definition. A complex SNR means that a signal can not only differ from noise because of its absolute value, but also because of its angle in the complex plane. This can be shown on a decibel scale if we extend the definition of decibels using the principal value of the complex logarithm of a complex number, such that for a real-valued SNR the result is equal to the normal definition:

$$\text{Log}(z) \triangleq \log_{10} |z| + j \angle z \quad (4.9)$$

$$\begin{aligned} \text{SNR}_{[\text{dB}]} &= 10 \cdot \text{Log} \left(\frac{\overline{H_{\mathcal{R}_1 \Xi} H_{\mathcal{R}_2 \Xi}} \cdot S_{\Xi \Xi}}{\sum_n \overline{H_{\mathcal{R}_1 N_n} H_{\mathcal{R}_2 N_n}} \cdot S_{N_n N_n}} \right) \text{ dB} \\ &= 10 \log_{10} \left| \frac{\overline{H_{\mathcal{R}_1 \Xi} H_{\mathcal{R}_2 \Xi}} \cdot S_{\Xi \Xi}}{\sum_n \overline{H_{\mathcal{R}_1 N_n} H_{\mathcal{R}_2 N_n}} \cdot S_{N_n N_n}} \right| + 10j \angle \left(\frac{\overline{H_{\mathcal{R}_1 \Xi} H_{\mathcal{R}_2 \Xi}} \cdot S_{\Xi \Xi}}{\sum_n \overline{H_{\mathcal{R}_1 N_n} H_{\mathcal{R}_2 N_n}} \cdot S_{N_n N_n}} \right) \text{ dB} \end{aligned} \quad (4.10)$$

Signal and noise transfer of the front end

Because only the passive front ends differ between the receiver with one antenna and the receiver with two antennas, it would be handy to be able to focus on the signal and noise transfer of this front end, instead of the systems as a whole. If we call the signals entering the mixers I and Γ respectively and the mixers, amplifiers and ADCs are modelled as a linear system with two inputs and two

outputs¹, we get the following equations:

$$I = H_{I\varepsilon}\varepsilon + \sum_n H_{IN_n}N_n \quad (4.11)$$

$$\Gamma = H_{\Gamma\varepsilon}\varepsilon + \sum_n H_{\Gamma N_n}N_n \quad (4.12)$$

$$\mathcal{Y}_1 = H_{\mathcal{Y}_1 I}I + H_{\mathcal{Y}_1 \Gamma}\Gamma \quad (4.13)$$

$$\mathcal{Y}_2 = H_{\mathcal{Y}_2 I}I + H_{\mathcal{Y}_2 \Gamma}\Gamma \quad (4.14)$$

$$\begin{aligned} S_{\mathcal{Y}_1 \mathcal{Y}_2} &= \overline{H_{\mathcal{Y}_1 I} H_{\mathcal{Y}_2 I}} S_{II} + \overline{H_{\mathcal{Y}_1 \Gamma} H_{\mathcal{Y}_2 \Gamma}} S_{\Gamma\Gamma} \\ &\quad + \overline{H_{\mathcal{Y}_1 I} H_{\mathcal{Y}_2 \Gamma}} S_{I\Gamma} + \overline{H_{\mathcal{Y}_1 \Gamma} H_{\mathcal{Y}_2 I}} S_{\Gamma I} \\ &= \left(\overline{H_{\mathcal{Y}_1 I} H_{I\varepsilon}} H_{\mathcal{Y}_2 \Gamma} H_{\Gamma\varepsilon} + \overline{H_{\mathcal{Y}_1 \Gamma} H_{\Gamma\varepsilon}} H_{\mathcal{Y}_2 I} H_{I\varepsilon} \right. \\ &\quad \left. + \overline{H_{\mathcal{Y}_1 I} H_{\mathcal{Y}_2 I}} |H_{I\varepsilon}|^2 + \overline{H_{\mathcal{Y}_1 \Gamma} H_{\mathcal{Y}_2 \Gamma}} |H_{\Gamma\varepsilon}|^2 \right) S_{\varepsilon\varepsilon} \\ &\quad + \sum_n \left(\overline{H_{\mathcal{Y}_1 I} H_{IN_n}} H_{\mathcal{Y}_2 \Gamma} H_{\Gamma N_n} + \overline{H_{\mathcal{Y}_1 \Gamma} H_{\Gamma N_n}} H_{\mathcal{Y}_2 I} H_{IN_n} \right. \\ &\quad \left. + \overline{H_{\mathcal{Y}_1 I} H_{\mathcal{Y}_2 I}} |H_{IN_n}|^2 + \overline{H_{\mathcal{Y}_1 \Gamma} H_{\mathcal{Y}_2 \Gamma}} |H_{\Gamma N_n}|^2 \right) S_{N_n N_n} \end{aligned} \quad (4.15)$$

From this it can be concluded that in order to calculate the output spectrum, all four transfer functions of this two-port are required, together with the power spectra and the cross spectrum at its input. These power spectra will presumably contain a larger portion of noise than the cross spectrum, as that is why a cross correlation receiver is supposed to have a better noise performance. Without knowledge or assumption of the transfer functions in Equation 4.13 and Equation 4.14, the output spectrum, according to Equation 4.16, can be any combination of these spectra. As already stated in Chapter 2 we either need to know the transfer functions of the rear end of the system, or presume there is no coupling between the branches between the mixer inputs and the correlator inputs, as was also suggested in the block diagrams in Figure 2.2 and Figure 2.3, so $H_{\mathcal{Y}_2 I} = 0$ and $H_{\mathcal{Y}_1 \Gamma} = 0$. The latter will be done, to obtain the situation depicted in Figure 4.3 on the left hand side. In equations this becomes:

¹Mixers are quadratic components, so they are definitely not linear. However, when the mixer input is sufficiently band-limited, the band-limited mixer output can be interpreted as a frequency-shifted version of the input. This results in measurement of a frequency-shifted version of the PSD to be measured. Because in that case there is a bijective relation between the actual measurement and the modelled measurement, the frequency shift can and will be cancelled at the output of the system for interpreting the data. Consequently, while modelling the mixers and ADCs as a black box, we can forget about the frequency shift altogether.

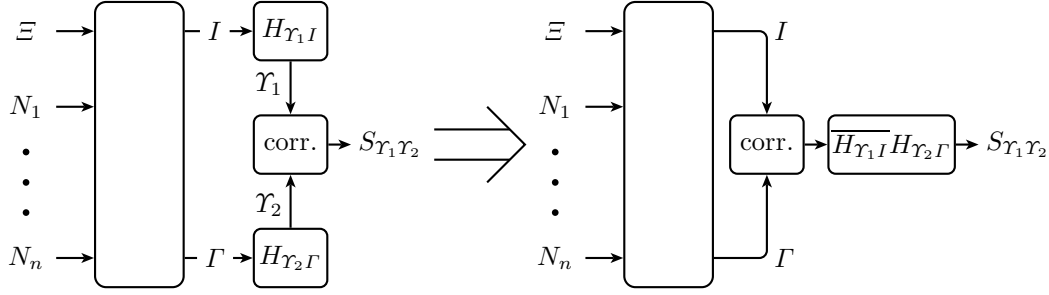


Figure 4.3: Equivalent block diagram in case of uncoupled noise at the rear end of the system. The signals I and Γ are the signals at the mixer inputs.

$$\gamma_1 = H_{\gamma_1 I} I + \underbrace{H_{\gamma_1 \Gamma} \Gamma}_0 \quad (4.16)$$

$$\gamma_2 = \underbrace{H_{\gamma_2 I} I}_0 + H_{\gamma_2 \Gamma} \Gamma \quad (4.17)$$

$$\begin{aligned} S_{\gamma_1 \gamma_2} &= \overline{H_{\gamma_1 I} H_{\gamma_2 \Gamma}} \cdot S_{\Gamma I} \\ &= \overline{H_{\gamma_1 I} H_{\gamma_2 \Gamma}} \cdot \left(\overline{H_{I \Xi} H_{\Gamma \Xi}} S_{\Xi \Xi} + \sum_n \overline{H_{I N_n} H_{\Gamma N_n}} S_{N_n N_n} \right) \end{aligned} \quad (4.18)$$

$$\text{SNR}_{[\text{dB}]} = 10 \cdot \text{Log} \left(\frac{\overline{H_{I \Xi} H_{\Gamma \Xi}} S_{\Xi \Xi}}{\sum_n \overline{H_{I N_n} H_{\Gamma N_n}} S_{N_n N_n}} \right) \text{ dB} \quad (4.19)$$

From Equation 4.19 it can be seen the SNR of the cross correlation of the signals I and Γ that enter the mixers is now equal to the SNR of the output $S_{\gamma_1 \gamma_2}$. Therefore by calculating $S_{I \Gamma}$, we can compare the noise performance of correlation receivers with one or two antennas, without having to bother about $H_{\gamma_1 I}$ and $H_{\gamma_2 \Gamma}$, as these form just a frequency dependent constant in all cases. This is shown in Figure 4.3 on the right hand side.

Transfer of signal and noise power spectral densities

To be able to make a clear distinction between signals referring to the receiver with one antenna and the receiver with two antennas, the signals entering the mixer in the two-antenna system will be referred to as I and Γ , whereas those signals in the one-antenna system will be referred to as Ψ and O , respectively.

If we see the spectrum $S_{\Xi \Xi}$ as a *signal* which we want to measure by using $S_{I \Gamma}$ or $S_{\Psi O}$ respectively as an estimator that is biased due to the noise spectra,

it makes sense to assign these spectra a name:

$$\Theta \triangleq S_{\Xi\Xi} \quad (4.20)$$

$$\Lambda_n \triangleq S_{N_n N_n} \quad (4.21)$$

$$\Pi \triangleq S_{I\Gamma} \quad (4.22)$$

$$\Phi \triangleq S_{\Psi O} \quad (4.23)$$

$$H_{\Pi\Theta} \triangleq \overline{H_{I\Xi}} \cdot H_{\Gamma\Xi} \quad (4.24)$$

$$H_{\Pi\Lambda_n} \triangleq \overline{H_{IN_n}} \cdot H_{\Gamma N_n} \quad (4.25)$$

$$H_{\Phi\Theta} \triangleq \overline{H_{\Psi\Xi}} \cdot H_{O\Xi} \quad (4.26)$$

$$H_{\Phi\Lambda_n} \triangleq \overline{H_{\Psi N_n}} \cdot H_{ON_n} \quad (4.27)$$

$$\Rightarrow \Pi = H_{\Pi\Theta} \cdot \Theta + \sum_n H_{\Pi\Lambda_n} \cdot \Lambda_n \quad (4.28)$$

$$\Rightarrow \Phi = H_{\Phi\Theta} \cdot \Theta + \sum_n H_{\Phi\Lambda_n} \cdot \Lambda_n \quad (4.29)$$

The transfer functions defined in Equation 4.24 to Equation 4.27 differ from the transfer functions from which they are defined, because they operate on (cross) PSD signals instead of voltage signals in the separate branches of the system. The input of the system is a signal power we would like to detect and its output is proportional to this power. However, this output is quadratically related to the voltage signals in both branches, so there is no linear transfer from, say, N_n to Π . What we have in our model is for both receiver types a linear system with the signal source and all noise sources as its inputs and the branch signals I and Γ or Ψ and O respectively as its outputs. The cross correlation of these branch signals is a linear combination of the *power spectra* of the signal source and all noise sources.

The SNR of both systems can be calculated according to Equation 4.30 and Equation 4.31 respectively:

$$\text{SNR}_{2\text{-antenna}} [\text{dB}] = 10 \cdot \text{Log} \left(\frac{H_{\Pi\Theta} \cdot \Theta}{\sum_n H_{\Pi\Lambda_n} \cdot \Lambda_n} \right) \text{ dB} \quad (4.30)$$

$$\text{SNR}_{1\text{-antenna}} [\text{dB}] = 10 \cdot \text{Log} \left(\frac{H_{\Phi\Theta} \cdot \Theta}{\sum_n H_{\Phi\Lambda_n} \cdot \Lambda_n} \right) \text{ dB} \quad (4.31)$$

Multiple signal and noise sources

In case multiple external sources are active, the contribution of signals in the output spectrum becomes a summation, just like the contribution of the internal noise:

$$\Pi = \sum_n H_{\Pi\Theta_n} \cdot \Theta_n + \sum_n H_{\Pi\Lambda_n} \cdot \Lambda_n \quad (4.32)$$

$$\Phi = \sum_n H_{\Phi\Theta_n} \cdot \Theta_n + \sum_n H_{\Phi\Lambda_n} \cdot \Lambda_n \quad (4.33)$$

If one wants to count the signal coming from some of these sources as noise, the SNR at the output of the (still partly idealized) XCSA will be:

$$\text{SNR}_{2\text{-antenna}} [\text{dB}] = 10 \cdot \text{Log} \left(\frac{\sum_{\text{signal sources}} H_{\Pi\Theta_n} \cdot \Theta_n}{\sum_{\text{noise sources}} H_{\Pi\Theta_n} \cdot \Theta_n + \sum_n H_{\Pi\Lambda_n} \cdot \Lambda_n} \right) \text{ dB} \quad (4.34)$$

$$\text{SNR}_{1\text{-antenna}} [\text{dB}] = 10 \cdot \text{Log} \left(\frac{\sum_{\text{signal sources}} H_{\Phi\Theta_n} \cdot \Theta_n}{\sum_{\text{noise sources}} H_{\Phi\Theta_n} \cdot \Theta_n + \sum_n H_{\Phi\Lambda_n} \cdot \Lambda_n} \right) \text{ dB} \quad (4.35)$$

Using these formulas, the SNR can be calculated if we know how much power is sent in which band by all sources within reach and what the transfer function from that source to the receiver is. The SNR can be estimated even more accurate by taking the noise contribution of the rear ends of both systems into account. This contribution would originate from noise that is generated by the rear end components and the error in the cross correlation estimate due to taking a finite amount of time.

Thermal noise power spectral density

It is well known that the noise power generated by a resistor is independent of the value of that resistor, but some care must be taken in the context of stochastic processes: When talking about the power of a stochastic process, normally the expectation of the square of that process is meant, so the unit of stochastic power is equal to the square of the unit of the signal. For a voltage signal this leads to a stochastic power that is expressed in V^2 . The Fourier transform of the stochastic power, the PSD, is then expressed in V^2s . When talking about physical power, one usually means an amount of energy per unit of time, commonly expressed in the unit W. The physical PSD is then expressed in Ws. Although the physical PSD of the thermal noise from a resistor in Ws does not depend on the value of that resistor, the stochastic PSD in V^2s is linearly dependent on the resistor value. As a consequence, Λ_n can not be taken out of the summations in Equation 4.32 and Equation 4.33. If we use Boltzmann's constant in JK^{-1} and the temperature in K, we get:

$$\begin{aligned}
 A_n &\triangleq S_{N_n N_n} = 2k_B \mathcal{T} (\text{Ws}) = 2k_B \mathcal{T} R_n (\text{V}^2\text{s}) \quad \text{see:[13]} \quad (4.36) \\
 \sum_{\text{resistor noise}} H_{\Pi \Lambda_n} \cdot A_n &= 2k_B \mathcal{T} \cdot \sum_{\text{resistor noise}} H_{\Pi \Lambda_n} \cdot R_n (\text{V}^2\text{s}) \\
 &= \frac{2k_B \mathcal{T}}{\sqrt{R_{l_I} R_{l_r}}} \cdot \sum_{\text{resistor noise}} H_{\Pi \Lambda_n} \cdot R_n (\text{Ws}) \quad (4.37)
 \end{aligned}$$

$$\begin{aligned}
 \sum_{\text{resistor noise}} H_{\Phi \Lambda_n} \cdot A_n &= 2k_B \mathcal{T} \cdot \sum_{\text{resistor noise}} H_{\Phi \Lambda_n} \cdot R_n (\text{V}^2\text{s}) \\
 &= \frac{2k_B \mathcal{T}}{\sqrt{R_{l_\psi} R_{l_O}}} \cdot \sum_{\text{resistor noise}} H_{\Phi \Lambda_n} \cdot R_n (\text{Ws}) \quad (4.38)
 \end{aligned}$$

Please note that the PSD in this report, as defined in Equation A.14 on Page 81, has a *double sided* spectrum, which means that the spectrum contains both positive and negative frequencies. As a consequence, if we would for example filter resistor noise with a passband filter with a bandwidth B and a passband gain of 1, the negative part of the spectrum needs to be taken into account as well. The resulting physical noise power would yield:

$$\mathcal{P} = 2B \cdot 2k_B \mathcal{T} (\text{W}) = 4Bk_B \mathcal{T} (\text{W}) \quad (4.39)$$

Comparison of signal and noise performance of the receivers

If we look back at the CR paradigm, our receiver is meant to give us information about which frequency bands we can use, ideally without knowledge of other transmitters in advance. However, because the SNR, according to Equation 4.34 or Equation 4.35 respectively, depends on complete knowledge of all sources within reach, it is practically impossible to give an insightful overview of possible situations and their corresponding SNR. To compare the performance of the one- and two-antenna system there are three parameters we can calculate and show for a representative selection of situations that give insight in the performance of the receivers:

- the transfer function from a representative selection of transmitters to the output of either system: $H_{\Pi \Theta}$ versus $H_{\Phi \Theta}$,
- the power spectrum at the output of either system due to thermal noise in the resistors of the front ends: $\sum_{\text{resistor noise}} H_{\Pi \Lambda_n} \Lambda_n$ versus $\sum_{\text{resistor noise}} H_{\Phi \Lambda_n} \Lambda_n$ and
- the transfer function from noise appearing at the mixer inputs to the output of the systems: $H_{\Pi \Lambda_I}$ and $H_{\Pi \Lambda_r}$ versus $H_{\Phi \Lambda_I}$ and $H_{\Phi \Lambda_r}$.

The first two of these performance parameters can be combined to give some more insight:

$$\mathcal{S}_{\text{two-antenna}} = \left| \frac{\sum H_{\Pi\Lambda_n} A_n}{\text{resistor noise}} \right| \frac{1}{H_{\Pi\Theta}} \quad (4.40)$$

$$\mathcal{S}_{\text{one-antenna}} = \left| \frac{\sum H_{\Phi\Lambda_n} A_n}{\text{resistor noise}} \right| \frac{1}{H_{\Phi\Theta}} \quad (4.41)$$

The parameter \mathcal{S} is the power spectral density for which at the output of the system, the magnitude of the signal contribution is equal to the magnitude of the thermal noise of the front end. This means that if a source has a PSD of \mathcal{S} , the real part of the SNR in decibels at the output of the system would be 0 dB, if there were no other noise sources than thermal noise from the front end resistors. It is a measure for the blind spot of the XCSAs due to noisy resistors in the front end.

4.2 Calculation of transfer functions

One-antenna system

The circuit diagram of the one-antenna system with noise sources is shown in Figure 4.4. To analyse the signal transfer of the one-antenna system, we need the transfer functions $H_{\Psi\Xi}$ and $H_{O\Xi}$ to calculate $H_{\Phi\Xi}$ according to Equation 4.26. To analyse its noise transfer, we need the transfer functions $H_{\Psi N_n}$ and $H_{O N_n}$ to calculate $H_{\Phi\Lambda_n}$ of each internal noise source according to Equation 4.27. These noise sources include thermal noise for each physical resistor, where the resistors with the same name in Figure 4.4 can be used in the calculation as being one: $H_{\Psi, a_{\Psi}}, H_{O, a_{\Psi}}, \dots, H_{O, c_O}$ to calculate $H_{\Phi, \Lambda_{a_{\Psi}}}, H_{\Phi, \Lambda_{b_{\Psi}}}, \dots, H_{O, \Lambda_{c_O}}$. Furthermore we will calculate the transfer from an arbitrary noise source at the mixer inputs using the same method: $H_{\Phi, \Lambda_{l_{\Psi}}}$ and $H_{\Phi, \Lambda_{l_O}}$.

Because the front end of the receiver is completely passive, all (voltage) transfer functions depend on all resistor values and the dimensions and relative position of the antennas. Although determining these transfers is a matter of accurate bookkeeping, listing them results in quite lengthy expressions. A slight simplification can be made by not using the impedance as seen from the antenna output, but just the antenna self impedance according to Equation 3.14 on Page 17. This means that the EM wave traveling from the receiving antenna to the transmitting antenna and back is ignored. Because the transmitting antenna is in general far away this effect will be small compared to the self impedance. Furthermore, in practice, there will probably be reflections close to the receiving antenna having a much bigger influence.

As the resulting transfer functions share a lot of equal sub-expressions, they are most compactly listed as block diagrams as shown in Figure 4.5. The diagram on the left is required for calculating eight equivalent impedances. A

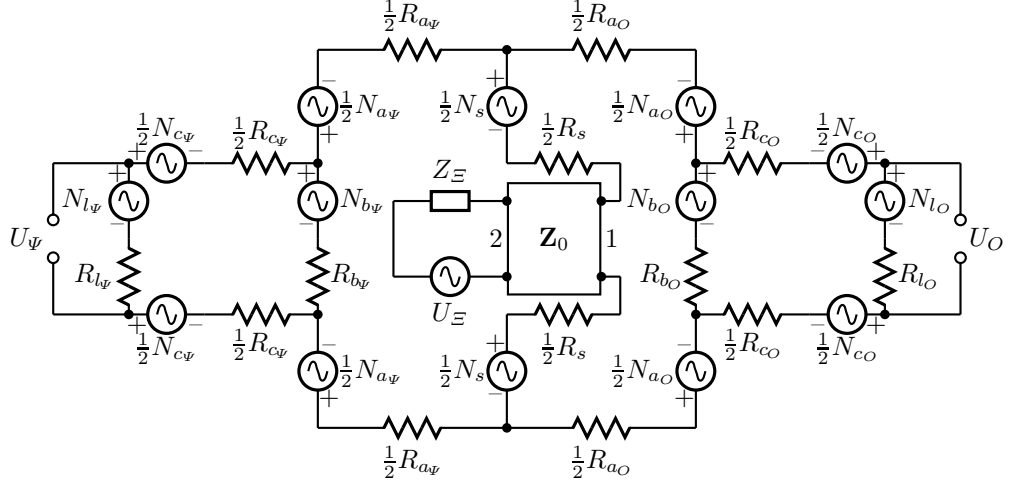


Figure 4.4: Circuit drawing of the one-antenna receiver with noise sources

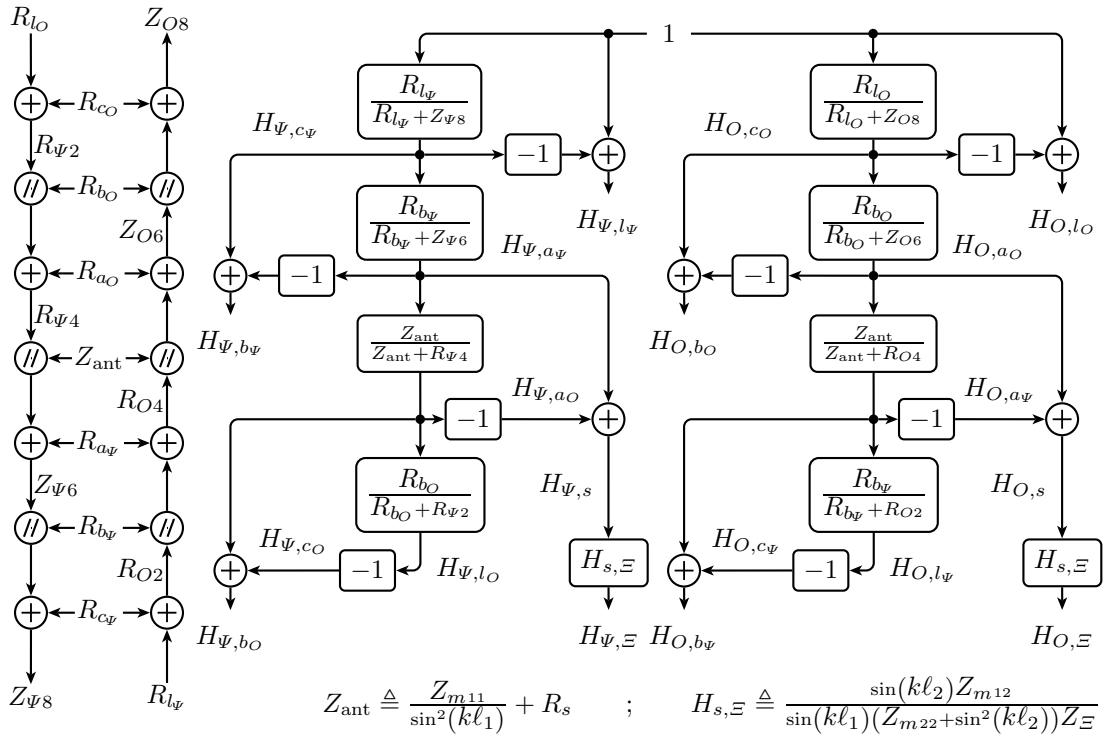


Figure 4.5: Block diagram for calculation of the transfer functions of the one-antenna system

plus sign indicates the equivalent impedance of the input impedances of this block as if they were connected in series. A double slash indicates the equivalent impedance of the input impedances of this block as if they were connected in parallel. The equivalent impedance of the antenna and the splitter resistance in series, Z_{ant} is shown at the bottom of the figure. The rest of Figure 4.5 can be used to calculate the voltage transfer functions. Care must be taken when implementing these diagrams in a script, to take limits in case some parameters become zero or infinity, which might be the case if any of the series resistors is set to zero or any of the parallel resistors is left out in a specific receiver design.

With the voltage transfer functions, the PSD transfer functions can be calculated according to Equation 4.26 and Equation 4.27 on Page 48, with the indices of the noise transfer functions according to the index of the corresponding resistance:

$$H_{\Phi\Theta} = \overline{H_{\Psi,\Xi}} \cdot H_{O,\Xi} \quad (4.42)$$

$$H_{\Phi\Lambda_{lO}} = \overline{H_{\Psi,lO}} \cdot H_{O,lO} \quad (4.43)$$

$$H_{\Phi\Lambda_{cO}} = \overline{H_{\Psi,cO}} \cdot H_{O,cO} \quad (4.44)$$

$$H_{\Phi\Lambda_{bO}} = \overline{H_{\Psi,bO}} \cdot H_{O,bO} \quad (4.45)$$

$$H_{\Phi\Lambda_{aO}} = \overline{H_{\Psi,aO}} \cdot H_{O,aO} \quad (4.46)$$

$$H_{\Phi\Lambda_s} = \overline{H_{\Psi,s}} \cdot H_{O,s} \quad (4.47)$$

$$H_{\Phi\Lambda_{a\Psi}} = \overline{H_{\Psi,a\Psi}} \cdot H_{O,a\Psi} \quad (4.48)$$

$$H_{\Phi\Lambda_{b\Psi}} = \overline{H_{\Psi,b\Psi}} \cdot H_{O,b\Psi} \quad (4.49)$$

$$H_{\Phi\Lambda_{c\Psi}} = \overline{H_{\Psi,c\Psi}} \cdot H_{O,c\Psi} \quad (4.50)$$

$$H_{\Phi\Lambda_{l\Psi}} = \overline{H_{\Psi,l\Psi}} \cdot H_{O,l\Psi} \quad (4.51)$$

Two-antenna system

The circuit of the two-antenna system with noise sources is shown in Figure 4.6. Calculating the required transfer functions of the two-antenna system can be done following the same procedure as with the one-antenna system. The antenna coupling can be expressed by calculating the open terminal voltage of one antenna with the other two connected to the circuit. This can be done with Equation 3.39, using 3×3 matrices and taking the limit of the load of the open terminal to infinity. The resulting transfer functions are shown in Figure 4.7, together with Equation 4.52 to Equation 4.57. Equations 4.56 and 4.57 differ from equations 4.54 and 4.55, because in the latter cases the presence of the transmitting antenna is ignored, just like we did with the one-antenna system. This means that in the transfer functions between the both antennas of the receiver ($H_{1,2}$ and $H_{2,1}$) all signal paths that pass the antenna of the transmitter, are ignored. This is done because the direct path between the two antennas of the receiver generally yields a much stronger signal and in practise nearby reflections will have a larger influence than the reflection at the antenna of the transmitter.

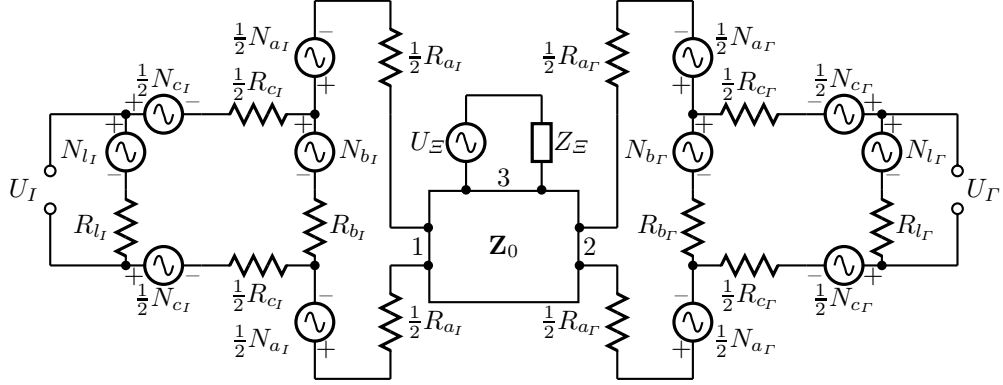


Figure 4.6: Circuit drawing of the two-antenna receiver with noise sources

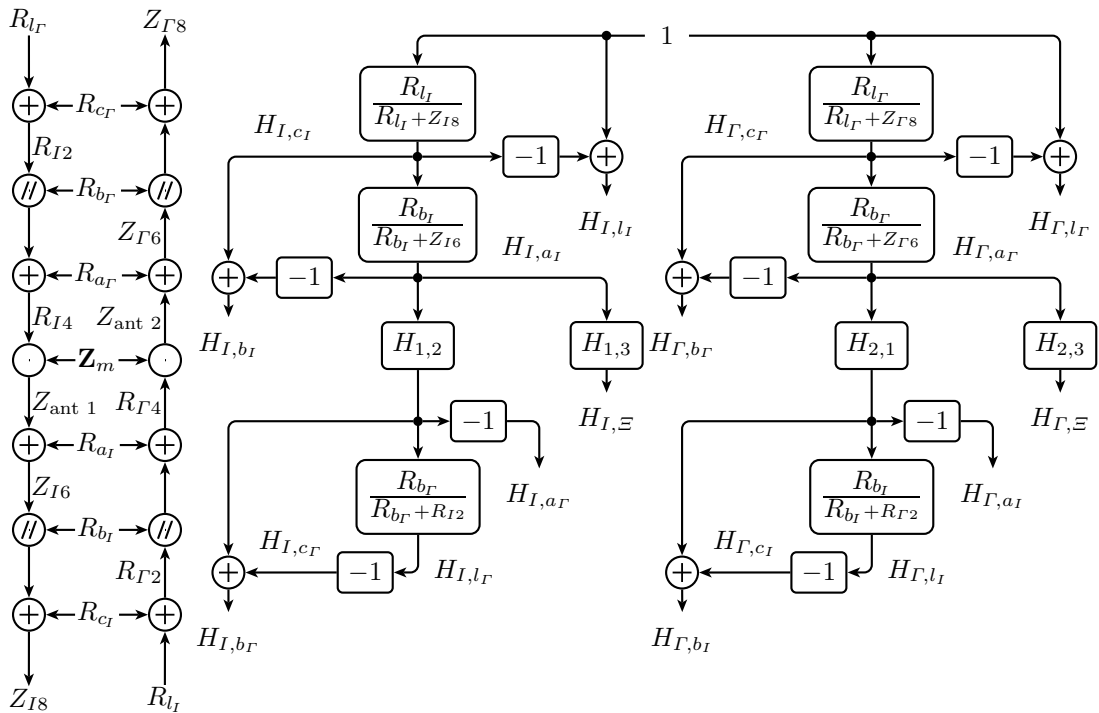


Figure 4.7: Block diagram for calculation of the transfer functions of the two-antenna system

$$Z_{\text{ant } 1} \triangleq \left(Z_{m11} - \frac{Z_{m12}^2}{Z_{m22} + R_{I4} \sin^2(k\ell_2)} \right) \sin^{-2}(k\ell_1) \quad (4.52)$$

$$Z_{\text{ant } 2} \triangleq \left(Z_{m22} - \frac{Z_{m12}^2}{Z_{m11} + R_{\Gamma 4} \sin^2(k\ell_1)} \right) \sin^{-2}(k\ell_2) \quad (4.53)$$

$$H_{1,2} \triangleq \frac{\sin(k\ell_2)}{\sin(k\ell_1)} \cdot \frac{Z_{m12}}{Z_{m22} + R_{I4} \sin^2(k\ell_2)} \quad (4.54)$$

$$H_{2,1} \triangleq \frac{\sin(k\ell_1)}{\sin(k\ell_2)} \cdot \frac{Z_{m12}}{Z_{m11} + R_{\Gamma 4} \sin^2(k\ell_1)} \quad (4.55)$$

$$H_{1,3} \triangleq \frac{\sin(k\ell_3)}{\sin(k\ell_1)} \cdot \frac{Z_{m13} (Z_{m22} + R_{I4} \sin^2(k\ell_2)) - Z_{m12} Z_{m23}}{(Z_{m22} + R_{I4} \sin^2(k\ell_2)) (Z_{mm33} + Z_{\Xi} \sin^2(k\ell_3)) - Z_{m23}^2} \quad (4.56)$$

$$H_{2,3} \triangleq \frac{\sin(k\ell_3)}{\sin(k\ell_2)} \cdot \frac{Z_{m23} (Z_{m11} + R_{\Gamma 4} \sin^2(k\ell_1)) - Z_{m12} Z_{m13}}{(Z_{m11} + R_{\Gamma 4} \sin^2(k\ell_1)) (Z_{m33} + Z_{\Xi} \sin^2(k\ell_3)) - Z_{m13}^2} \quad (4.57)$$

With the voltage transfer functions, the PSD transfer functions can be calculated according to Equation 4.24 and Equation 4.25 on Page 48, with the indices of the noise transfer functions according to the index of the corresponding resistance:

$$H_{\Pi\Theta} = \overline{H_{I,\Xi}} \cdot H_{\Gamma,\Xi} \quad (4.58)$$

$$H_{\Pi\Lambda_{l\Gamma}} = \overline{H_{I,l\Gamma}} \cdot H_{\Gamma,l\Gamma} \quad (4.59)$$

$$H_{\Pi\Lambda_{c\Gamma}} = \overline{H_{I,c\Gamma}} \cdot H_{\Gamma,c\Gamma} \quad (4.60)$$

$$H_{\Pi\Lambda_{b\Gamma}} = \overline{H_{I,b\Gamma}} \cdot H_{\Gamma,b\Gamma} \quad (4.61)$$

$$H_{\Pi\Lambda_{a\Gamma}} = \overline{H_{I,a\Gamma}} \cdot H_{\Gamma,a\Gamma} \quad (4.62)$$

$$H_{\Pi\Lambda_{aI}} = \overline{H_{I,aI}} \cdot H_{\Gamma,aI} \quad (4.63)$$

$$H_{\Pi\Lambda_{bI}} = \overline{H_{I,bI}} \cdot H_{\Gamma,bI} \quad (4.64)$$

$$H_{\Pi\Lambda_{cI}} = \overline{H_{I,cI}} \cdot H_{\Gamma,cI} \quad (4.65)$$

$$H_{\Pi\Lambda_{lI}} = \overline{H_{I,lI}} \cdot H_{\Gamma,lI} \quad (4.66)$$

4.3 Plots

We have derived equations for the transfer of signal and noise cross power spectral densities at the mixer inputs of the one-antenna and two-antenna receiver. We have seen that in case we assume no coupling between both receiver paths behind the mixers, these cross-PSDs are proportional to the expectation of the signal and noise PSDs as measured by both systems. Unfortunately from these equations it is not clear how the design parameters of the systems, like antenna size and positioning and the choice of resistances, affect the measurement. Also the sensitivity of the system with respect to the location and design of the transmitters is unclear. In the following pages some example configurations are described of which plots show how both systems compare.

These examples include a discussion of how certain (design) parameters could optimize the system design.

In all configurations we have chosen the system of coordinates such that the plane in which both receiving antennas are, is the plane $y = 0$. We choose z in the longitudinal direction of the antennas, such that x is orthogonal to the antennas and in the plane $y = 0$. In all configurations the center of the antenna of the one-antenna system is chosen as the origin. The two antennas of the two-antenna system are placed symmetrically with respect to the antenna of the one-antenna system to which it is compared. The parameters with subscript “one” refer to the receiving antenna of the one-antenna system. The parameters with subscript “TX” refer to the transmitter. The parameters with subscripts 1 and 2 refer to the receiving antennas of the two-antenna system. In all examples a temperature of 300K is assumed.

Please note that the situations we compare are a one antenna system with some transmitter on one hand and a two antenna system with that same transmitter on the other hand. This means we do not consider a situation with three receiving antennas at the same time.

Parallel receiving antennas of equal length at different spacings

We start with a symmetric system with two parallel antennas of equal length at different spacings, which we compare to a one-antenna system. We assume a transmitter that is far away, on the perpendicular bisector of the two antennas. In the receivers we take only one impedance in series with the load impedance formed by the mixer inputs. The transmitter is assumed to have a conjugate matching impedance compared to its antenna. The situation is listed below. Configuration 1:

$$\begin{array}{llll}
 r_{x,\text{one}} \triangleq 0 & r_{x,\text{TX}} = 0 & r_{x1} = \text{variable} & r_{x2} = -r_{x1} \\
 r_{y,\text{one}} \triangleq 0 & r_{y,\text{TX}} = 1000\ell_1 & r_{y1} \triangleq 0 & r_{y2} \triangleq 0 \\
 r_{z,\text{one}} \triangleq 0 & r_{z,\text{TX}} = 0 & r_{z1} = 0 & r_{z2} = 0 \\
 \ell_{\text{one}} = \ell_1 & \ell_{\text{TX}} = \ell_1 & \ell_1 = \text{unit} & \ell_2 = \ell_1 \\
 a_{\text{one}} = \ell_{\text{one}}/100 & a_{\text{TX}} = \ell_{\text{TX}}/100 & a_1 = \ell_1/100 & a_2 = \ell_2/100 \\
 R_s = 0 & Z_{\Xi} = \overline{Z_{0,\text{TX},\text{TX}}} & & \\
 R_{a_v} = 100\Omega & R_{a_o} = 100\Omega & R_{a_l} = 100\Omega & R_{a_r} = 100\Omega \\
 R_{b_v} = \infty\Omega & R_{b_o} = \infty\Omega & R_{b_l} = \infty\Omega & R_{b_r} = \infty\Omega \\
 R_{c_v} = 0\Omega & R_{c_o} = 0\Omega & R_{c_l} = 0\Omega & R_{c_r} = 0\Omega \\
 R_{l_v} = 50\Omega & R_{l_o} = 50\Omega & R_{l_l} = 50\Omega & R_{l_r} = 50\Omega
 \end{array}$$

In Figure 4.8 the cross-PSD is shown due to the thermal noise of the series resistors R_{a_v} and R_{a_o} or R_{a_l} and R_{a_r} respectively. The antenna separation of the two-antenna system is taken between $0.2\ell_1$ and $1.2\ell_1$.

The first thing to notice is that in most cases this cross-PSD has a negative value. A cross-PSD can be any complex number, but because of the symmetry of Configuration 1 we find only real numbers in this case. The negative values

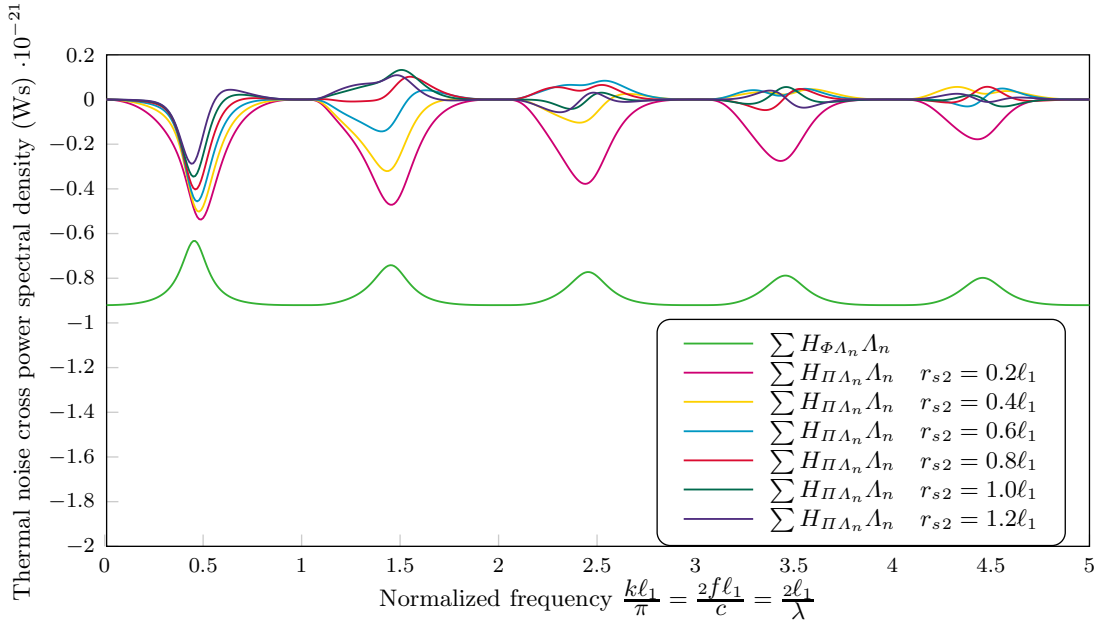


Figure 4.8: Cross power spectral density of at the mixer inputs due to noisy resistors in Configuration 1

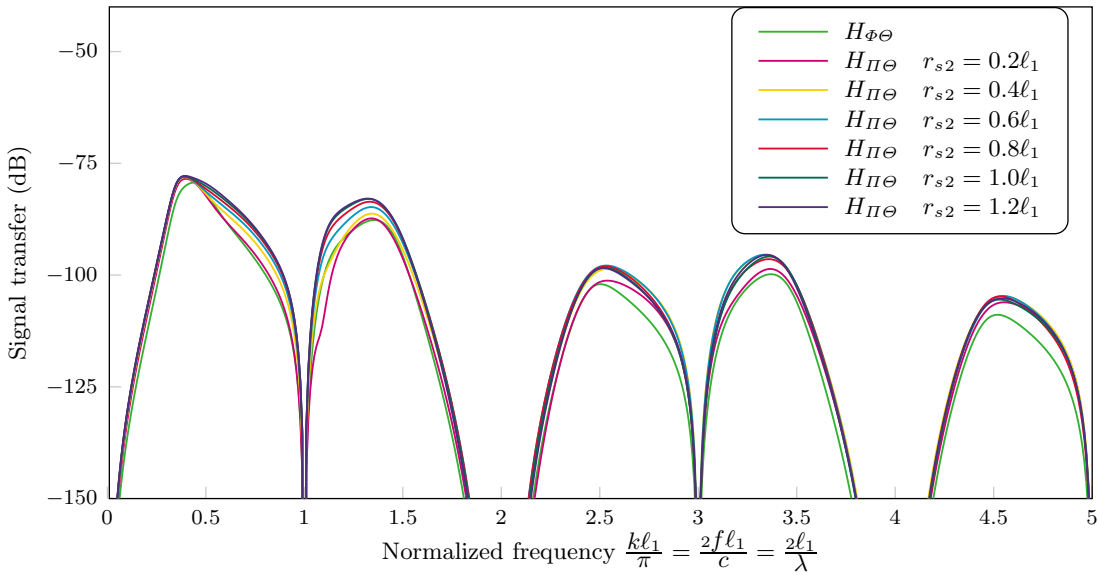


Figure 4.9: Signal transfer function to the cross power spectral density at the mixer inputs in Configuration 1

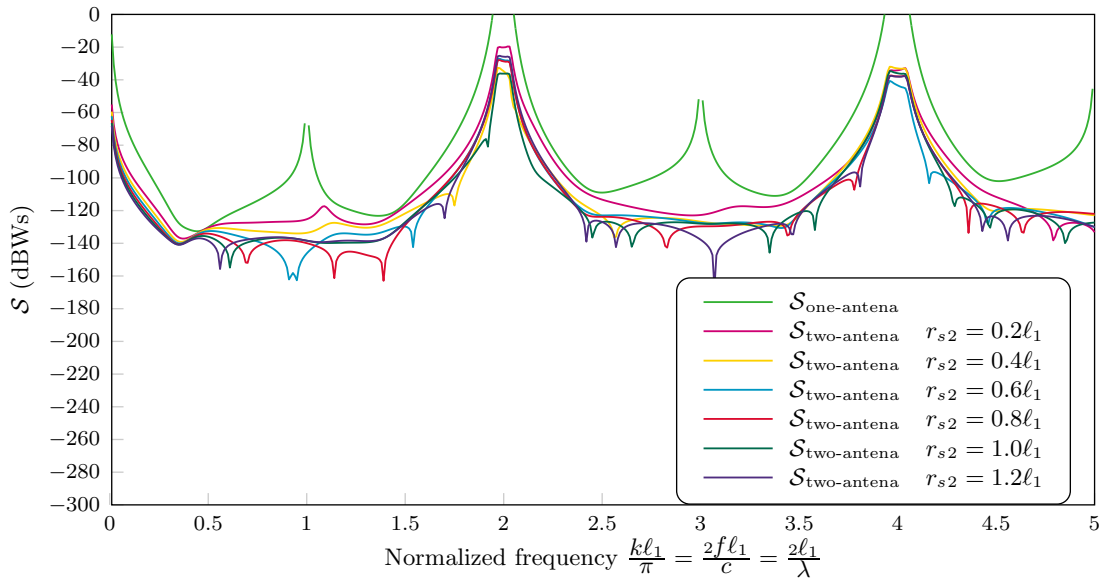


Figure 4.10: Power spectral density for which at the output of the system, the magnitude of the signal contribution is equal to the magnitude of the thermal noise of the front end in Configuration 1

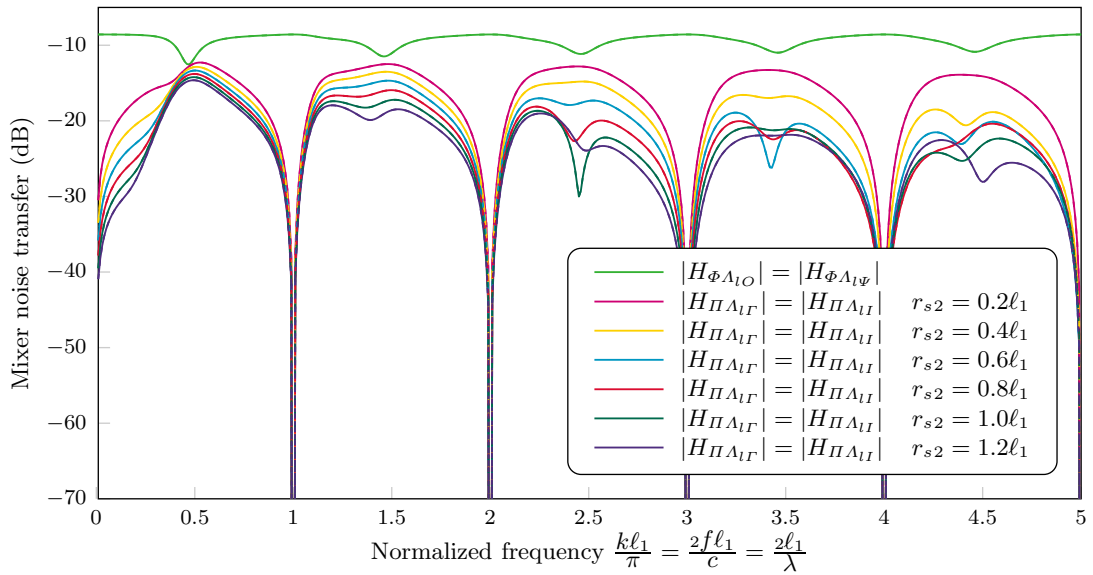


Figure 4.11: Transfer function of noise at the mixer inputs to the cross power spectral density at the mixer inputs

indicate that these noisy resistors cause a current in opposite directions through the load impedances. If we look at the magnitude of the cross-PSD, we see that the one-antenna system suffers from higher thermal noise than the two-antenna systems that are shown. This confirms the reason for considering a two-antenna system: reduction of correlated noise.

At frequencies for which the antenna lengths 2ℓ are odd multiples of 0.5λ , the dipole antennas are known to “work best”: they radiate energy easily. This causes peaks in Figure 4.8. In case of a one antenna system these are the frequencies at which a large portion of the noise is radiated, such that a smaller portion is reflected back into the system, resulting in a lower absolute noise cross-PSD at the mixer inputs. In case of two antennas it is the other way around: Because at these frequencies a large portion of noise from one branch of the system is radiated by one antenna and picked up by the other, we get an increase in absolute noise cross-PSD.

As expected, a larger separation of the antennas yields a lower absolute amount of noise cross-PSD. We can see that in case of a larger separation, the value can be positive. At higher frequencies, the peaks appear to be lower.

We should also look at the transfer of signals. Because of the symmetry in Configuration 1, we find real values, as shown in Figure 4.9. Even in a decibel scale we see a large variation in signal reception in every case. This is one of the reasons why dipole antennas are not suitable for wideband systems. Compared to these variations the differences between different antenna spacings are almost imperceptible. Below a normalized frequency of 2, the signal reception appears to become a few decibels higher at a larger antenna spacing. This can be specific to the plotted cases, as the antenna spacing determines how well the receiver impedance is matched to the antennas. Above a normalized frequency of 2.5 we see that all but the closest two-antenna case result in a higher signal perception of about 5 dB.

In Figure 4.10 the parameter \mathcal{S} , as defined in Equation 4.40 and Equation 4.41 on Page 51, is plotted. This is the power spectral density for which at the output of the system, the magnitude of the signal contribution is equal to the magnitude of the thermal noise of the front end, so a higher value indicates that the transmitter must have a higher power in order to be still received by our system. First of all we see that in all plotted cases, the two-antenna systems have a better performance than the one-antenna system. The closest spacing yields a slightly worse performance than the other two-antenna cases, but the other spacings yield comparable results, depending on the frequency.

The most remarkable thing is that the peak at odd values of the normalized frequency, which is clearly visible in the one-antenna case and which could be expected from the preceding plots, is gone in all two-antenna cases. This means that the two-antenna systems can be used close to these frequencies as far as thermal noise is concerned. We must remember, however, that this effect does not occur in case of additional sources of coupled noise in the receiver, such as power lines. Such sources will have a relatively large influence near these odd normalized frequencies.

In Figure 4.11 we see the magnitude of the transfer function from a noise source in series with either of the mixers to the cross-PSD at the mixer inputs. Because we only have a series impedance between the antennas and the mixers, this plot shows almost the same information as Figure 4.8.

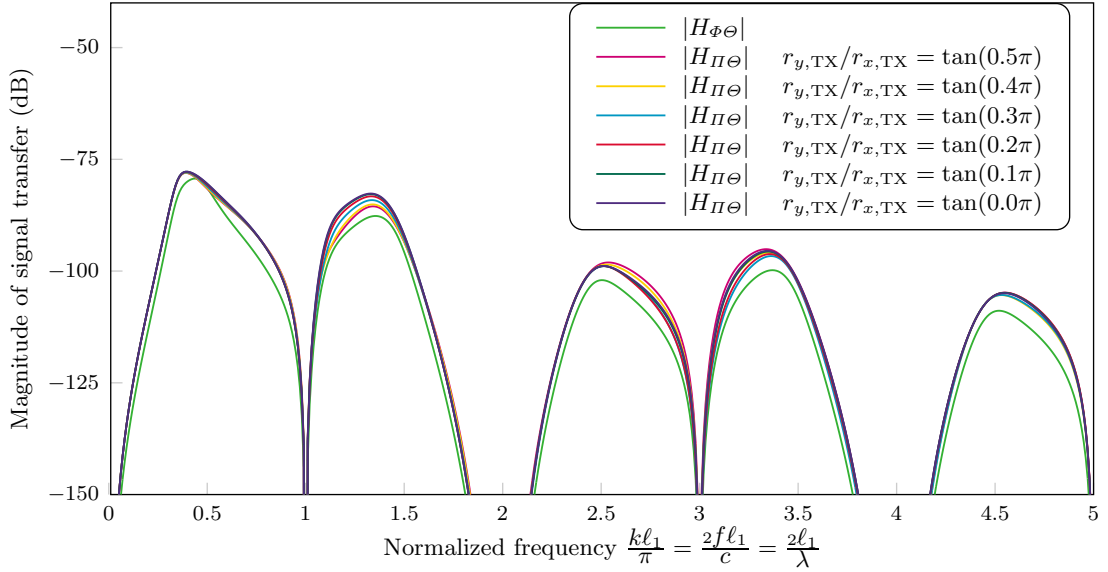


Figure 4.12: Magnitude of the signal transfer function to the cross power spectral density at the mixer inputs in Configuration 2

Configuration 1 shows the expected benefit from using a two-antenna system: less coupled noise. The disadvantage of using two antennas is that in general the signal as received by the antennas is unequal. This does not show up in Configuration 1, because the transmitter is on the perpendicular bisector of the two antennas. In Configuration 2 the distance between the antennas is fixed and the transmitter is chosen at different positions at a quarter circle in the plane $z = 0$ at a distance of $1000\ell_1$. The other parameters are equal to Configuration 1.

Configuration 2:

$r_{x,\text{one}} \triangleq 0$	$r_{x,\text{TX}} = 0$	$r_{x1} = 0.5\ell_1$	$r_{x2} = -r_{x1}$
$r_{y,\text{one}} \triangleq 0$	$r_{y,\text{TX}} = \text{variable}$	$r_{y1} \triangleq 0$	$r_{y2} \triangleq 0$
$r_{z,\text{one}} \triangleq 0$	$r_{z,\text{TX}} = \text{variable}$	$r_{z1} = 0$	$r_{z2} = 0$
$\ell_{\text{one}} = \ell_1$	$\ell_{\text{TX}} = \ell_1$	$\ell_1 = \text{unit}$	$\ell_2 = \ell_1$
$a_{\text{one}} = \ell_{\text{one}}/100$	$a_{\text{TX}} = \ell_{\text{TX}}/100$	$a_1 = \ell_1/100$	$a_2 = \ell_2/100$
$R_s = 0$	$r_{s,\text{TX}} = 1000\ell_1$	$Z_{\Xi} = \overline{\mathbf{Z}}_{0,\text{TX},\text{TX}}$	
$R_{a_{\psi}} = 100\Omega$	$R_{a_o} = 100\Omega$	$R_{a_I} = 100\Omega$	$R_{a_r} = 100\Omega$
$R_{b_{\psi}} = \infty\Omega$	$R_{b_o} = \infty\Omega$	$R_{b_I} = \infty\Omega$	$R_{b_r} = \infty\Omega$
$R_{c_{\psi}} = 0\Omega$	$R_{c_o} = 0\Omega$	$R_{c_I} = 0\Omega$	$R_{c_r} = 0\Omega$
$R_{l_{\psi}} = 50\Omega$	$R_{l_o} = 50\Omega$	$R_{l_I} = 50\Omega$	$R_{l_r} = 50\Omega$

Because in the calculation of the thermal noise cross-PSD, the position of a far transmitter is ignored, the plots in Figure 4.8 of the one-antenna system

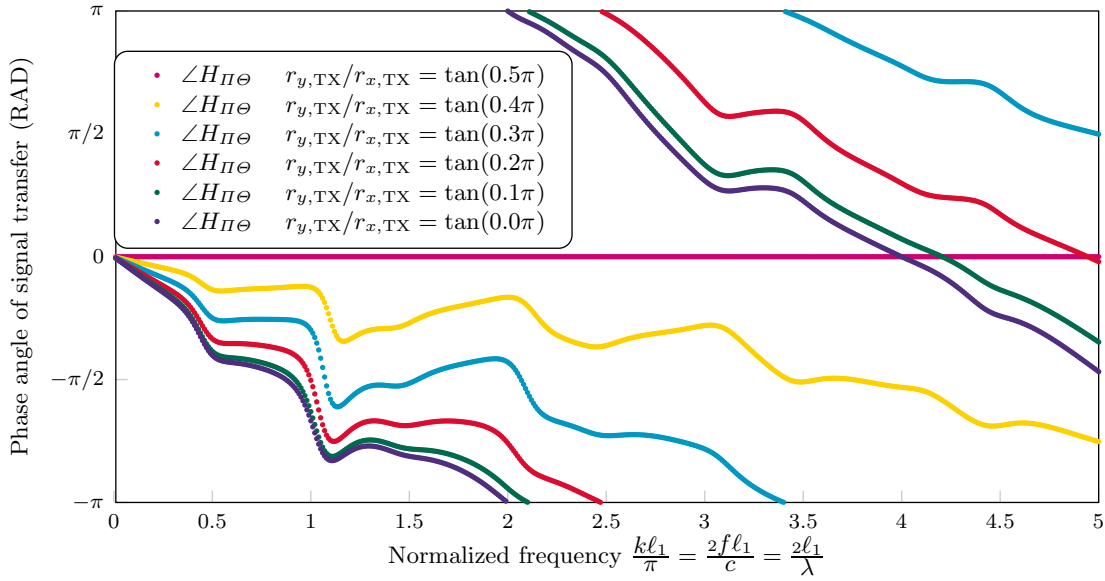


Figure 4.13: Angle of the signal transfer function to the cross power spectral density at the mixer inputs in Configuration 2

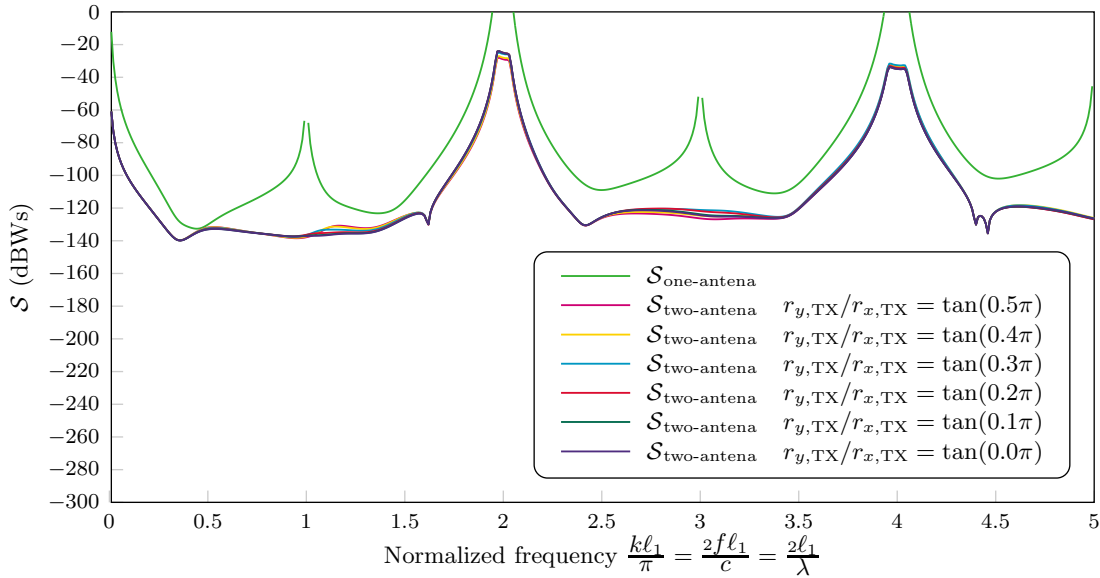


Figure 4.14: Power spectral density for which at the output of the system, the magnitude of the signal contribution is equal to the magnitude of the thermal noise of the front end in Configuration 2

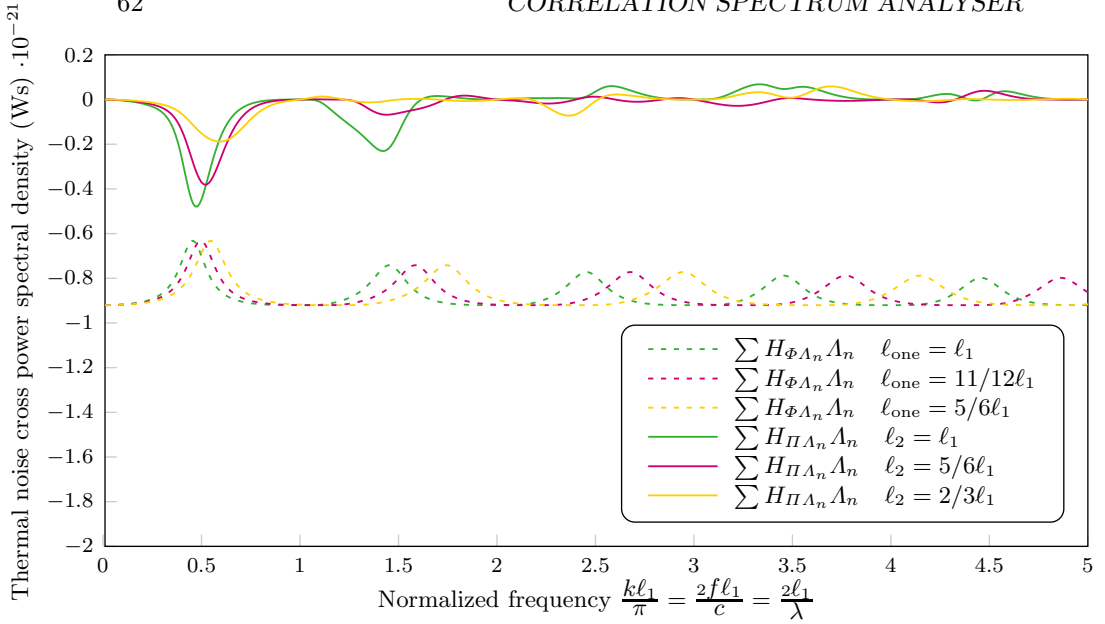


Figure 4.15: Cross power spectral density of at the mixer inputs due to noisy resistors in Configuration 3

and the two-antenna system with an antenna separation of $1.0\ell_1$ are valid for Configuration 2 as well.

Figure 4.12 shows only a small spread. This tells us that the magnitude of the signal transfer function barely depends on the direction of the transmitter in the plane $z = 0$. Figure 4.13 shows this is not the case with the complex angle of the transfer function. When the distance between the transmitter and one antenna and the distance between the transmitter and the other antenna, differs more, the complex angle plot gets steeper. A simple planar wave model of the situation would suggest a linear relation between the complex angle and the normalized frequency. However, because the antenna mutual antenna impedances do not have a constant phase, this relation deviates somewhat from a linear relation. Because in practice we cannot choose the angle of the incident wave, the detector that interprets the measurements of a two-antenna receiver, must be able to deal with a random angle of the incident signal.

In Figure 4.14 we can see again that as far as the magnitude of the signal compared to the noise is concerned, the direction of the transmitter in the plane $z = 0$ barely changes the sensitivity of the two-antenna receiver.

Parallel receiving antennas of different length

As a possibility to optimize the receiver design for some required frequency band, one could think of an asymmetric two-antenna receiver. This could reduce noise coupling or flatten the signal transfer in some frequency band of interest. One possibility to do so, is using antennas of different lengths.

Configuration 3:

$$\begin{array}{llll}
 r_{x,\text{one}} \triangleq 0 & r_{x,\text{TX}} = 0 & r_{x1} = 0.5\ell_1 & r_{x2} = -r_{x1} \\
 r_{y,\text{one}} \triangleq 0 & r_{y,\text{TX}} = 1000\ell_1 & r_{y1} \triangleq 0 & r_{y2} \triangleq 0 \\
 r_{z,\text{one}} \triangleq 0 & r_{z,\text{TX}} = 0 & r_{z1} = 0 & r_{z2} = 0 \\
 \ell_{\text{one}} = \text{variable} & \ell_{\text{TX}} = \ell_1 & \ell_1 = \text{unit} & \ell_2 = \text{variable} \\
 a_{\text{one}} = \ell_{\text{one}}/100 & a_{\text{TX}} = \ell_{\text{TX}}/100 & a_1 = \ell_1/100 & a_2 = \ell_2/100 \\
 R_s = 0 & Z_{\Xi} = \overline{\mathbf{Z}_{0,\text{TX},\text{TX}}} & & \\
 R_{a_{\text{v}}} = 100\Omega & R_{a_{\text{O}}} = 100\Omega & R_{a_{\text{I}}} = 100\Omega & R_{a_{\text{r}}} = 100\Omega \\
 R_{b_{\text{v}}} = \infty\Omega & R_{b_{\text{O}}} = \infty\Omega & R_{b_{\text{I}}} = \infty\Omega & R_{b_{\text{r}}} = \infty\Omega \\
 R_{c_{\text{v}}} = 0\Omega & R_{c_{\text{O}}} = 0\Omega & R_{c_{\text{I}}} = 0\Omega & R_{c_{\text{r}}} = 0\Omega \\
 R_{l_{\text{v}}} = 50\Omega & R_{l_{\text{O}}} = 50\Omega & R_{l_{\text{I}}} = 50\Omega & R_{l_{\text{r}}} = 50\Omega
 \end{array}$$

In Configuration 3 the length of the antenna of the one-antenna system is altered as well in such a way that its length is the average between the lengths of the antennas of the two-antenna system.

The plots in Figure 4.15 show what happens to the thermal noise cross-PSD. In the plots about the one-antenna system we see a horizontal stretch, because the normalized frequency is linearly dependent on the antenna length. In the two antenna system the peaks corresponding to both antennas are shifted (and stretched) with respect to each other. Therefore the graphs show that in these cases a more unequal antenna length yields some lower and shifted combined peaks.

If we take a look at Figure 4.16, we immediately notice the extra zeros resulting from the second antenna. This comes with the advantage that the zeros corresponding to the length of the first antenna are smaller in frequency, compared to the case of equal lengths. This is most clear near the normalized frequency of 2, where the dip of the equal length case in green is clearly wider than the dip of the unequal length case plots.

Because the two-antenna system is no longer symmetric, the phase angle of the signal transfer is no longer zero, even though the transmitter is on the perpendicular bisector of the two antennas. This phase angle is shown in Figure 4.17. We see a lot of phase jumps at the zeros of the transfer magnitude. The reason these jumps do not occur when the antenna lengths are equal is that in that case both antennas jump at the same frequency, cancelling each other. A phase inversion is very inconvenient for a detector: If we look at a transmitter that radiates a signal in a band that happens to be right across a phase jump in the receiver, a part of the signal will have the opposite sign compared to the rest of the signal. This causes (partial) self-cancellation in the measurement, which obviously hinders signal detection. Also, apart from the jumps, the phase plots are rather steep at some points. This also makes

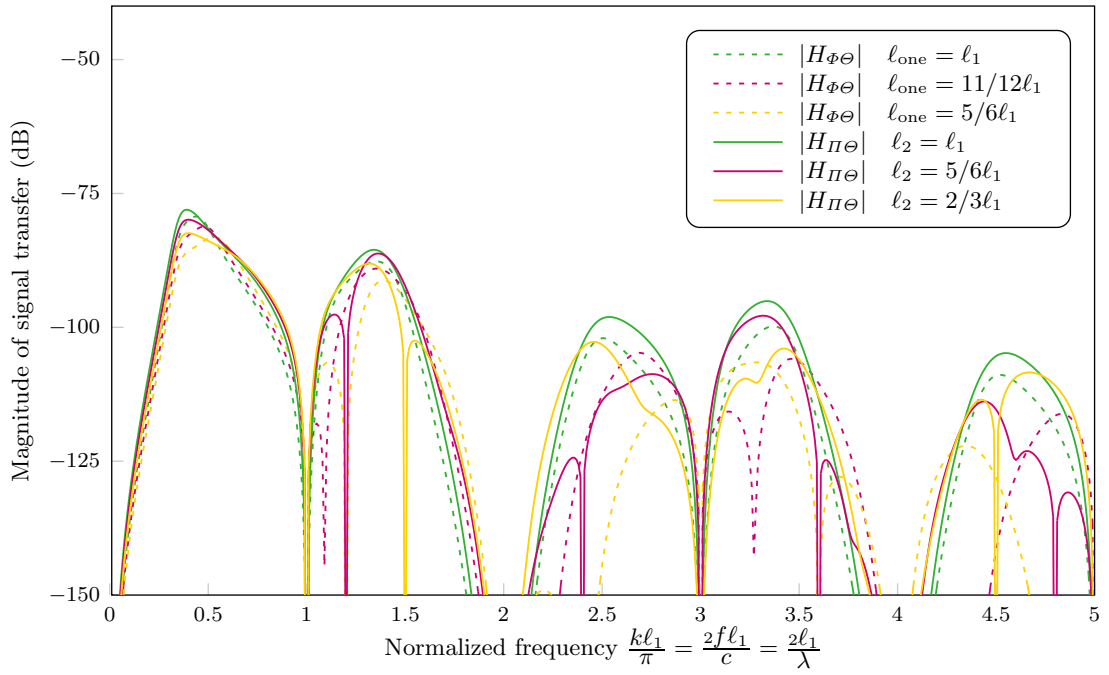


Figure 4.16: Magnitude of the signal transfer function to the cross power spectral density at the mixer inputs in Configuration 3

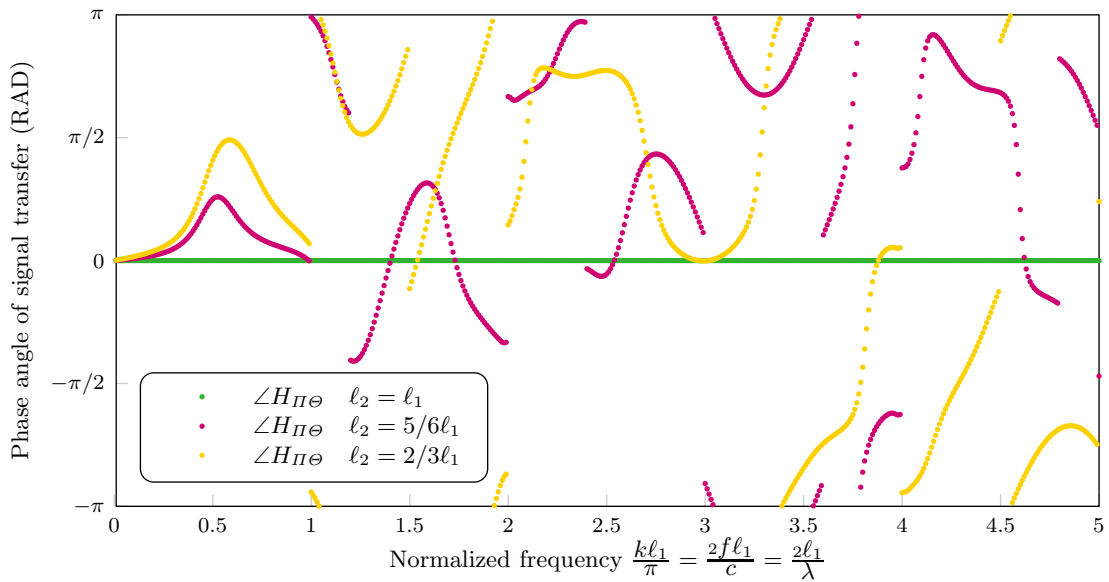


Figure 4.17: Angle of the signal transfer function to the cross power spectral density at the mixer inputs in Configuration 3

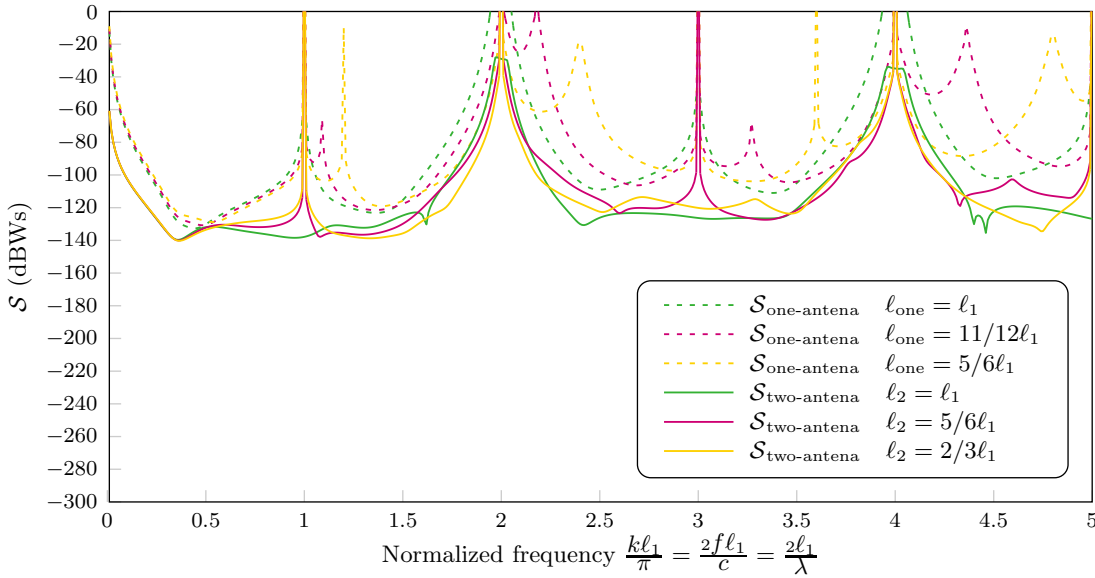


Figure 4.18: Power spectral density for which at the output of the system, the magnitude of the signal contribution is equal to the magnitude of the thermal noise of the front end in Configuration 3

detection more difficult. Please note that if we were to build any of these asymmetric systems, we will not know the direction of the transmitter, so the actual phase plot is unknown. To use such a system, we must use a detector that can cope with random, steeply varying, phases. This probably requires measurements with a relatively high frequency resolution.

In Figure 4.18 we can see that it differs from one frequency to another whether the sensitivity is improved by choosing unequal antenna lengths. For example between a normalized frequency of 1 and 2, we see that a design with $\ell_2 = 2/3\ell_1$ in yellow yields a higher sensitivity than the design with antennas of equal length in green, provided that the detector can cope with the variation in phase angle.

Collinear antennas

Another approach to reduce the coupling between the receiving antennas is to put them in a collinear position. In this way the coupling will be already quite low at a moderate spacing between the antennas, as we are about to see. However, if we have to integrate the antennas in a mobile device, the total length of both antennas and their spacing will have to be smaller than the length of the device. In case of parallel antennas, both antennas separately need to be smaller than the length of the device and their spacing needs to be smaller than the width of the device. This means that in practice the antennas can be about twice as long in the parallel configuration as in the collinear configuration.

Because of the circular symmetry, a receiver with two collinear antennas will

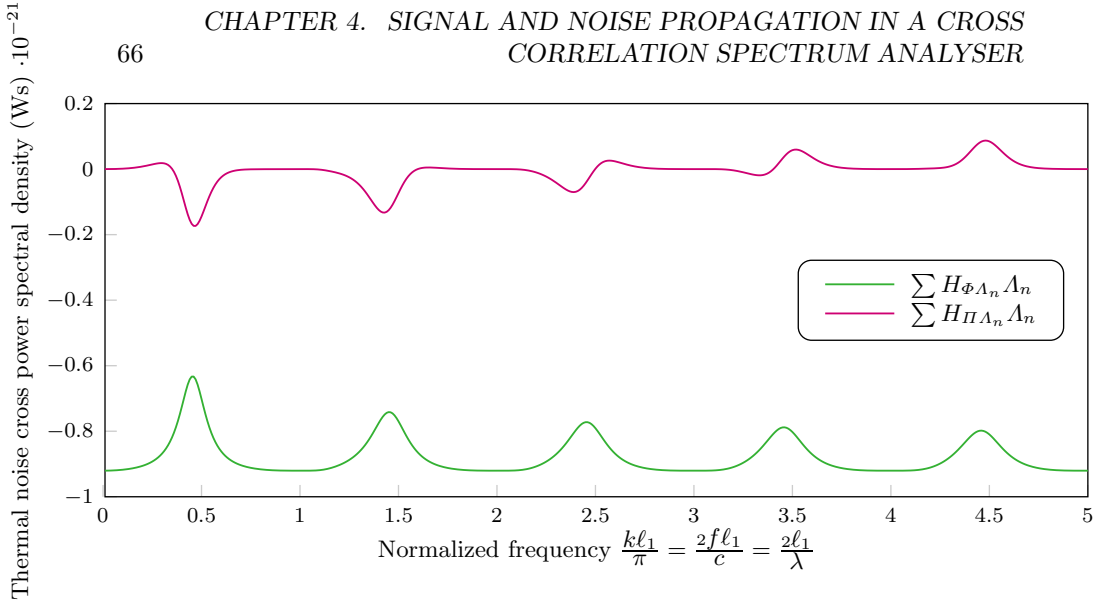


Figure 4.19: Cross power spectral density of at the mixer inputs due to noisy resistors in Configuration 4

be indifferent to the direction of a transmitter in the plane $z = 0$, but it will be sensitive to the elevation angle in the plane $y = 0$. Especially when the antenna of the transmitter is collinear with the antennas of the receiver, practically no signal is received. This is due to the well-known doughnut-shaped (far-field) antenna pattern of dipole antennas. In Configuration 4 the elevation angle is varied, while the receiver is fixed.

Configuration 4:

$r_{x,\text{one}} \triangleq 0$	$r_{x,\text{TX}} = 0$	$r_{x1} = 0$	$r_{x2} = -r_{x1}$
$r_{y,\text{one}} \triangleq 0$	$r_{y,\text{TX}} = \text{variable}$	$r_{y1} \triangleq 0$	$r_{y2} \triangleq 0$
$r_{z,\text{one}} \triangleq 0$	$r_{z,\text{TX}} = \text{variable}$	$r_{z1} = 1.1\ell_1$	$r_{z2} = -1.1\ell_1$
$\ell_{\text{one}} = \text{variable}$	$\ell_{\text{TX}} = \ell_1$	$\ell_1 = \text{unit}$	$\ell_2 = \ell_1$
$a_{\text{one}} = \ell_{\text{one}}/100$	$a_{\text{TX}} = \ell_{\text{TX}}/100$	$a_1 = \ell_1/100$	$a_2 = \ell_2/100$
$R_s = 0$	$\sqrt{r_{y,\text{TX}}^2 + r_{z,\text{TX}}^2} = 1000\ell_1$	$Z_{\Xi} = \overline{\mathbf{Z}}_{0,\text{TX},\text{TX}}$	
$R_{a_y} = 100\Omega$	$R_{a_o} = 100\Omega$	$R_{a_l} = 100\Omega$	$R_{a_r} = 100\Omega$
$R_{b_y} = \infty\Omega$	$R_{b_o} = \infty\Omega$	$R_{b_l} = \infty\Omega$	$R_{b_r} = \infty\Omega$
$R_{c_y} = 0\Omega$	$R_{c_o} = 0\Omega$	$R_{c_l} = 0\Omega$	$R_{c_r} = 0\Omega$
$R_{l_y} = 50\Omega$	$R_{l_o} = 50\Omega$	$R_{l_l} = 50\Omega$	$R_{l_r} = 50\Omega$

If we compare Figure 4.19 to Figure 4.8 on Page 57, we see that the coupling of noise in the collinear position at low frequencies, is lower than all plotted parallel configurations, while the space between the tips of the antennas is only $0.2\ell_1$. We could place the antennas even closer in practice, but in that case our model will probably not be accurate, due to capacitive effects between the antenna tips that alter the current distribution in the antennas.

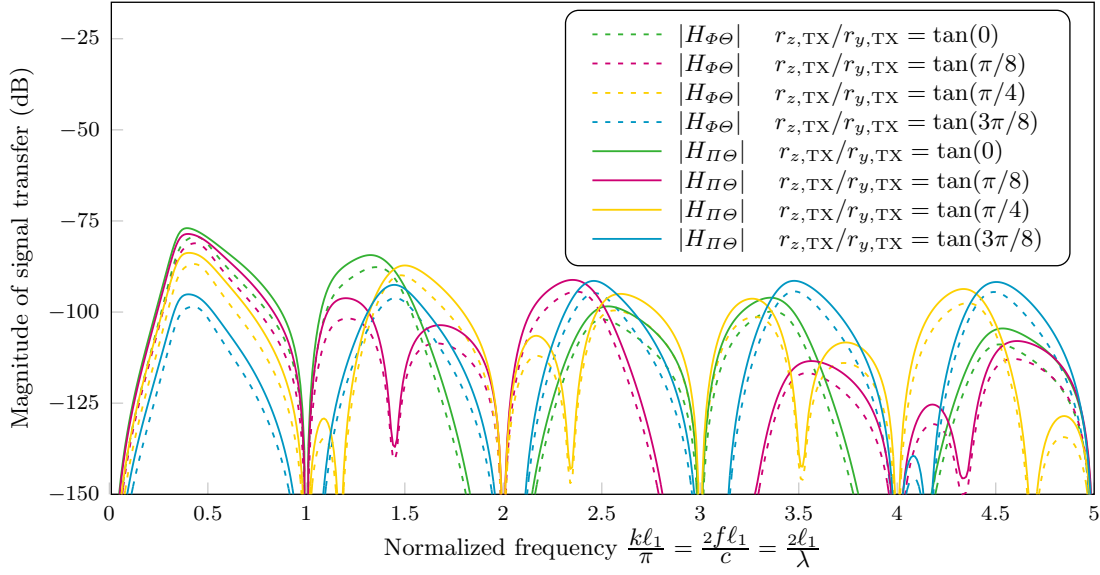


Figure 4.20: Magnitude of the signal transfer function to the cross power spectral density at the mixer inputs in Configuration 4

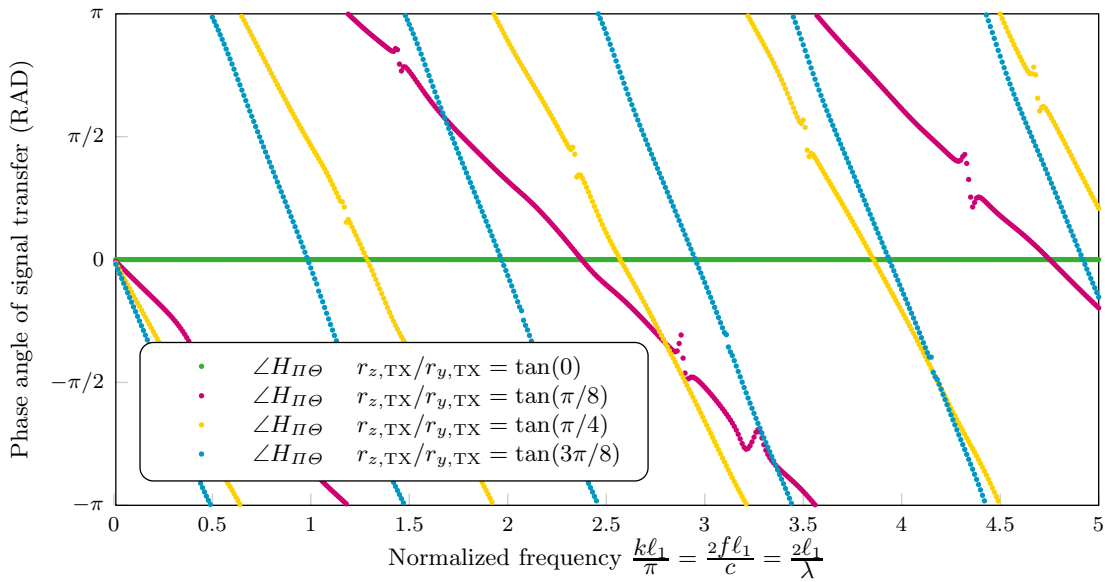


Figure 4.21: Angle of the signal transfer function to the cross power spectral density at the mixer inputs in Configuration 4

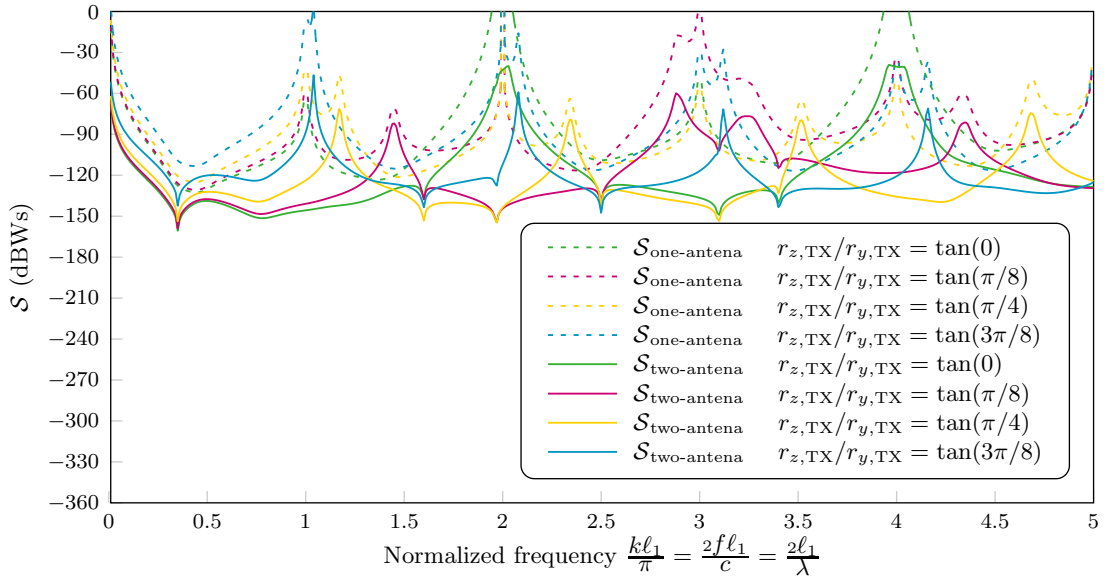


Figure 4.22: Power spectral density for which at the output of the system, the magnitude of the signal contribution is equal to the magnitude of the thermal noise of the front end in Configuration 4

In Figure 4.20 we see the transfer of signal from a transmitter at different elevation angles. The first thing we notice is that besides the zeros that correspond to the antenna length, some extra zeros show up. This means that the receiver will have blind spots, each consisting of a combination of a direction and a frequency of a transmitter. For example at a normalized frequency just below 1.5, we see that a transmitter at an elevation angle of $\pi/8$ RAD has a transfer that is about -50dB compared to a transmitter that is at an elevation angle of 0 RAD or $\pi/4$ RAD. The second thing we notice about Figure 4.20 is that the transfers of the one-antenna system are almost parallel to those of the two-antenna system. This is because the transmitter at a large distance has about an equal position with respect to each of the three receiving antennas, while the coupling between the antennas of the two-antenna system is negligible. This means that the attenuation of the signal at each of the receiving antennas is about equal and the major difference is the splitter that reduces the total power measured by the one-antenna system. This tells us that the blind spots at different elevation angles are not due to the use of dipole antennas, rather than the collinear positioning.

Because of a different path length between the transmitter and each of the receivers, there is a phase shift of the signal cross-PSD at the mixer inputs, as shown in Figure 4.21. This phase shift is notably higher than the phase shift seen at feasible parallel configurations, shown in Figure 4.13 on Page 61.

Figure 4.22 shows what we already suspected from Figure 4.20: The sensitivity of the system varies largely, depending on the elevation angle, but in all cases the two-antenna system is more sensitive than the one-antenna system.

Different attenuators

Apart from the antennas, we can also change the attenuator. Please recall that the input attenuator is part of the design, because an attenuation before the non-linear parts of the system improves the linearity of the system as a whole, as a trade-off against SNR. [7] In Figure 3.16 on Page 30 it was already seen that if we enlarge the ohmic load of two dipole antennas, the transfer function between the two has a flatter, attenuated magnitude and a smoother phase curve. When we assume we cannot change the input resistances of the mixers R_{l*} , we can increase the load as seen from the antenna terminals by increasing the series resistances R_{a*} . By doing so we increase both the ohmic load of the antenna and the attenuation, so we increase both the smoothness of the transfer function and the linearity of the system as a whole, at the cost of a lowering of the SNR.

It seems to be not beneficial to include the parallel resistances R_{b*} , for it will increase the attenuation, but also decrease the load as seen from the antenna terminals, which is undesired. However, one may want to use R_{b*} in combination with capacitors or inductors to optimize the receiver for a certain frequency band. This optimization is out of the scope of this report.

Another reason for including the parallel resistances is that the thermal noise of the series impedances most of the times have a negative contribution to the cross-glspsd, whereas the parallel resistances have a positive contribution. By choosing the resistances carefully it might be possible to bring the expectation of the thermal noise cross-PSD at the mixer inputs closer to zero at the cost of a larger variance, because of the added noise sources. This possibility was also suggested by Smeenge [11, Appendix A]. However, this larger variance makes it more difficult to detect a signal, despite of the zero expectation. After all, we could better subtract any known expectation of the noise cross-PSD from the total measured cross-PSD, to obtain a measurement with a noise expectation of zero *without* increasing the noise variance.

In this example we choose to leave R_{b*} out. Consequently, R_{c*} cannot be distinguished from R_{a*} , so we can leave it at 0Ω .

Configuration 5:

$$\begin{array}{llll}
 r_{x,\text{one}} \triangleq 0 & r_{x,\text{TX}} = 1000\ell_1 & r_{x1} = 0.5\ell_1 & r_{x2} = -r_{x1} \\
 r_{y,\text{one}} \triangleq 0 & r_{y,\text{TX}} = 1000\ell_1 & r_{y1} \triangleq 0 & r_{y2} \triangleq 0 \\
 r_{z,\text{one}} \triangleq 0 & r_{z,\text{TX}} = 0 & r_{z1} = 0 & r_{z2} = 0 \\
 \ell_{\text{one}} = \ell_1 & \ell_{\text{TX}} = \ell_1 & \ell_1 = \text{unit} & \ell_2 = \ell_1 \\
 a_{\text{one}} = \ell_{\text{one}}/100 & a_{\text{TX}} = \ell_{\text{TX}}/100 & a_1 = \ell_1/100 & a_2 = \ell_2/100 \\
 R_s = 0 & Z_\varepsilon = \overline{\mathbf{Z}}_{0,\text{TX},\text{TX}} & & \\
 R_{a\psi} = \text{variable} & R_{aO} = R_{a\psi} & R_{aI} = R_{a\psi} & R_{a\Gamma} = R_{a\psi} \\
 R_{b\psi} = \infty\Omega & R_{bO} = \infty\Omega & R_{bI} = \infty\Omega & R_{b\Gamma} = \infty\Omega \\
 R_{c\psi} = 0\Omega & R_{cO} = 0\Omega & R_{cI} = 0\Omega & R_{c\Gamma} = 0\Omega \\
 R_{l\psi} = 50\Omega & R_{lO} = 50\Omega & R_{lI} = 50\Omega & R_{l\Gamma} = 50\Omega
 \end{array}$$

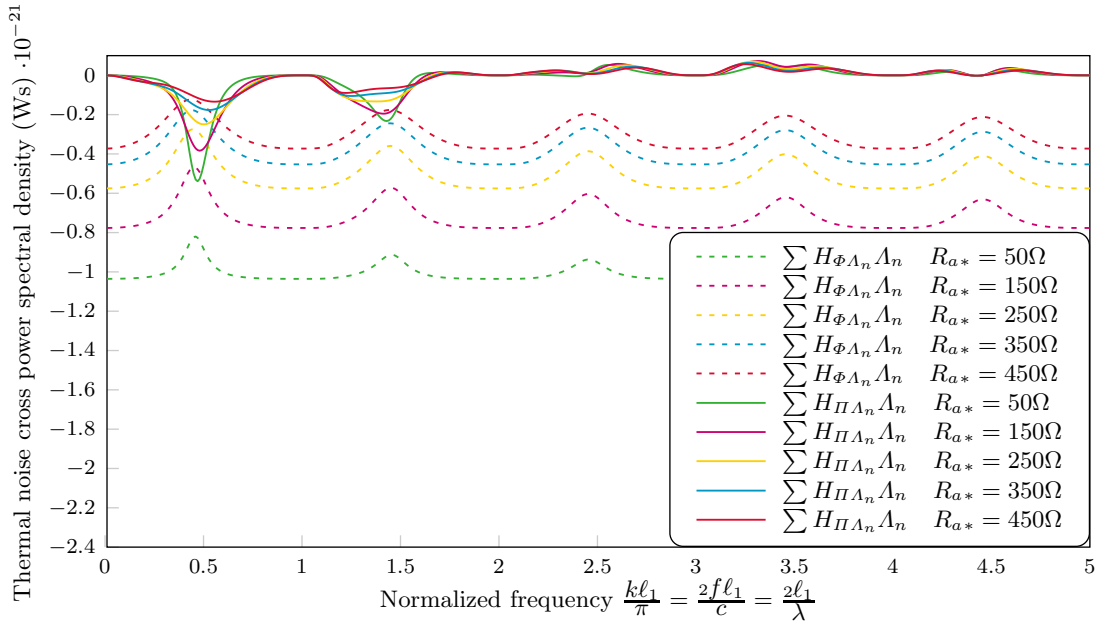


Figure 4.23: Cross power spectral density of at the mixer inputs due to noisy resistors in Configuration 5

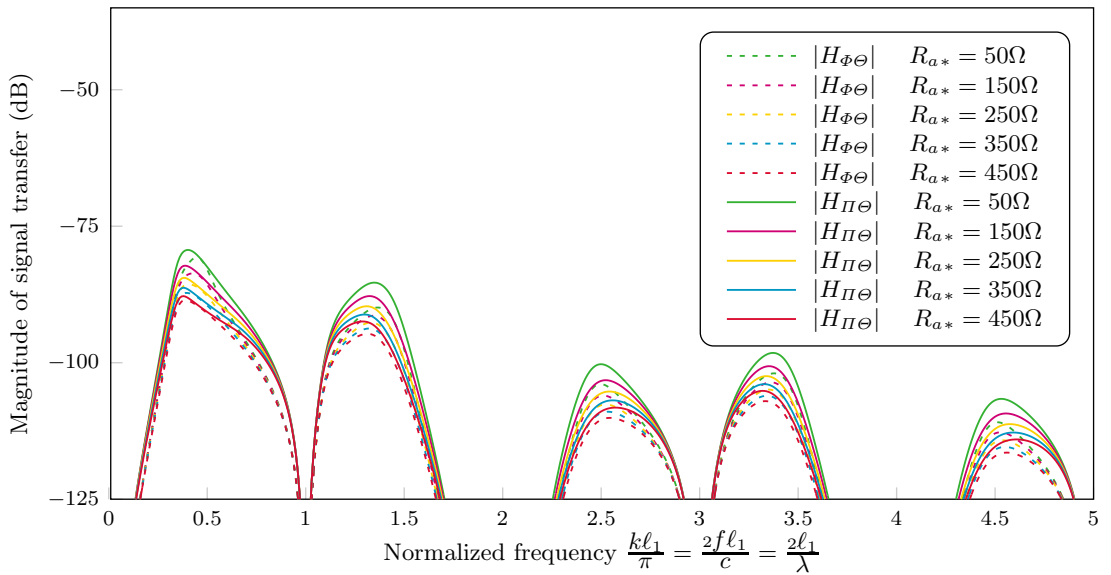


Figure 4.24: Magnitude of the signal transfer function to the cross power spectral density at the mixer inputs in Configuration 5

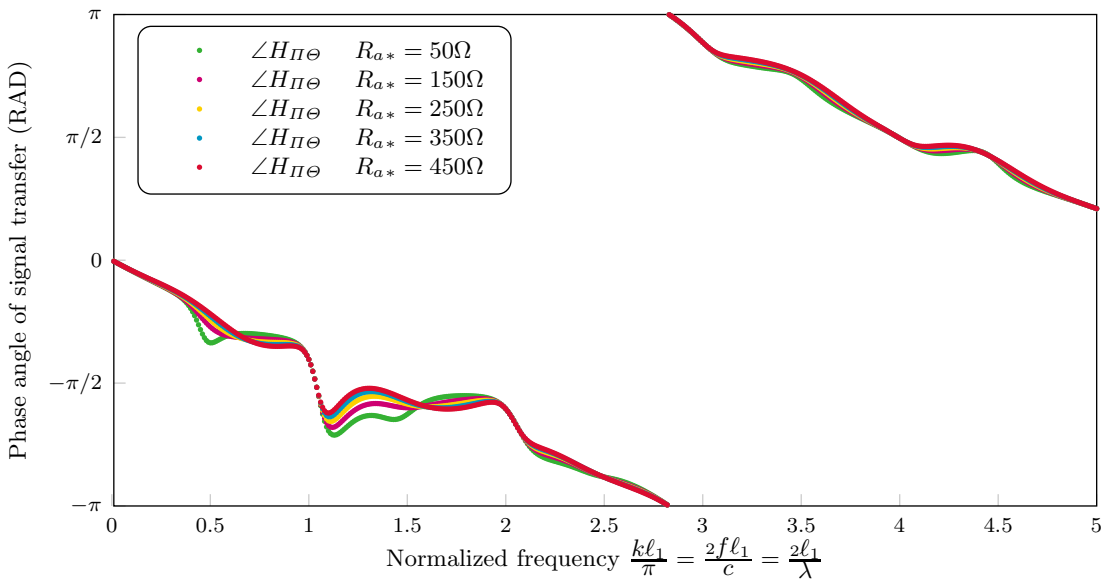


Figure 4.25: Angle of the signal transfer function to the cross power spectral density at the mixer inputs in Configuration 5

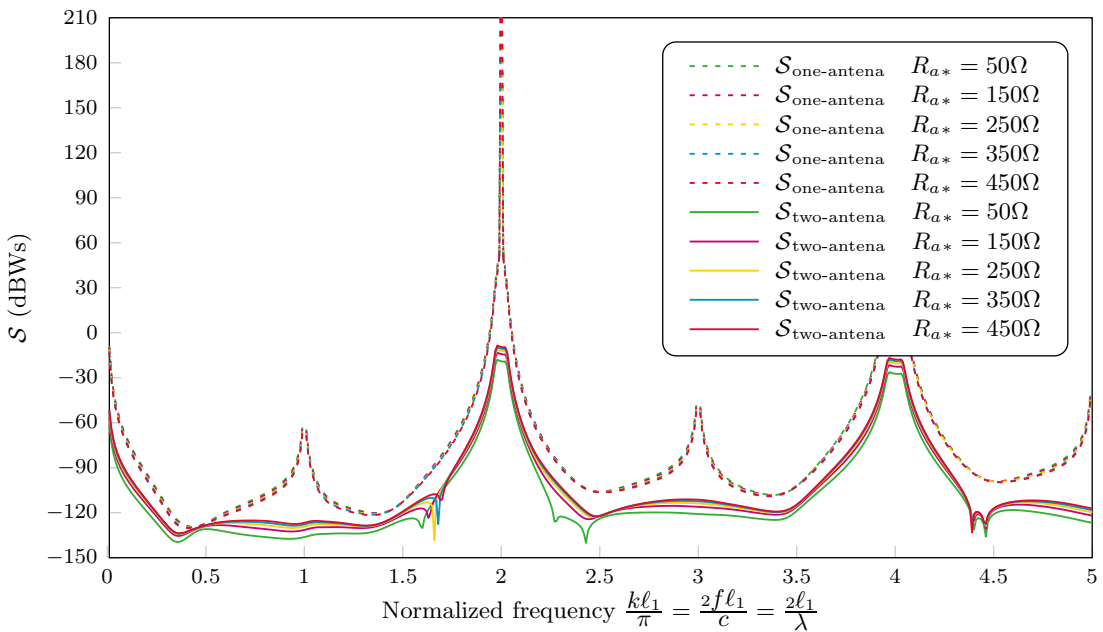


Figure 4.26: Power spectral density for which at the output of the system, the magnitude of the signal contribution is equal to the magnitude of the thermal noise of the front end in Configuration 5

In Figure 4.23 we see that an increase of the series impedance lowers the absolute noise level of the one-antenna system greatly. We see that the peaks of the curves belonging to the two-antenna system become lower and wider as the series impedances increase, such that the curve becomes flatter.

The flattening of the transfer functions can be seen in in Figure 4.24, especially below a normalized frequency of 1. This is the case for both the one-antenna system and the two-antenna system. We also see an overall decrease of the magnitude of the transfer functions, as expected. Because in Configuration 5 the transmitter is placed in the plane $z = 0$ at an angle of $\pi/4$ RAD to the parallel antennas, the signal transfer function has a non-zero phase curve, as shown in Figure 4.25. We see that an increase of the series impedances tends to flatten the phase plot, towards a linear decay.

Because both the amount of signal and the amount of noise in the cross-PSD at the mixer inputs is decreased by the series impedance, we have to take a look at Figure 4.26 to see the overall effect on the sensitivity of the system. For the two-antenna system the sensitivity appears to be reduced by an increase of the series resistance, at least in the plotted cases. The sensitivity of the one-antenna system is barely changed by the larger resistance. A larger series impedance yields a small increase in sensitivity, but still far worse than the sensitivity of the two-antenna system.

4.4 Summary

In this chapter, we have derived expressions for the signal and noise contributions to the expected measurement by both a two-antenna receiver and a one-antenna receiver.

For this purpose we assumed that there is no coupling between the two receiver paths after the mixers and that these receiver paths could each be modelled as linear and time-invariant. We showed that under these assumptions, the expectation of the output of the system is linearly dependent on the cross-PSD of the signals that enter the mixers. Because this linear dependency is the same for both one-antenna receivers and two-antenna receivers, this allowed us to compare these receivers by looking only at their analogue front ends.

Using the impedance matrix representation of the antenna configuration and straightforward network theory, the voltage transfer functions from all noisy resistors in the receiver to both mixer inputs were calculated and listed. The same was done for the transfer from a signal source. It was shown that there is also a linear PSD transfer function from a signal or noise PSD to the cross-PSD at the mixer inputs, which can be calculated from the two voltage transfer functions to the mixer inputs.

Finally, we selected some configurations consisting of a two-antenna receiver design, a specific transmitter at a known location and a reference one-antenna system. From this moderate selection of designs, it can be concluded that a two-antenna receiver has a lower amount of thermal system noise at its output than a comparable one-antenna receiver. Furthermore, the magnitude of the signal reception of a two-antenna receiver is in most designs higher or about equal to the signal reception of a comparable one-antenna receiver, such that the expectation of a measurement with a two-antenna receiver will have a higher (real) SNR. However, the considered two-antenna systems have a signal PSD transfer function that generally has a non-zero phase, depending on the direction of the signal source relative to the receiver and the distance between the antennas. This increases the demands on the digital part of the receiver and complicates the task of interpreting the measurement results.

Some approaches for optimization of the two-antenna receiver were discussed. Increasing the spacing between two equal parallel receiving antennas appeared not to be beneficial in general above a spacing of about a quarter of the total length of the antennas. Making the system asymmetric by choosing antennas of different lengths, yields very irregular signal PSD transfer functions and should only be considered for optimization at a certain limited frequency band. Receivers with collinear antennas have a low coupling of noise, but have the disadvantage that often the antennas need to be about 50% shorter compared to a parallel configuration, to fit in a casing. Furthermore, measurement with such receivers will suffer from a large phase dependency on the elevation angle of the signal source. It was discussed that a pure resistive attenuator is probably best implemented by means of series resistors only, because it will make the the signal transfer function more flat.

Chapter 5

Conclusion and recommendations

5.1 Conclusion

The research question “What is the effect of antenna coupling on spectrum sensing for cognitive radio using a cross-correlation spectrum analyser with two antennas?”, will be answered by answering the sub-questions.

How can we model antenna coupling?

When antennas are not moving and the medium they are both in is linear, passive and isotropic, the antenna coupling can be modelled in an electric circuit as a linear n -port, where n equals the number of antennas. The electric circuit properties of this linear n -port are fully described by an impedance matrix. The impedance matrix describing the situation of parallel dipole antennas, can be approximated according to the induced electromagnetic force method.

How is the propagation of system noise to the output effected by antenna coupling in a two-antenna xcsa?

The effect of system noise to the output of the considered XCSAs in terms of SNR or as a comparison to another XCSA with the same mixers, ADCs and digital part, can be calculated without a need to know the propagation from the mixer inputs to the system outputs if the branches are uncoupled in this part of the system. Only in that case the expectation of the output of the system will be proportional to the cross-PSD of the voltages at the mixer inputs.

To find this cross-PSD, we need to multiply the noise spectrum of each noise source with the voltage transfer function to one mixer input times the complex conjugate of the voltage transfer function to the other mixer input. These voltage transfer functions were found using circuit theory. If the receiver is symmetric, the system noise contribution to the output is real-valued, but can be negative. If the system is asymmetric, the noise contribution to the output is generally complex-valued.

In case of a two-antenna receiver with dipole antennas of equal total length 2ℓ , the system noise contribution to the output shows peaks around frequencies for which 2ℓ equals an odd multiple of a half wavelength, because at those frequencies the antenna coupling has a maximum. In case of a one-antenna receiver, we find the opposite: At these frequencies a dip is found, because at

these frequencies the antenna radiates the most system noise power, such that it cannot contribute to the noise power at the output of the system.

How is the measurement of signals effected by using two antennas instead of one?

The magnitude of signal reception by a two-antenna XCSA was seen to be usually higher than the signal reception with a comparable one-antenna receiver. Relatively small deviations occur due to coupling between the receiving antennas.

When measuring a signal with a two-antenna XCSA, the angle of the received PSD will differ, depending on the direction of the transmitter, the frequency and the spacing between the antennas. In case of parallel dipole antennas it was seen that this complex angle is not as linear dependent on the frequency as far-field models suggest. While spectrum sensing for CR, we do not know the direction of a transmitter in advance, so when measuring with two antennas a random phase must be assumed.

Which antenna designs are promising for a two-antenna xcsa for cognitive radio?

Due to the large number of parameters which do not all have a univocal effect on the sensitivity of an XCSA, it is impossible to draw unambiguous conclusions from the limited amount of parameter sweeps that were shown. However, some design approaches seem more promising than others.

A design with parallel dipole antennas of equal length seems to have an optimal distance between the antennas around a quarter of the total length of the antennas. Here “optimal” means the distance for which the ratio between the magnitude of the contribution of thermal system noise and the magnitude of the contribution of the received signal, is not further improved by increasing that distance. Depending on the chosen attenuator, this distance may differ.

A design with dipole antennas of unequal length reduces the noise coupling compared to a similar design with antennas of equal length, but increases the number of zeros in the signal transfer and yields a more capricious phase plot of the measurement result. Such a design seems only suitable for spectrum sensing on a relatively small band.

A two-antenna receiver with collinear dipole antennas has a real-valued transfer function for signals from transmitters in the H-plane. Furthermore, it has a low coupling between the antennas, which reduces the noise. The only drawbacks of a collinear two-antenna receiver compared to a one-antenna receiver are the large phase shift for signals from transmitters at an elevation angle and the length that is required to fit the antennas in a device.

5.2 Recommendations

Validation

All models in this report are based on calculations. None of the results that are shown are validated by measurements. It would be wise to do so, to ensure that the simplifications that are used in the derivations indeed do not have a large influence on the validity of the model.

Noise variance

In this report we only looked at the expectation of the noise at the output of the system. However, measurement inaccuracies come from *uncertainty* of the noise: both its magnitude and its phase. Knowledge of this uncertainty is required for designing a good detector that interprets the measurements to determine whether or not a signal is present.

Direction-tolerant antenna design

Uncertainty of the direction of a transmitter leads to uncertainty of of the frequency-dependent complex angle of the signal component in the measurement result. This complicates the demands on the detector that interprets the measurement results. One could also try to find an antenna configuration that is less sensitive to the direction of the transmitter, while having a sufficiently small coupling. A possible candidate is a configuration with two orthogonal dipole antennas of which the centres are aligned.

Appendix A

Correlation

This appendix is a reference for the stochastic signal theory required in this report. The information is mostly based on [13].

A.1 Stochastic process

The concept of a stochastic process is fundamental to statistical signal processing, but it is often found difficult to understand on first encounter. We will use an example to explain this concept.

Suppose we have a regular die with each side marked with a different number of dots between one and six. A die is usually used to obtain a *random number* between one and six. Therefore we throw the die and discern between six possible results, being either side facing upwards. These six results are called the *sample space*. To each outcome in the sample space we assign a number, being the number of dots on the side facing upward. In mathematics this rather trivial process can be written down as a sample space $\mathcal{S} = \{s_1, s_2, \dots, s_6\}$ with $s_1 \triangleq$ "The side with one dot is facing upward" and so on. Next we have a well-defined process $X(s)$ according to which we assign a number to each event in the sample space: $X(s_1) \triangleq 1$, $X(s_2) \triangleq 2$ and so on.

Now if instead of a number we would assign a function of time to each event in the sample space, we get a well-defined process $X(t, s)$ according to which we assign a function to each event in the sample space \mathcal{S} . We could for example define $X(t, s_1) \triangleq \sin(t)$, $X(t, s_2) \triangleq \cos(t)$, $X(t, s_3) \triangleq 0$, or whatever suits our needs and obtain a function of time by rolling the die. This process $X(t, s)$ is called a stochastic process.

A.2 Cumulative probability distribution function

The size of the sample space associated with a stochastic process is not necessarily a finite number. It can be infinite or continuous as well. The latter is the case when we use a stochastic variable to describe the thermal noise of a resistor, for example. Furthermore the probability for each outcome within the sample space is not necessarily equal. To describe a stochastic process mathematically the cumulative probability distribution function is defined for a fixed instant of time as:

$$F_X(x_1; t_1) \triangleq P\{X(t_1, s) \leq x_1\} \quad (\text{A.1})$$

The cumulative probability distribution function is a monotonically rising function from $\lim_{x_1 \rightarrow -\infty} F_X(x_1; t_1) = 0$ to $\lim_{x_1 \rightarrow \infty} F_X(x_1; t_1) = 1$. When two random values are considered by looking at the same stochastic process at two instants of time:

$$F_X(x_1, x_2; t_1, t_2) \triangleq P\{X(t_1, s) \leq x_1 \wedge X(t_2, s) \leq x_2\} \quad (\text{A.2})$$

When two random values are considered by looking at two stochastic processes, the joint cumulative probability distribution function is defined as:

$$F_{XY}(x_1; y_1; t_1; t'_1) \triangleq P\{X(t_1, s) \leq x_1 \wedge Y(t'_1, s) \leq y_1\} \quad (\text{A.3})$$

A.3 Probability density function

The (joint) PDF is found by taking the derivative of the (joint) cumulative probability distribution functions:

$$f_X(x_1; t_1) \triangleq \frac{\partial F_X(x_1; t_1)}{\partial x_1} \quad (\text{A.4})$$

$$f_X(x_1, x_2; t_1, t_2) \triangleq \frac{\partial^2 F_X(x_1, x_2; t_1, t_2)}{\partial x_1 \partial x_2} \quad (\text{A.5})$$

$$f_{XY}(x_1; y_1; t_1; t'_1) \triangleq \frac{\partial^2 F_{XY}(x_1; y_1; t_1; t'_1)}{\partial x_1 \partial y_1} \quad (\text{A.6})$$

The PDF $f_X(x_1; t_1)$ describes, roughly speaking, the chance $P\{X(t_1, s) \approx x_1\}$. This can be shown by:

$$\begin{aligned} P\{x_1 - \epsilon \leq X(t_1, s) \leq x_1 + \epsilon\} &= P\{X(t_1, s) \leq x_1 + \epsilon\} - P\{X(t_1, s) \leq x_1 - \epsilon\} \\ &= F_X\{x_1 + \epsilon; t_1\} - F_X\{x_1 - \epsilon; t_1\} \\ &= \int_{-\infty}^{x_1 + \epsilon} f_X(x; t_1) dx - \int_{-\infty}^{x_1 - \epsilon} f_X(x; t_1) dx \\ &= \int_{x_1 - \epsilon}^{x_1 + \epsilon} f_X(x; t_1) dx \\ &\approx 2\epsilon f_X(x; t_1) \end{aligned} \quad (\text{A.7})$$

A.4 Averages

The mean value of a stochastic process is a weighted average of all sample functions assigned to a possible outcome in the sample space:

$$\mathbb{E}[X(t_1; s)] \triangleq \int x f_X(x; t_1) dx \quad (\text{A.8})$$

The mean value is a function of time, but may be constant. An other kind of average is the time average:

$$A[X(t; s_1)] \triangleq \lim_{T \rightarrow \infty} \frac{1}{2T} \int_{-T}^T x(t; s_1) dt \quad (\text{A.9})$$

The time average may be different for different sample functions.

A.5 Autocorrelation

The autocorrelation of a real stochastic process is a function of two time parameters, defined according to:

$$\begin{aligned} R_{XX}(t_1, t_1 + \tau) &\triangleq E[X(t_1; s) \cdot X(t_1 + \tau; s)] \\ &= \iint x_1 x_2 f_X(x_1, x_2; t_1, t_1 + \tau) dx_1 dx_2 \end{aligned} \quad (\text{A.10})$$

For many stochastic processes of practical use the autocorrelation does not depend on the absolute time. In that case it can be written as:

$$R_{XX}(t, t + \tau) = R_{XX}(\tau) \quad (\text{A.11})$$

If furthermore $E[X(t_1, s)]$ is independent of t_1 , the process X is called wide-sense stationary. A wide sense stationary process is called ergodic if and only if that process satisfies the following two conditions:

$$A[X(t; s)] \equiv E[X(t; s)] = \text{constant} \quad (\text{A.12})$$

$$A[X(t; s)X(t + \tau; s)] \equiv E[X(t; s)X(t + \tau; s)] = R_{XX}(\tau) \quad (\text{A.13})$$

Proving ergodicity of a stochastic process encountered in practice is hard if not impossible. Usually ergodicity is assumed unless the contrary is evident. In this report when the autocorrelation is discussed, actually the Fourier transform of the autocorrelation of an ergodic process is meant:

$$S_{XX}(\omega) \triangleq \int_{-\infty}^{\infty} R_{XX}(\tau) \exp(-j\omega\tau) d\tau \quad (\text{A.14})$$

The function $S_{XX}(\omega)$ is a measure for the way in which the total power of the process is spread over the different frequency components. Therefore it is called the power spectral density (PSD) or just the power spectrum of the process X .

A.6 Cross-correlation

The cross-correlation of two real stochastic processes is defined according to:

$$\begin{aligned} R_{XY}(t_1, t_1 + \tau) &\triangleq E[X(t_1; s) \cdot Y(t_1 + \tau; s)] \\ &= \iint x_1 y_1 f_X(x_1, y_1; t_1, t_1 + \tau) dx_1 dy_1 \end{aligned} \quad (\text{A.15})$$

In many cases the cross-correlation of two stochastic processes does not depend on the absolute time. In that case it can be written as:

$$R_{XY}(t, t + \tau) = R_{XY}(\tau) \quad (\text{A.16})$$

If this is the case and furthermore the stochastic processes X and Y are wide-sense stationary, X and Y are jointly wide sense stationary. These processes are called jointly ergodic if and only if both of them are ergodic and furthermore:

$$A[X(t; s)Y(t + \tau; s)] \equiv E[X(t; s)Y(t + \tau; s)] = R_{XY}(\tau) \quad (\text{A.17})$$

The function $R_{XY}(\tau)$ is related to $R_{YX}(\tau)$ according to:

$$\begin{aligned} R_{YX}(\tau) &= E[Y(t_1; s) \cdot X(t_1 + \tau; s)] = E[X(t_1 + \tau; s) \cdot Y(t_1; s)] \\ &= E[X(t'_1) \cdot Y(t'_1 - \tau; s)] = R_{XY}(-\tau) \end{aligned} \quad (\text{A.18})$$

In this report when the cross correlation is discussed, actually the Fourier transform of the cross-correlation of two jointly ergodic process is meant:

$$S_{XY}(\omega) \triangleq \int_{-\infty}^{\infty} R_{XY}(\tau) \exp(-j\omega\tau) d\tau \quad (\text{A.19})$$

The function $S_{XY}(\omega)$ is called the cross-power spectral density or just the cross-power spectrum. The cross-power spectrum shows up, for example, when the autocorrelation of the sum of two stochastic processes is calculated:

$$Z(t, s) \triangleq X(t, s) + Y(t, s) \quad (\text{A.20})$$

$$\Rightarrow R_{ZZ}(\tau) = R_{XX}(\tau) + R_{YY}(\tau) + R_{XY}(\tau) + R_{YX}(\tau) \quad (\text{A.21})$$

$$\Rightarrow S_{ZZ}(\omega) = S_{XX}(\omega) + S_{YY}(\omega) + S_{XY}(\omega) + S_{YX}(\omega) \quad (\text{A.22})$$

From this it can be seen (although it is not a complete proof) that the autocorrelation of a sum of processes is equal to the sum of the autocorrelations of those processes, if and only if those processes are uncorrelated: if their cross-power spectrum is zero.

The function $S_{XY}(\omega)$ is related to $S_{YX}(\omega)$ according to:

$$\begin{aligned} S_{YX}(\omega) &= \int_{-\infty}^{\infty} R_{YX}(\tau) \exp(-j\omega\tau) d\tau = \int_{-\infty}^{\infty} R_{XY}(-\tau) \exp(-j\omega\tau) d\tau \\ &= \int_{-\infty}^{\infty} R_{XY}(\tau') \exp(j\omega\tau') d\tau' = \int_{-\infty}^{\infty} \overline{R_{XY}(\tau') \exp(-j\omega\tau')} d\tau' \\ &= \overline{S_{XY}(\omega)} \end{aligned} \quad (\text{A.23})$$

When a wide sense stationary stochastic process $Z(t, s_1)$ is filtered twice in parallel, such that $X(t, s_1) = h_{ZX}(t) * Z(t, s_1)$ and $Y(t, s_1) = h_{ZY}(t) * Z(t, s_1)$,

where the symbol $*$ is the convolution operator. the cross correlation yields:

$$\begin{aligned}
R_{XY}(\tau) &= \text{E} [X(t; s_1) \cdot Y(t + \tau; s - 1)] \\
&= \text{E} \left[\left(h_{ZX}(t) * Z(t, s_1) \right) \cdot \left(h_{YZ}(t + \tau) * Z(t + \tau, s_1) \right) \right] \\
&= \text{E} \left[\int_{-\infty}^{\infty} h_{XZ}(\theta_1) \cdot Z(t - \theta_1) d\theta_1 \cdot \int_{-\infty}^{\infty} h_{YZ}(\theta_2) \cdot Z(t + \tau - \theta_2) d\theta_2 \right] \\
&= \int \int_{-\infty}^{\infty} \text{E} [Z(t - \theta_1) \cdot Z(t + \tau - \theta_2)] \cdot h_{XZ}(\theta_1) \cdot h_{YZ}(\theta_2) d\theta_1 d\theta_2 \\
&= \int \int_{-\infty}^{\infty} R_{ZZ}((\tau + \theta_1) - \theta_2) \cdot h_{XZ}(\theta_1) \cdot h_{YZ}(\theta_2) d\theta_1 d\theta_2 \\
&= \int_{-\infty}^{\infty} \left(R_{ZZ}(\tau + \theta_1) * h_{YZ}(\tau + \theta_1) \right) \cdot h_{XZ}(\theta_1) d\theta_1 \\
&= R_{ZZ}(\tau) * h_{YZ}(\tau) * h_{XZ}(-\tau) \tag{A.24}
\end{aligned}$$

$$\Rightarrow S_{XY}(\omega) = \overline{H_{XZ}(\omega)} \cdot H_{YZ}(\omega) \cdot S_{ZZ}(\omega) \tag{A.25}$$

A.7 Correlation estimator

In this section we will discuss how to estimate a cross-correlation function in practice. The results are valid for an autocorrelation as well, by choosing $Y = X$ and consequently $y(t) \equiv x(t)$.

To measure a correlation function in practice, requires knowledge of all possible functions that can result from a stochastic process as can be seen from Equation A.10. This is not possible. However when (joint) ergodicity is assumed the time average can be used instead of the ensemble average:

$$\begin{aligned}
R_{XY}(\tau) &= R_{XY}(t, t + \tau) && \text{by Equation A.16} \\
&= \text{E} [X(t) \cdot Y(t + \tau)] && \text{by Equation A.15} \\
&= \text{A} [X(t) \cdot Y(t + \tau)] && \text{by Equation A.17} \\
&= \lim_{T \rightarrow \infty} \frac{1}{2T} \int_{-T}^T x(t) \cdot y(t + \tau) dt && \text{by Equation A.9} \tag{A.26}
\end{aligned}$$

This equation can still not be used for measuring, because an infinite amount of time would be required. However an estimate can be made by taking a sufficiently long time in the future, resulting in an implementable calculation:

$$\hat{R}_{XY}(\tau, T) = \frac{1}{T} \int_0^T x(t) \cdot y(t + \tau) dt \tag{A.27}$$

Having estimated the cross-correlation, any suitable estimator for a Fourier transform can be used to obtain the cross-power spectrum.

In this report another approach is used, which is found by rewriting the cross-power spectrum as a function of the Fourier transforms of the input sam-

ple functions:

$$\begin{aligned}
S_{XY}(\omega) &= \int_{-\infty}^{\infty} \left[\lim_{T \rightarrow \infty} \frac{1}{2T} \int_{-T}^T x(t) \cdot y(t + \tau) dt \right] \exp(-j\omega\tau) d\tau \\
&= \lim_{T \rightarrow \infty} \frac{1}{2T} \int_{-T}^T x(t) \exp(j\omega t) \left[\int_{-\infty}^{\infty} y(t + \tau) \exp(-j\omega(t + \tau)) d(t + \tau) \right] dt \\
&= \lim_{T \rightarrow \infty} \frac{1}{2T} \int_{-\infty}^{\infty} \overline{\text{rect}\left(\frac{t}{2T}\right)} x(t) \exp(-j\omega t) \cdot Y(\omega) dt \\
&= \lim_{T \rightarrow \infty} \frac{1}{2T} \left(\frac{2 \sin(\omega T)}{\omega} * X(\omega) \right) \cdot Y(\omega) \\
&= \lim_{T \rightarrow \infty} \left(\frac{\sin(\omega T)}{\omega T} * \overline{X(\omega)} \right) \cdot Y(\omega) \tag{A.28}
\end{aligned}$$

with:

$$\text{rect}\left(\frac{t}{2T}\right) \triangleq \begin{cases} 1 & |t| < T \\ \frac{1}{2} & |t| = T \\ 0 & |t| > T \end{cases} \tag{A.29}$$

The rect-function and its Fourier transform are found in [19]. The result of Equation A.28 shows an unexpected asymmetry, as convolution and multiplication are not mutually distributive or associative, so we cannot remove the brackets. This becomes more clear by using Equation A.23:

$$\begin{aligned}
S_{XY}(\omega) &= \overline{S_{YX}(\omega)} = \overline{\lim_{T \rightarrow \infty} \left(\frac{\sin(\omega T)}{\omega T} * \overline{Y(\omega)} \right) \cdot X(\omega)} \\
&= \lim_{T \rightarrow \infty} \left(\frac{\sin(\omega T)}{\omega T} * Y(\omega) \right) \cdot \overline{X(\omega)} \tag{A.30}
\end{aligned}$$

To give a weak mathematical explanation of why Equation A.28 and Equation A.30 are equivalent, we need the following limit that represents a nascent delta function [20]:

$$\lim_{T \rightarrow \infty} \frac{\sin(\omega T)}{\omega\pi} = \lim_{\epsilon \rightarrow 0} \frac{1}{\omega\pi} \sin\left(\frac{\omega}{\epsilon}\right) = \delta(\omega) \tag{A.31}$$

When applied to either Equation A.28 or Equation A.30 this results in:

$$\begin{aligned}
S_{XY}(\omega) &= \lim_{T \rightarrow \infty} \left(\frac{\pi \sin(\omega\pi)}{T \omega T} * \overline{X(\omega)} \right) \cdot Y(\omega) \\
&= \lim_{T \rightarrow \infty} \left(\frac{\pi}{T} \cdot \delta(\omega) * \overline{X(\omega)} \right) \cdot Y(\omega) \\
&= \lim_{T \rightarrow \infty} \frac{\pi}{T} \cdot \overline{X(\omega)} \cdot Y(\omega) \tag{A.32}
\end{aligned}$$

Although Equation A.32 contains the expected symmetry, the description is not entirely correct. Because $X(\omega)$ and $Y(\omega)$ do not depend on the time period T ,

the limit will either be zero or undefined as:

$$\lim_{T \rightarrow \infty} \frac{\pi}{T} \cdot \delta(\omega - \omega_0) = \begin{cases} \text{undefined} & \omega = \omega_0 \\ 0 & \omega \neq \omega_0 \end{cases} \quad (\text{A.33})$$

While:

$$\lim_{T \rightarrow \infty} \frac{\sin(\omega T)}{\omega T} * \delta(\omega - \omega_0) = \lim_{T \rightarrow \infty} \frac{\sin((\omega - \omega_0)T)}{(\omega - \omega_0)T} = \begin{cases} 1 & \omega = \omega_0 \\ 0 & \omega \neq \omega_0 \end{cases} \quad (\text{A.34})$$

This means the representation in Equation A.32 can only be used when every delta peak in $X(\omega)$ and $Y(\omega)$ is interpreted as:

$$\lim_{T \rightarrow \infty} \delta(\omega) = \begin{cases} \lim_{T \rightarrow \infty} T & \omega = 0 \\ 0 & \omega \neq 0 \end{cases} \quad (\text{A.35})$$

Fortunately, when a finite amount of time is used for estimating the cross-PSD, neither T nor the estimation of the delta peak is infinite, so the problem with an undefined value as in Equation A.33 will not occur. The cross correlation of two jointly ergodic processes can be estimated by approximating Equation A.32 using a finite amount of measurement time that is not in the past:

$$\hat{S}_{XY}(\omega, T) = \frac{2\pi}{T} \cdot \overline{\hat{X}(\omega, T)} \cdot \hat{Y}(\omega, T) \quad (\text{A.36})$$

With:

$$\hat{X}(\omega, T) = \int_0^T x(t) \exp(-j\omega t) dt \quad (\text{A.37})$$

$$\hat{Y}(\omega, T) = \int_0^T y(t) \exp(-j\omega t) dt \quad (\text{A.38})$$

Appendix B

Derivation of the self-impedance of a dipole antenna

This appendix shows how to solve the integral describing the impedance of a dipole antenna according to the induced EMF method as used in Section 3.1 on Page 15.

$$\frac{4\pi}{\eta} Z_m = \int_{-\ell}^{\ell} j \sin(k(\ell - |z|)) \left(\frac{e^{-jkR_1}}{R_1} + \frac{e^{-jkR_2}}{R_2} - 2 \cos(k\ell) \frac{e^{-jkr}}{r} \right) \Big|_{s=a} dz \quad (\text{B.1})$$

with:

$$\begin{aligned} r &= \sqrt{s^2 + z^2} \\ R_1 &\triangleq \sqrt{s^2 + (z - \ell)^2} \\ R_2 &\triangleq \sqrt{s^2 + (z + \ell)^2} \end{aligned}$$

Noting the integrand is even symmetric in $z = 0$:

$$\frac{4\pi}{\eta} Z_m = \int_0^{\ell} \left(e^{jk(\ell-z)} - e^{-jk(\ell-z)} \right) \left(\frac{e^{-jkR_1}}{R_1} + \frac{e^{-jkR_2}}{R_2} - 2 \cos(k\ell) \frac{e^{-jkr}}{r} \right) \Big|_{s=a} dz \quad (\text{B.2})$$

Substitution of R_1 , R_2 and r , combining all exponentials and splitting the integral in a sum of integrals, yields:

$$\begin{aligned}
\frac{4\pi}{\eta} Z_m &= \int_0^\ell \frac{e^{jk(\ell-z-\sqrt{a^2+(z-\ell)^2})}}{\sqrt{a^2+(z-\ell)^2}} dz + \int_0^\ell \frac{e^{jk(\ell-z-\sqrt{a^2+(z+\ell)^2})}}{\sqrt{a^2+(z+\ell)^2}} dz \\
&+ \int_0^\ell -\frac{e^{jk(z-\ell-\sqrt{a^2+(z-\ell)^2})}}{\sqrt{a^2+(z-\ell)^2}} dz + \int_0^\ell -\frac{e^{jk(z-\ell-\sqrt{a^2+(z+\ell)^2})}}{\sqrt{a^2+(z+\ell)^2}} dz \\
&+ \int_0^\ell -\frac{e^{jk(2\ell-z-\sqrt{a^2+z^2})}}{\sqrt{a^2+z^2}} - \frac{e^{jk(-z-\sqrt{a^2+z^2})}}{\sqrt{a^2+z^2}} dz \\
&+ \int_0^\ell \frac{e^{jk(z-\sqrt{a^2+z^2})}}{\sqrt{a^2+z^2}} + \frac{e^{jk(z-2\ell-\sqrt{a^2+z^2})}}{\sqrt{a^2+z^2}} dz
\end{aligned} \tag{B.3}$$

Making a substitution $v = z \pm \ell$ where applicable, yielding $dv = dz$, and rewriting the last two integrals:

$$\begin{aligned}
\frac{4\pi}{\eta} Z_m &= \int_{-\ell}^0 \frac{e^{jk(-v-\sqrt{a^2+v^2})}}{\sqrt{a^2+v^2}} dv - \int_{-\ell}^0 \frac{e^{jk(v-\sqrt{a^2+v^2})}}{\sqrt{a^2+v^2}} dv \\
&+ e^{2jk\ell} \int_\ell^{2\ell} \frac{e^{jk(-v-\sqrt{a^2+v^2})}}{\sqrt{a^2+v^2}} dv - e^{-2jk\ell} \int_\ell^{2\ell} \frac{e^{jk(v-\sqrt{a^2+v^2})}}{\sqrt{a^2+v^2}} dv \\
&- (1 + e^{2jk\ell}) \int_0^\ell \frac{e^{jk(-v-\sqrt{a^2+v^2})}}{\sqrt{a^2+v^2}} dv + (1 + e^{-2jk\ell}) \int_0^\ell \frac{e^{jk(v-\sqrt{a^2+v^2})}}{\sqrt{a^2+v^2}} dv
\end{aligned} \tag{B.4}$$

Making a second substitution $w = jk(u \pm \sqrt{a^2 + u^2})$, yielding $dw = \pm w du / \sqrt{a^2 + u^2}$, results in:

$$\begin{aligned}
\frac{4\pi}{\eta} Z_m &= \int_{jk(\sqrt{a^2+\ell^2}-\ell)}^{jka} \frac{\exp(-w)}{w} dw + \int_{jk(\sqrt{a^2+\ell^2}+\ell)}^{jka} \frac{\exp(-w)}{w} dw + e^{2jk\ell} \cdot \int_{jk(\sqrt{a^2+\ell^2}+\ell)}^{jk(\sqrt{a^2+(2\ell)^2+2\ell})} \frac{\exp(-w)}{w} dw \\
&+ e^{-2jk\ell} \cdot \int_{jk(\sqrt{a^2+(2\ell)^2}-2\ell)}^{jk(\sqrt{a^2+\ell^2}-\ell)} \frac{\exp(-w)}{w} dw - (1 + e^{2jk\ell}) \cdot \int_{jka}^{jk(\sqrt{a^2+\ell^2}+\ell)} \frac{\exp(-w)}{w} dw - (1 + e^{-2jk\ell}) \cdot \int_{jka}^{jk(\sqrt{a^2+\ell^2}-\ell)} \frac{\exp(-w)}{w} dw
\end{aligned} \tag{B.5}$$

These integrands do not have an antiderivative that can be expressed in elementary functions. Instead, the solution can be given in terms of the E_1 -

function:

$$E_1(z) \triangleq \int_z^\infty \frac{\exp(-w)}{w} dw \quad \Re(z) \geq 0 \quad (\text{B.6})$$

$$E_1'(a, x) \triangleq E_1 \left(jk(\sqrt{a^2 + x^2} + x) \right) \quad (\text{B.7})$$

$$\begin{aligned} \frac{4\pi}{\eta} Z_m &= -\exp(2jk\ell) \cdot E_1'(a, 2\ell) + (2 \cdot \exp(2jk\ell) + 2) \cdot E_1'(a, \ell) \\ &\quad + (-\exp(2jk\ell) - \exp(-2jk\ell) - 4) \cdot E_1'(a, 0) \\ &\quad + (2 \cdot \exp(-2jk\ell) + 2) \cdot E_1'(a, -\ell) - \exp(-2jk\ell) \cdot E_1'(a, -2\ell) \\ &= 2E_1'(a, \ell) - 4E_1'(a, 0) + 2E_1'(a, -\ell) + \cos(2k\ell) \\ &\quad \cdot \left[-E_1'(a, 2\ell) + 2E_1'(a, \ell) - 2E_1'(a, 0) + 2E_1'(a, -\ell) - E_1'(a, -2\ell) \right] \\ &\quad + j \sin(2k\ell) \cdot \left[-E_1'(a, 2\ell) + 2E_1'(a, \ell) - 2E_1'(a, -\ell) + E_1'(a, -2\ell) \right] \end{aligned} \quad (\text{B.8})$$

As the dipole radius a is in general very small compared to its length 2ℓ , three values applied to the E_1 -function are close to zero, resulting in very large numbers that are subtracted to obtain a small number. Using numerical evaluation, this might easily give rise to errors. These errors can be circumvented by using the following series expansion for the exponential integral to obtain a useful approximation to Equation B.8 [21]:

$$E_1(z) = -\gamma - \ln(z) - \sum_{n=1}^{\infty} \frac{(-z)^n}{n \cdot n!} \quad (\text{B.9})$$

$$\text{with } \gamma \triangleq \lim_{N \rightarrow \infty} \left(\sum_{n=1}^N n^{-1} - \ln(N) \right) \approx 0.5772 \quad (\text{B.10})$$

When z is a small positive imaginary number, we can rewrite the series as:

$$\begin{aligned} -\sum_{n=1}^{\infty} \frac{(-j\epsilon)^n}{n \cdot n!} &= -\sum_{n=0}^{\infty} \left[\frac{\epsilon^{2(n+1)}}{2(n+1) \cdot (2(n+1))!} (-1)^{n-1} \right] \\ &\quad - j \cdot \sum_{n=0}^{\infty} \left[\frac{\epsilon^{2n+1}}{(2n+1) \cdot (2n+1)!} (-1)^{n-1} \right] \\ &= j\epsilon + \frac{\epsilon^2}{4} - j \frac{\epsilon^3}{18} - \frac{\epsilon^4}{96} + \dots \end{aligned} \quad (\text{B.11})$$

Here, ϵ is a small positive real number. Using the alternating series estimation theorem (see: [22]) with the first two terms of both series, we can conclude:

$$\begin{cases} \epsilon^2 \left(\frac{1}{4} - \frac{\epsilon^2}{96} \right) \leq \left| \Re \left\{ \sum_{n=1}^{\infty} \frac{(-j\epsilon)^n}{n \cdot n!} \right\} \right| \leq \epsilon^2 \left(\frac{1}{4} + \frac{\epsilon^2}{96} \right) \\ \epsilon \left(1 - \frac{\epsilon^2}{18} \right) \leq \left| \Im \left\{ \sum_{n=1}^{\infty} \frac{(-j\epsilon)^n}{n \cdot n!} \right\} \right| \leq \epsilon \left(1 + \frac{\epsilon^2}{18} \right) \end{cases} \quad (\text{B.12})$$

When z is sufficiently close to zero, the series in Equation B.9 can be neglected compared to the natural logarithm:

$$\left\{ \begin{array}{l} \left| \Re \left\{ \sum_{n=1}^{\infty} \frac{(-j\epsilon)^n}{n \cdot n!} \right\} \right| \leq \epsilon^2 \left(\frac{1}{4} + \frac{\epsilon^2}{96} \right) \ll |\Re \{\ln(j\epsilon)\}| = |\ln(\epsilon)| \\ \left| \Im \left\{ \sum_{n=1}^{\infty} \frac{(-j\epsilon)^n}{n \cdot n!} \right\} \right| \leq \epsilon \left(1 + \frac{\epsilon^2}{18} \right) \ll |\Im \{\ln(j\epsilon)\}| = \frac{\pi}{2} \end{array} \right. \quad (\text{B.13})$$

$$\Rightarrow E_1(j\epsilon) \approx -\gamma - \ln(j\epsilon) = -\gamma - \ln(\epsilon) - \frac{j\pi}{2} \quad (\text{B.14})$$

$$\begin{aligned} \Rightarrow \lim_{a \rightarrow \epsilon} c_0 \cdot E_1'(a, 0) + c_1 \cdot E_1'(a, -\ell) + c_2 \cdot E_1'(a, -2\ell) \approx \\ - (c_0 + c_1 + c_2) \cdot \left(\gamma + \frac{j\pi}{2} \right) + \\ \ln \left(\lim_{a \rightarrow \epsilon} \left((ka)^{c_0} \cdot (k(\sqrt{a^2 + \ell^2} - \ell))^{c_1} \cdot (k(\sqrt{a^2 + (2\ell)^2} - 2\ell))^{c_2} \right) \right) \end{aligned} \quad (\text{B.15})$$

In these equations γ is the Euler-Mascheroni constant (0.577...). Application of this approximation to Equation B.8 yields for small antenna radii a :

$$\begin{aligned} \frac{4\pi}{\eta} Z_m \approx & 2E_1'(a, \ell) + 2\gamma + j\pi + \ln \left(\frac{k^2 a^4}{(\sqrt{a^2 + \ell^2} - \ell)^2} \right) \\ & + \cos(2k\ell) \left[-E_1'(a, 2\ell) + 2E_1'(a, \ell) + \gamma + \frac{j\pi}{2} + \ln \left(\frac{k(\sqrt{a^2 + (2\ell)^2} - 2\ell) a^2}{(\sqrt{a^2 + \ell^2} - \ell)^2} \right) \right] \\ & + j \sin(2k\ell) \left[-E_1'(a, 2\ell) + 2E_1'(a, \ell) + \gamma + \frac{j\pi}{2} + \ln \left(\frac{k(\sqrt{a^2 + \ell^2} - \ell)^2}{\sqrt{a^2 + 2\ell^2} - 2\ell} \right) \right] \end{aligned} \quad (\text{B.16})$$

$$\begin{aligned} \approx & 2E_1(2jk\ell) + 2\gamma + j\pi + 2 \ln(2k\ell) \\ & + \cos(2k\ell) \left[-E_1(4jk\ell) + 2E_1(2jk\ell) + \gamma + \frac{j\pi}{2} + \ln(k\ell) \right] \\ & + j \sin(2k\ell) \left[-E_1(4jk\ell) + 2E_1(2jk\ell) + \gamma + \frac{j\pi}{2} + \ln \left(\frac{ka^2}{\ell} \right) \right] \end{aligned} \quad (\text{B.17})$$

The argument to the last natural logarithm in equation B.16 limits to zero, so the second order Taylor-approximation of this argument is given in equation B.17 instead, for approximating for small dipole diameters. The real and imaginary part of Equation B.17 are shown in Equation 3.15 and Equation 3.16

on Page 18. This result can be found by writing the E_1 -function as:

$$\begin{aligned}
 E_1(jx) &= \int_{jx}^{\infty} \frac{\exp(-w)}{w} dw = \int_x^{\infty} \frac{\exp(-jv)}{v} dv \\
 &= \int_x^{\infty} \frac{\cos(v)}{v} - j \frac{\sin(v)}{v} dv \\
 &= \int_x^{\infty} \frac{\cos(v)}{v} dv - j \left(\int_0^{\infty} \frac{\sin(v)}{v} dv - \int_0^x \frac{\sin(v)}{v} dv \right) \\
 &= \text{Ci}(x) + j \text{Si}(x) - \frac{j\pi}{2} \tag{B.18}
 \end{aligned}$$

$$\text{with:} \quad \text{Si}(x) \triangleq \int_0^x \frac{\sin(w)}{w} dw \quad \text{Ci}(x) \triangleq \int_x^{\infty} \frac{\cos(w)}{w} dw$$

Bibliography

- [1] N Sampietro, G Accomando, L G Fasoli, G Ferrari, and E C Gatti. High sensitivity noise measurement with a correlation spectrum analyzer. *Instrumentation and Measurement IEEE Transactions on*, 49(4):820–822, 2000. URL http://ieeexplore.ieee.org/xpl/freeabs_all.jsp?arnumber=863931.
- [2] Carmine Ciofi, Felice Crupi, and Calogero Pace. A new method for high-sensitivity noise measurements. *IEEE T. Instrumentation and Measurement*, 51(4):656–659, 2002. URL <http://dblp.uni-trier.de/db/journals/tim/tim51.html#CiofiCP02>.
- [3] André B.J. Kokkeler and André W. Gunst. Modeling correlation of quantized noise and periodic signals. *IEEE Signal Processing Letters*, 11(10):802–805, 2004. URL <http://doc.utwente.nl/49362/>.
- [4] Felice Crupi, Gino Giusi, Carmine Ciofi, and Calogero Pace. Enhanced sensitivity cross-correlation method for voltage noise measurements. *IEEE T. Instrumentation and Measurement*, 55(4):1143–1147, 2006. URL <http://dblp.uni-trier.de/db/journals/tim/tim55.html#CrupiGCP06>.
- [5] M.S. Oude Alink. Increasing the spurious-free dynamic range of an integrated spectrum analyzer. Master’s thesis, University of Twente, Faculty of Electrical Engineering, Mathematics & Computer Science, November 2008. URL <http://essay.utwente.nl/58500/>.
- [6] M. Heskamp and C. H. Slump. Sub-noise primary user detection by cross-correlation. In *Proceedings IEEE International Conference on Communication, ICC 2009, Dresden, Germany*, pages 1–6, USA, June 2009. IEEE Communications Society.
- [7] M.S. Oude Alink, E.A.M. Klumperink, M.C.M. Soer, A.B.J. Kokkeler, and B. Nauta. A 50Mhz-to-1.5Ghz cross-correlation CMOS spectrum analyzer for cognitive radio with 89dB SFDR in 1Mhz RBW. In *New Frontiers in Dynamic Spectrum, 2010 IEEE Symposium on*, pages 1–6, april 2010. doi: 10.1109/DYSPAN.2010.5457887.
- [8] Mark S. Oude Alink, Eric A.M. Klumperink, André B.J. Kokkeler, Michiel C.M. Soer, Gerard J.M. Smit, and Bram Nauta. A cmos-compatible spectrum analyzer for cognitive radio exploiting crosscorrelation to improve linearity and noise performance. *IEEE Transactions on Circuits and Systems I: Regular papers*, PP(99):1–14, November 2011. URL <http://doc.utwente.nl/79000/>.

- [9] Mark S. Oude Alink, André B.J. Kokkeler, Eric A.M. Klumperink, Gerard J.M. Smit, and Bram Nauta. Lowering the snr-wall for energy detection using crosscorrelation. *IEEE Transactions on Vehicular Technology*, 60(8):3748–3757, August 2011. URL <http://doc.utwente.nl/78308/>.
- [10] Carlo P. Domizioli, Brian L. Hughes, Kevin G. Gard, and Gianluca Lazzi. Noise correlation in compact diversity receivers. *Trans. Comm.*, 58:1426–1436, May 2010. ISSN 0090-6778. doi: <http://dx.doi.org/10.1109/TCOMM.2010.05.080601>. URL <http://dx.doi.org/10.1109/TCOMM.2010.05.080601>.
- [11] A.R. Smeenge. Improving cross-correlation spectrum sensing using two antennas. Master’s thesis, University of Twente, Faculty of Electrical Engineering, Mathematics & Computer Science, October 2010. URL <http://essay.utwente.nl/59734/>.
- [12] M.S. Oude Alink, A.R. Smeenge, A.B.J. Kokkeler, E.A.M. Klumperink, G.J.M. Smit, and B. Nauta. Exploring the use of two antennas for cross-correlation spectrum sensing. In *IEEE Vehicular Technology Conference, VTC Fall 2011*, pages 1–5, Piscataway, September 2011. IEEE Press. URL <http://doc.utwente.nl/78999/>.
- [13] Wim C. van Etten. *Random Signals and Noise*. John Wiley & Sons Ltd., 2005.
- [14] *The American Heritage dictionary of the English language*. American Heritage Dictionary of the English Language. Houghton Mifflin, 2000. ISBN 9780395825174.
- [15] Constantine A. Balanis. *Antenna theory*. John Wiley & Sons, Inc., second edition, 1982.
- [16] Edward C. Jordan and Keith G. Balmain. *Electromagnetic waves and radiating systems*. Prentice-Hall Electrical Engineering series. Prentice-Hall, second edition, 1968.
- [17] J. Richmond. A reaction theorem and its application to antenna impedance calculations. *Antennas and Propagation, IRE Transactions on antennas and propagation*, 9(6):515–520, november 1961. ISSN 0096-1973. doi: 10.1109/TAP.1961.1145068.
- [18] Howard E. King. Mutual impedance of unequal length antennas in echelon. *IRE Transactions on antennas and propagation*, AP-5:306–313, july 1957.
- [19] Samir S. Soliman and Mandyam D. Srinath. *Continuous and discrete signals and systems*. Prentice-Hall, Inc., second edition, 1990.
- [20] Eric W. Weisstein. *Delta Function*. From MathWorld—A Wolfram Web Resource, september 2011. URL <http://mathworld.wolfram.com/DeltaFunction.html>.
- [21] Eric W. Weisstein. *En-Function*. From MathWorld—A Wolfram Web Resource, september 2011. URL <http://mathworld.wolfram.com/En-Function.html>.

- [22] James Stewart. *Calculus: early transcendentals*. Thomson/Brooks/Cole, fifth edition, 2003. ISBN 0534274099.